Dendroclimatology using stable isotopes from subfossil tree-rings: A Late Glacial Investigation

Maren Isabelle Pauly

Freie Universitat Berlin
Department of Earth Sciences - Paleontology
2021

Dendroclimatology using stable isotopes from subfossil tree-rings: A Late Glacial Investigation

---

A Dissertation

Submitted in Partial Fulfilment of the
Requirements for the Degree of
Ph.D.

to the Department of Earth Sciences
of Freie Universität Berlin

by Maren Isabelle Pauly

Berlin, 2021

Thesis Committee

Chair: Prof. Dr. Anne Bernhardt, Tectonics and Sedimentary Systems Professor
Department of Earth Sciences at the Freie Universität Berlin

Deputy Chair: Prof. Dr. Harry Becker, Head of the Geochemistry group
Department of Earth Sciences at the Freie Universität Berlin

First Referee: Prof. Dr. Frank Riedel, Paleontology Univ.-Professor
Department of Earth Sciences at the Freie Universität Berlin

Second Referee: Prof. Dr. Achim Brauer
Head of Section 5.2 Climate Dynamics and Landscape Evolution, GFZ Potsdam
Außerplanmäßiger Professor in the Institute of Earth and Environmental Science at Universität Potsdam

Inspector: Prof. Dr. Stephan Pfahl
Institute for Meteorology Professor at the Freie Universität Berlin

Date of defense: August 16, 2021

A SPECIAL THANKS TO...

The Deutsche Forschungsgemeinschaft for funding this research

My wonderful co-authors and members of the Binz team for all of your hard work and determination

Professor Frank Riedel for welcoming me into the department and providing insightful feedback and recommendations

Dr. Gerhard Helle for always being a positive ray of sunshine, even when all of the lab equipment broke and we were left without a technician

Professor Achim Brauer for his continuous support and patience, particularly in explaining volcanic tie points on multiple occasions

All of my friends in Berlin for distracting me in times I probably should have been focussing on this PhD

Tim, Otto and Rudi for never reading a single one of my papers, but supporting and entertaining me nonetheless

My parents and sister for pretending to care about paleontology and encouraging me throughout these past 5 years

Contents

List of Figures

ZUSAMMENFASSUNG

Das übergeordnete Ziel dieser Dissertation ist der Aufbau von Jahrring-Isotopenchronologien von Kohlenstoff ($\delta^{13}C$) und Sauerstoff ($\delta^{18}O$) spätglazialer Hölzer der Nord- und Südhemisphäre und die Extraktion und Interpretation möglicher Klimasignale. Dazu wurden (1) jährlich aufgelöste mehrhundertjährige Zeitreihen der stabilen Isotope in Jahrringen subfossiler Kiefernhölzer (Pinus sylvestris) von Fundorten in der Schweiz (Binz) und (2) den südfranzösischen Alpen (Barbiers) erstellt, und (3) eine etwas mehr als tausendjährige Jahrring-Isotopenchronologie von neuseeländischen Kauribäumen (Agathis australis) entwickelt. Anschließend wurden folgende Teilziele verfolgt: (1) ermitteln potenzieller Klimasignale in den erstellten Isotopendatensätzen, (2) identifizieren und beschreiben möglicher Signalstörungen infolge diagenetischer Veränderungen einzelner Hölzer durch Vergleiche der Isotopentrends gleichalter Bäume, sowie in Einzelbäumen, (3) Ableitung des Quellwasser-$\delta^{18}O$ (Niederschlag) aus dualen ($\delta^{13}C$, $\delta^{18}O$) Isotopenmodellen, und (4) Erstellung und Interpretation von Rekon¬struktionen der Klimavariabilität in den untersuchten Regionen und Zeitabschnitten.

Die älteste der drei Isotopenchronologien wurde aus 27 Schweizer Kiefern entwickelt. Sie umfasst den Zeitraum ~ 14.050 - 12.795 cal BP (Kapitel 6). Der Jahrring Datensatz ($\delta^{18}O_{tree}$) wurde mit Eisbohrkern-$\delta^{18}O$ Daten (NGRIP) verglichen, um zu testen, ob die während des Sommers in der Zellulose der Jahrringe festgelegten Isotopenverhältnisse des Schweizer Plateaus die grönländischen Klimaphasen ebenso widerspiegeln wie mitteleuropäische Seesedimente. Zwei extreme Einbrüche des $\delta^{18}O_{tree}$ zeigen Bezug zu GI-1c und GS-1, während z.B. GI-1b in $\delta^{18}O_{tree}$ nicht klar zum Ausdruck kommt. Einbrüche in $\delta^{18}O_{tree}$ können nicht ausschließlich in Verbindung mit extremen Kältephasen gebracht werden, sondern sie sind auch Ausdruck deutlich erhöhter Niederschläge. In solchen Phasen zeigen sich $\delta^{18}O$-Zeitreihen der Einzelbäume deutlich kohäsiver (höheres Populationssignal), was wahrscheinlich auf den geringeren Einfluss der Stomata-Apertur der Nadeln auf die Isotopenfraktionierung bei hoher Luftfeuchtigkeit deutet. Im Allgemeinen kann $\delta^{18}O_{tree}$ Klimaschwankungen erfassen, jedoch in geringerem Maße als NGRIP $\delta^{18}O$. Die dort dokumentierten Kältephasen sind in der Sommer¬saison auf dem Schweizer Plateau eventuell weniger stark ausgeprägt.

Anhand von 7 Kiefern aus den südfranzösischen Alpen wurden der Beginn (~ 12 900 - 12 600 cal BP) von GS-1 (Grönland) bzw. Jüngerer Dryas (Europa) untersucht (Kapitel 7). Aus $\delta^{18}O_{tree}$ Quellwasser-$\delta^{18}O$ abgeleitet, wodurch sich Veränderungen des Ursprungs feuchter Luftmassen in S-Frankreich zeigten. Eine erhöhte $\delta^{18}O_{tree}$-Variabilität deutet auf ein Wechselspiel zwischen Nordatlantik (niedriges $\delta^{18}O$) und im Mittelmeerraum (hohes δ18O) hin, wahrscheinlich infolge starker Oszillationen einer generell nach Süden wandernden Polarfront.

Die jüngste Chronologie wurde unter Verwendung von 6 Kauri-Bäumen aus Neuseeland erstellt. Der Zeitraum wurde ~ 13 020 - 11 850 cal BP ist in dekadischer Auflösung, ein kurzer Teilabschnitt in jährlicher Auflösung (~ 12 520 - 12 400 cal BP) untersucht (Kapitel 8). Anders als im nordatlantischen Raum erwärmt sich die südliche Hemisphäre im Spätglazial eher allmählich. Ein markanter Klimaabschwung (~ 12 625 - 12 375 cal BP) wurde allerdings von den Bäumen dokumentiert. Kennzeichnend waren hohe Niederschläge/Luftfeuchtigkeit und niedrige Temperaturen, möglicherweise ausgelöst durch Veränderungen der Ozeanzirkulation.

Insgesamt zeigen die Jahrringisotope das gute Potenzial subfossiler Bäume zur Rekonstruktion der hydroklimatischen Variabilität des Spätglazials. Allerdings zeichnen sie eher hochfrequente Signale auf und spiegeln oft nicht bekannte Klimatrends anderer Archive wider. Dies hängt einerseits mit dem biologischen Charakter des Archivs „Baum“ zusammen, andererseits sind mögliche Signalveränderungen durch Zersetzungsprozesse während und nach der Einbettung im Sediment derzeit nur schwer zu quantifizieren. Insgesamt zeigen die Baumring-Chronologien in dieser Dissertation das Potenzial, subfossile Bäume zur Rekonstruktion der Variabilität des Hydroklimas während des späten Gletschers zu verwenden.

SUMMARY

The overall goal of this PhD dissertation is to develop multi-centennial stable isotope chronologies in annual rings of subfossil pine trees (Pinus sylvestris) from sites in (1) Switzerland (Binz) and (2) the southern French Alps (barbers), as well as (3) decadal records from subfossil New Zealand kauri trees (Agathis australis). After establishing these three chronologies, this dissertation explored the following objectives: (1) detect any potential climatic signal contained within the developed $\delta^{18}O$ and $\delta^{13}C$ records, (2) identify any probable diagenetic biases impacting the inter- and intra- tree stable isotope correlations (e.g. wood decay), (3) develop a technique to estimate sourcewater $\delta^{18}O$ (precipitation) from dual stable isotope models, and (4) reconstruct high frequency climate variability across the Late Glacial.

The oldest chronology was developed from 27 Swiss subfossil pine trees, covering ~14,050 – 12,795 cal BP; described in the Chapter 6 paper. The tree-ring $\delta^{18}O$ record was compared to ice core $\delta^{18}O$ (NGRIP) to investigate whether Greenland Stadial "events", which are often discernible in European lake records, are also recorded in the Swiss plateau during the summer growing season. Two examples of $\delta^{18}O_{tree}$ extreme depletions did parallel known North Atlantic 'cool periods' (GI-1c, GS-1), while another LG oscillation (GI-1b) is not clearly expressed in $\delta^{18}O_{tree}$. The trees tended to record events more cohesively (higher population signal) during extreme $\delta^{18}O_{tree}$ depletions in relatively wet conditions (high precipitation amount); likely due to the lack of stomata influence on stable isotope fractionation in high humidity. Generally, this record was able to capture North Atlantic climate oscillations, but to a lesser degree than Greenland ice core δ18O, suggesting the "events" may be less extreme in the summer season.

The GS-1 (Younger Dryas) cold reversal recorded in the Swiss pine trees was also documented in 7 pine trees from the southern French alps, as described in the Chapter 7 paper. A short chronology was developed during this interval, covering ~12 900 – 12 600 cal BP. Estimates of sourcewater $\delta^{18}O$ ($\delta^{18}O_{SW}$) recorded changes in air mass origin in southern France over the cooling event, indicating an amplification of both North Atlantic (depleted $\delta^{18}O_{SW}$) as well as Mediterranean (high $\delta^{18}O_{SW}$) originating storms. Higher magnitude and frequency of precipitation from both origins would likely have been due to the oscillating, southward moving polar front as Europe plunged into near-Glacial conditions.

The youngest chronology was established using 6 kauri trees from New Zealand, covering ~13 020 – 11 850 cal BP at decadal resolution and a subset at annual resolution (~12 520 – 12 400 cal BP), as explained in the Chapter 8 paper. Whilst North Atlantic climate oscillations are occurring in Europe, the Southern Hemisphere is going through a gradual warming. The kauri trees recorded a significant climate downturn (~12 625 – 12 375 cal BP: low tree-ring growth, depleted $\delta^{18}O_{tree}$, $\delta^{18}O_{SW}$ and $\delta^{13}C_{tree}$), undetected in Antarctic ice core data, which was characterised by sustained high precipitation, low temperature and high humidity. In conjunction with global climate model outputs, this research suggests this climate downturn may have been triggered by ocean circulation changes, resulting in a prolonged shift in hydroclimate conditions in New Zealand.

Overall, the tree-ring chronologies presented in this dissertation from Switzerland, France and New Zealand demonstrate the potential to use subfossil trees to reconstruct hydroclimate variability during the Late Glacial using dual stable isotopes and sourcewater reconstructions. However, they tend to record high-frequency signals and often reflect unknown climate trends from other archives. On the one hand, this is related to the biological character of the "tree" archive, on the other hand, possible signal changes due to decomposition processes during and after embedding in the sediment are currently difficult to quantify

I hereby declare in lieu of oath that I wrote this dissertation independently and without any unauthorized help. When writing the dissertation there were no aids other than those listed in the text are used. All statements within the present work, which in terms of wording or meaning from other sources have been taken, are identified in the text and are in a full reference list. I have not started a doctoral procedure previously with another university and have never made an application with this wor to another department.

Maren Isabelle Pauly

Toronto, 28. February 2021

Publications and Contributions

First-author:

Paper1: Pauly, M., Helle, G., Büntgen, U., Wacker, L., Treydte, K., Reinig, F., Turney, C., Nievergelt, D., Kromer, B., Friedrich, M. and Sookdeo, A., 2020. An annual-resolution stable isotope record from Swiss subfossil pine trees growing in the late Glacial. *Quaternary Science Reviews*, 247, 106550. https://doi.org/10.1016/j.quascirev.2020.106550

The trees for this paper were dated by colleagues at WSL with assistance by MP. The tree selection, sample cross-dating and preparation, cellulose extraction and stable isotope measurement were done by MP. MP performed analysis and evaluation of all data, designed the figures and wrote the MS. GH designed and directed the project (DFG HE3089/9-1), together with AB he supervised the project providing feedback at all stages. All other authors assisted in choosing research design and editing manuscript drafts.

Paper2: Pauly, M., Helle, G., Miramont, C., Büntgen, U., Treydte, K., Reinig, F., Guibal, F., Sivan, O., Heinrich, I., Riedel, F. and Kromer, B., 2018. Subfossil trees suggest enhanced Mediterranean hydroclimate variability at the onset of the Younger Dryas. *Scientific reports*, 8(1), pp.1-8. https://doi.org/10.1038/s41598-018-32251-2

The initial stable isotope data was existing and belonging to GH, it was previously measured but not published by another student. MP performed analytic calculations, tree-ring physiological modeling (sourcewater) and interpreted all data. MC, FG, OS, FR and BK provided radiocarbon and dendrochronological dating of all samples. MP designed the figures and wrote the MS with input from all co-authors. GH designed and directed the project (DFG HE3089/9-1), together with AB he supervised the project providing feedback at all stages.

Paper3: Pauly, M., Turney, C.S.M., Palmer, J.G., Büntgen, U., Brauer, A. and Helle, G., 2020. Kauri tree-ring stable isotopes reveal a centennial climate downturn following the Antarctic Cold Reversal in New Zealand. *Geophysical Research Letters. vol. 48, Issue 2. e2020GL090299*
https://doi.org/10.1029/2020GL090299

The initial stable isotope data was existing and belonging to GH, it was previously measured but not published by another student. The data was interpreted, and a tree-ring physiological model (sourcewater) was developed by MP to utilize the data for publication. MP also ran global climate models (TraCE21ka) as part of the methodology. The manuscript draft and revisions were done by MP. GH designed and directed the project (DFG HE3089/9-1), together with AB he supervised the project providing feedback at all stages. All other authors assisted in choosing research design and editing manuscript drafts.

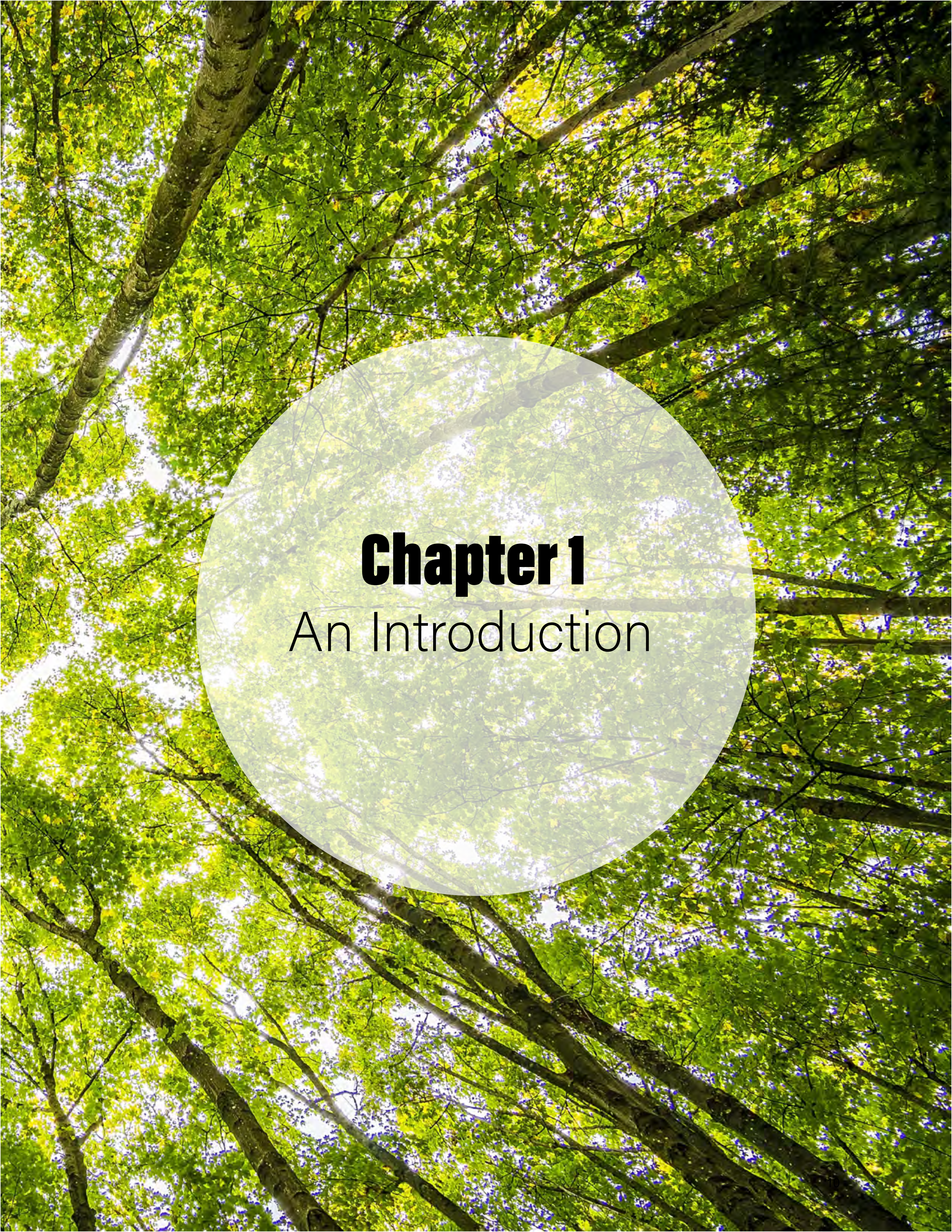

Chapter 1
An Introduction

1. Introduction

1.1. Climate change and paleoclimatology

Climate change and related hazards are some of the most significant and likely risks projected to negatively impact society by the end of the century (World Economic Forum, 2019). Much of these environmental challenges are catalysed by extreme changes to the climate system's hydrological cycle, amplifying the magnitude and frequency of extreme weather events (cyclones, flooding, drought); the effects of which cascade into loss of habitats, as well as threats in food and water security.

Evidence of global warming was first detected in the instrumental record as a steady rise in atmospheric CO_2 at Mauna Loa Observatory in Hawaii (313ppm in 1958 to 416ppm in 2020; NOAA 2020), which was connected to anthropogenic fossil fuel emissions and warming temperatures across the globe. The mechanism behind contemporary climate change has been confirmed in Global Climate Models (GCMs) and put into context from examples of past climate oscillations using environmental archives.

Despite the advantage of using GCMs in estimating the future rate and magnitude of local change, one of the primary uncertainties in climate models is the regional projection of precipitation in the future (Stocker et al. 2014). This is partly due to the strong modulation of weather systems by complex atmosphere-ocean linked phenomena (e.g. ENSO, NAO, AO, AMOC), which are responsible for distributing moisture across the globe, with cycle frequencies reaching beyond the instrumental record. For example, although a reduction in Atlantic Meridional Overturning Circulation (AMOC) is predicted by GCMs at high confidence, the subsequent reactions of more localised systems (i.e. North Atlantic Oscillation) remain unclear. Moreover, while the immediate effects of modified atmosphere-ocean systems could potentially be interpreted from the enhanced frequency and intensity of storm events within the instrumental record, it is difficult to decipher whether any discovered trends are within the envelope of natural variability or a result of anthropogenic alteration of the system.

The study of past climate (paleoclimatology) using nature archives (trees, corals, ice cores, lake sediments) offers a critical opportunity to improve the predictability of future climate change. Examples from the past provide a validation to the scale of possible oscillations in the climate system, beyond the modern observational time threshold. By improving the understanding of the physical dynamics controlling climate variability on long time scales, GCM projections can potentially be constrained.

The most recent and extreme examples of past climate change occurred at the transition from the last glaciation to the current interglacial (Holocene) - The Late Glacial (~ 14,600 – 11,700 calendar years before present (cal BP); Steffensen et al. 2008; Chapter 3). Given a collection of paleoclimate datasets exemplifying such chaotic and complex climate events, one can investigate the underlying patterns, resilience, variability, extremes and feedbacks of the climate system. In this way, new independent benchmarks can be established to evaluate sensitivities of climate parameters beyond the instrumental record with which GCMs were built.

1.2 Dendrochronology

Trees offer an advantageous proxy archive for past environments within their high-resolution annual rings, which record indirect signatures of climate variation. They have long individual chronologies with wide spatial and temporal coverage, and the synthesis of latewood and earlywood potentially allows the reconstruction of seasonality and abrupt climate events (Fritts 1971, Hughes 2011, Speer 1971, Stokes 1968). Earlywood is growth with a low density structure at the beginning of the growing season, whereas latewood is the denser growth near the end of the growing season; the former appears rather light in colour, whereas the latter is comparably dark, with clear periodicity allowing for the delineating of individual years (Figure 1.1). The boundaries between years and growth types tends to be more severe in climates with strong seasonality (Fritts 1971).

Each tree represents an individual record, which must be joined together by matching tree ring widths and finding synchronous growth patterns to create a full chronology (Speer 1971, Stokes 1968). Chronology precision is not homogenous and is dependent on sample size and the "common signal". The common signal is the degree to which the trees within a group are recording the same environmental signal(s); the strength of which can be overshadowed by local influences (age, stand evolution, competition, slope). in regions with weak limiting growth factors. For this reason, larger sample sizes and multiple tree-proxies are preferred to ensure accuracy of the chronological climate representation (Esper 2002, LaMarche 1974, Fritts 1971, Fritts 1974, Fritts 1976).

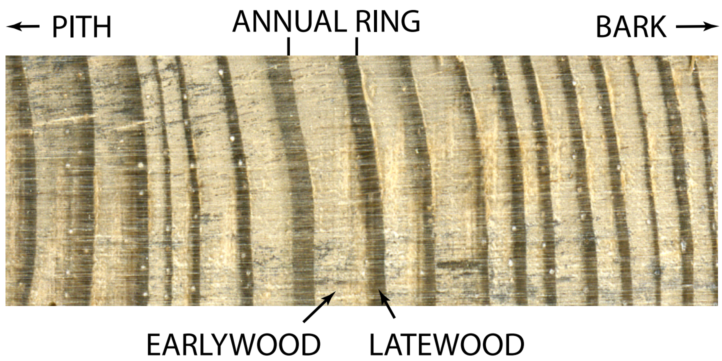

Figure 1.1: An example of tree-rings within a subfossil pine (*Pinus sylvestris*) from the Binz wood material with typical structures highlighted, including earlywood and latewood within an annual ring.

The tendency for trees to accurately record climate depends on the degree to which their growth is limited by the environmental factors that define the local climate ('limiting growth factors'). For example, in areas of climate extremes, parameters such as temperature and precipitation may constraint the growth and prosperity of vegetation; trees in arid regions would be limited by moisture availability, while trees along high latitude or altitude boundaries would be limited by temperature (Fritts 1971). As a result, the growth rings of trees existing in these areas would be a product of the strong variability in such limiting growth factors, and therefore these factors could theoretically be reconstructed from tree-ring widths through time (Fritts 1971, Hughes 2011, Speer 1971, Stokes 1968).

References (Chapter 1)

Esper, J., Cook, E.R. and Schweingruber, F.H., "Low-frequency signals in long tree-ring chronologies for reconstructing past temperature variability". Science, 295 (2002), pp.2250-2253.

Fritts, Harold C. "Dendroclimatology and dendroecology." *Quaternary Research* 1.4 (1971): 419-449.

Fritts, Harold C. "Relationships of ring widths in arid-site conifers to variations in monthly temperature and precipitation." *Ecological Monographs* 44.4 (1974): 411-440.

Hughes, Malcolm K. "Dendroclimatology in high-resolution paleoclimatology." *Dendroclimatology*. Springer, Dordrecht, 2011. 17-34.

LaMarche, Valmore C. "Paleoclimatic Inferences from Long Tree-Ring Records: Intersite comparison shows climatic anomalies that may be linked to features of the general circulation." *Science* 183.4129 (1974): 1043-1048.

NOAA/GML, Dr. Pieter Tans (www.esrl.noaa.gov/gmd/ccgg/trends/) and Dr. Ralph Keeling, Scripps Institution of Oceanography (scrippsco2.ucsd.edu/)

Steffensen, Jørgen Peder, et al. "High-resolution Greenland ice core data show abrupt climate change happens in few years." *Science* 321.5889 (2008): 680-684.

Stokes, M. A., and T. L. Smiley. "Introduction to tree-ring dating. University of Chicago." (1968).

Stocker, T. F., et al. "Contribution of working group I to the fifth assessment report of the intergovernmental panel on climate change." *Climate change* (2013).

World Economic Forum "The Global Risks Report 2020". (2020) Insight Report, 15th Edition.

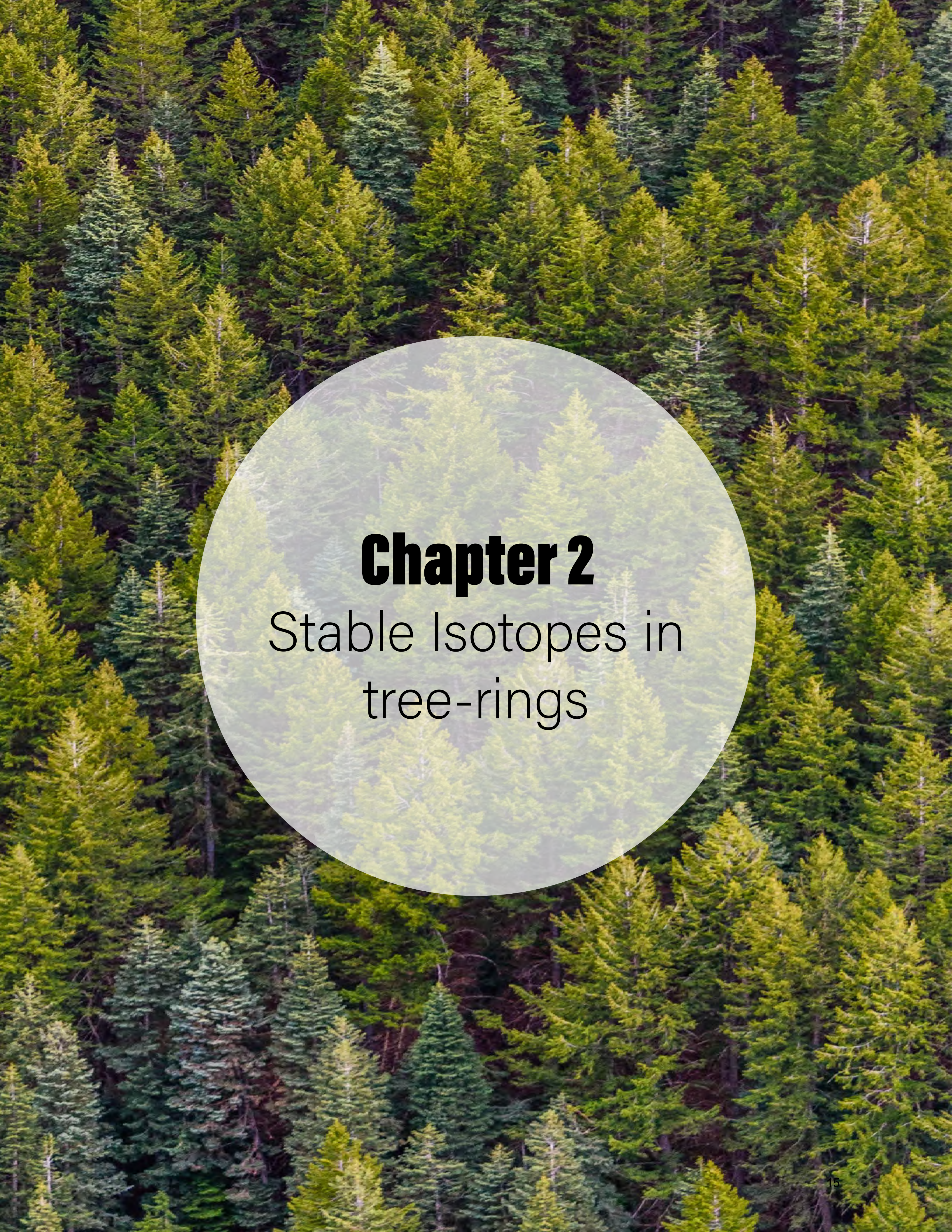

Chapter 2
Stable Isotopes in tree-rings

2. Stable isotopes in tree-rings

Numerous environmental conditions that may result in a particular physical tree response (via growth dynamics) can be greatly refined when combined with the analysis of chemical tree response (via stable isotopes) (McCarroll & Loader 2004). Hence, the analysis of stable isotopes improves the climate signal provided by tree ring width and wood density alone, by reducing noise in the weight of controlling factors, tree-level sensitivity and physiological responses.

Oxygen and carbon are two major constituents in tree wood material, which exist in different stable isotopic forms in the natural world. The slight mass differences impart bias in the physical and chemical processes that drive elemental uptake, internal fractionations and eventual storage into tree growth rings. Consequently, the isotopic records in tree rings reveal dynamic signatures of the environmental conditions during growth as a function of multifaceted, non-linear tree-level processes (McCarroll & Loader 2004, Gessler 2014, Schleser 1999).

2.1 Oxygen Isotope Theory

The environmental oxygen stable isotope ($\delta^{18}O$) signal is imparted in tree rings through numerous exchange mechanisms on different parts of the tree (McCarroll & Loader 2004). Most importantly, the main driver is the exchange at the roots through precipitation and groundwater. The isotopic signature is not a simple representation of source water which is firstly determined by the air temperature during condensation in a rain cloud, as well as by the intensity of the rain-out process, i.e. the amount of precipitation, but rather, is subject to alteration depending on specific local soil conditions including soil moisture and relative humidity (Dawson 1993, Dawson 1996, Dansgaard 1987). In drier conditions, light oxygen (16O) is preferentially evaporated from the upper soil layers, developing a depth gradient within the soil, thus creating fractionation at the point of uptake. This is particularly true for younger trees with less developed root systems that rely on upper soil layer water. Following uptake, the water is transferred up the trunk to the leaves without any isotopic changes. At this point, further fractionation can occur at the leaf level by evapotranspiration (Saurer 1998ab, Barbour 2001). Under warm and dry conditions, transpiration rates are higher than under cool and wet conditions, because transpiration is controlled by vapour pressure deficit (vpd) between leaf and atmosphere (Scheidegger 2000). Water loss through transpiration can be reduced through stomatal closure and lowering of conductance between the atmosphere and leaf as an adaptive response to moisture loss (Roden 2000). However, stomatal conductance can only modify transpiration rates, as the main driver of transpiration is vpd. During transpiration, light H_2O molecules ($H_2{}^{16}O$) are preferentially released from leaf water into air, leading to higher $\delta^{18}O$ values of water at the leaf level, a process called leaf water enrichment (Saurer 1998ab). Due to oxygen isotope exchange between leaf water and leaf internal CO_2, as well as due to water splitting and subsequent biochemical processes in the chloroplasts, leaf water oxygen is finally incorporated into assimilates (sugars) that are ultimately moved down the trunk, where some oxygen isotope exchange with trunk water may occur before it is eventually laid down as woody material (lignin and cellulose) (Sternberg 1986, Hill 1995, Barbour 2001, McCarroll & Loader 2004).

On the whole, at the tree level, oxygen stable isotopes may be used as a predictor of air temperature (due to fractionation processes in the clouds) and, more strongly, drought conditions due to preferential enrichment of heavy oxygen during uptake and leaf level processes (transpiration). The oxygen isotope signal nevertheless contains larger scale signatures of low frequency global change if high frequency plant level processes are considered.

2.2 Carbon Isotope Theory

Stable isotopes of carbon ($\delta^{13}C$) are incorporated into a tree at the leaf level in the form of CO_2 (McCarroll & Loader 2004). This uptake is significantly influenced by the differential partial pressure of CO_2 between the external environment and internal leaf space (Farquhar 1982). As with any isotopic exchange across surfaces, isotopes move from a region of higher density to lower density, as represented by differential CO_2 partial pressure of the leaf interior and the atmosphere (c_i/c_a) (McCarroll & Loader 2004, Farquhar 1982). The photosynthetic uptake of CO2 or carboxylation is performed by a special enzyme (RubisCO), that preferentially fixes CO_2 with the lighter carbon isotope (^{12}C). However, this so-called discrimination of heavier ^{13}C is dependent on the availability of CO_2 in the leaf (Park 1960, Melander 1980). In principle, drier conditions lead to wood or cellulose with relatively more ^{13}C, i.e. less negative $\delta^{13}C$ values. Under cool and wet conditions, with stomata wide open, the CO2 fixing enzyme can strongly discriminate against ^{13}C, so that wood/cellulose has lower (more negative) $\delta^{13}C$-values. However, increasing air temperatures under ample moisture supply may also lead to increased $\delta^{13}C$-values, when higher assimilation rates lower the ci/ca ratio and reduce ^{13}C discrimination of RubisCO. So, ^{13}C of plant organic matter is always governed by both stomatal conductance (driven by moisture conditions) and photosynthetic rate (driven by temperature). It is important to note that carboxylation is part of photosynthesis, a complex process that is influenced by other factors like solar irradiance etc. As a consequence, these other factors may enhance or hinder photosynthesis efficiency, modifying the ^{13}C-discrimination at leaf level.

The predictability of these $\delta^{13}C$ shifts and resultant tree ring signatures are not straightforward due to the conflicting and additive leaf-level processes (McCarroll & Loader 2004). This is further complicated by $\delta^{13}C$ discrimination at the stand level, where near soil (atmospheric) levels are relatively depleted of $\delta^{13}C$ due to collection of respired CO_2 (Dawson 1996, 1993). Shorter, younger trees that are subject to this preferential uptake of ^{13}C-depleted soil respired CO_2 and might show juvenile trends (Schleser 1985). All in all, processes that influence CO_2 uptake, controlling factors of photosynthesis efficiency and stand dynamics should be considered.

2.3 Dual Isotope Theory

The relationship between hydrological conditions and stable isotope signatures in tree rings is complex and most likely non-linear (Figure 2.1). Individually, enhanced $\delta^{13}C$ could represent drought conditions due to stomata conductance reduction, or non-hydrological conditions of enhanced photosynthetic efficiency (Scheidegger 2000). In an effort to interpret the main driver, oxygen isotopes can provide additional information, since theoretically, $\delta^{18}O$ is negatively correlated to relative humidity (DeNiro 1979, Sternberg 1989, Farquhar 1998, Scheidegger 2000). This is conversely true during times of high humidity. Since juvenile trees complicate this relationship, as previously discussed, the first 40 years of tree growth are normally left out for reconstructions from stable isotopes.

Tree ring width and cell density measurements are obligatory to gain an understanding of the overarching growth dynamics and may provide information on fires, frost, drought and other factors that have implications in the interpretation of stable isotopes (Fritts 1971, Hughes 2011, Speer 1971, Stokes 1968). For example, a period of drought (as interpreted by high $\delta^{18}O$ and $\delta^{13}C$) should be exemplified by low tree ring widths (Treydte 2001); a marked drop in $\delta^{13}C$ could be a result of forest fire, visible as a fire scar within tree rings (Beghin 2011, Schweingruber 2007), rather than degraded climate conditions. Moreover, while stable isotopes from any site provide better information on hydrological variability (McCarroll & Loader 2004, Hughes 2002, Hughes 2011), tree ring growth from high latitudes or high elevation sites is most reflective of temperature variability, and tree-ring growth from temperate sites show only weak climate signals due to many other interfering environmental factors (Speer 1971, Mikola 1962, Hughes 2011).

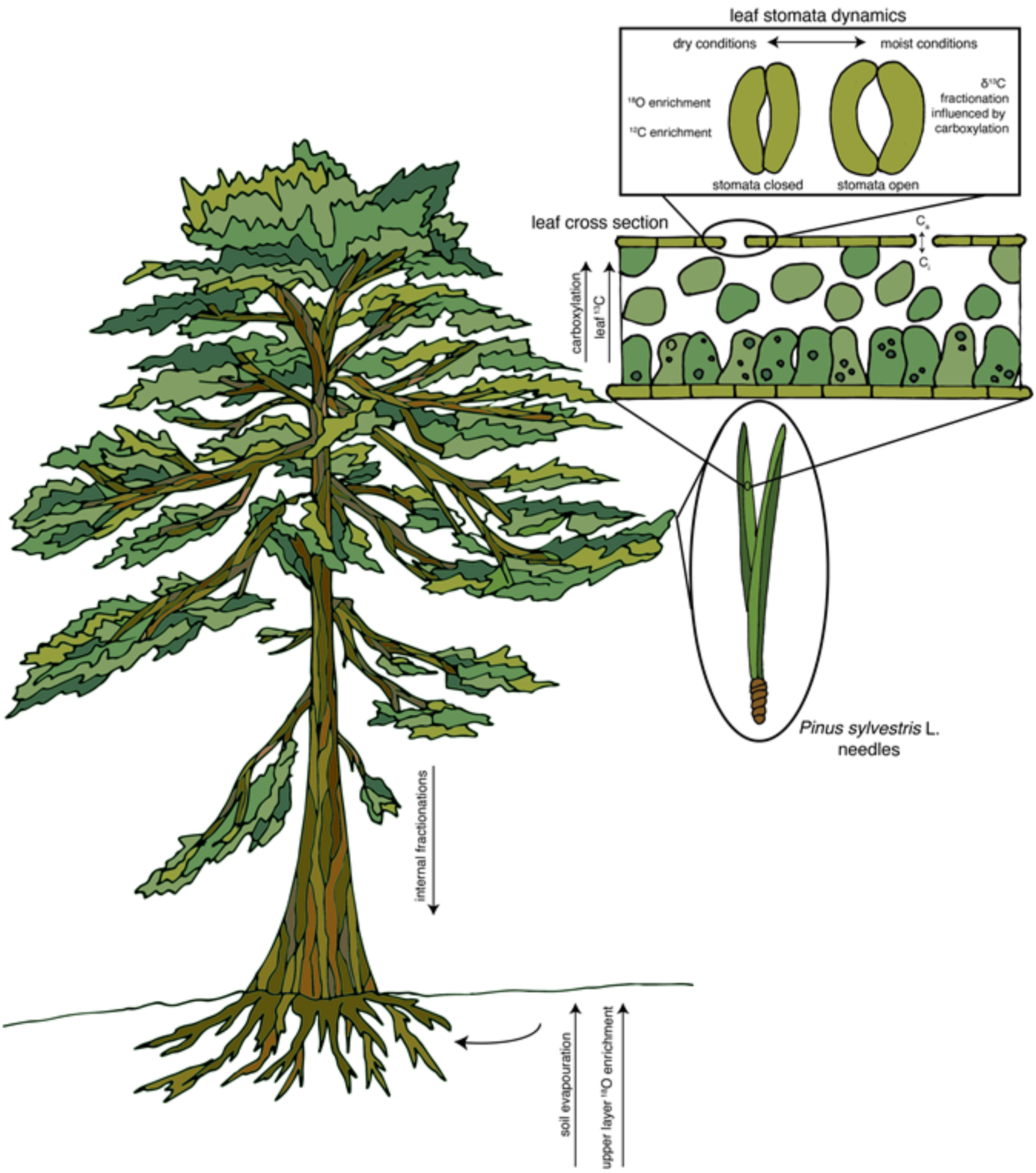

Figure 2.1: Summary of factors influencing $\delta^{18}O$ and $\delta^{13}C$ fractionation in Pinus sylvestris L. (illustrated by Maren Pauly with information from McCarroll & Loader 2004, Farquhar et al. 1982)

Establishing climate signals from stable isotopes in tree-ring cellulose firstly relies on calibration and verification of modern stable isotope time series with instrumental climate data by inferring and testing transfer functions derived from regression analyses. A large number of calibration studies have demonstrated a high sensitivity of stable isotope fractionation to external drivers, such as weather conditions making them a valuable tool to reconstruct climatic influences during tree growth (e.g.

Loader et al. 2004, Helle and Schleser 2004). However, relationships were frequently found to be unstable over time, as dominating climatic factors can change according to changes in environmental boundary conditions. Furthermore, internal drivers - such as species-specific physiology - can constrain climatic significance of tree-ring stable isotopes. Hence, a thorough interpretation of tree-ring stable isotope data has to be further based on the knowledge of the trees' response behaviour and model conceptions of stable isotope fractionation in the arboreal system (e.g. Schleser et al. 1999, e.g. Farquhar et al., 1982; Farquhar and Cernusak 2012: Roden et al. 2000; Kahmen et al. 2011; Treydte et al. 2014 and citations therein).

Knowledge of trees' response behaviour and related isotope fractionations to changing climatic quantities is derived not only from field observations, but also from numerous greenhouse experiments (e.g. Schleser et al. 1999) and the fractionation models developed from these studies have proven to be quite robust. They mainly address key isotope fractionations occurring as a result of CO_2 and H_2O integration during photosynthesis in the leaves but also consider modifications during post-photosynthetic physiological processes.

References (Chapter 2)

Barbour, Margaret M., T. John Andrews, and Graham D. Farquhar. "Correlations between oxygen isotope ratios of wood constituents of Quercus and Pinus samples from around the world." Functional Plant Biology 28.5 (2001): 335-348.

Beghin, Rachele, et al. "Tree-ring growth and stable isotopes (13 C and 15 N) detect effects of wildfires on tree physiological processes in Pinus sylvestris L." Trees 25.4 (2011): 627-636.

Dansgaard, W. "Ice core evidence of abrupt climatic changes." Abrupt climatic change. Springer, Dordrecht, 1987. 223-233.

Dawson, Todd E. "Water sources of plants as determined from xylem-water isotopic composition: perspectives on plant competition, distribution, and water relations." Stable isotopes and plant carbon-water relations. Academic Press, 1993. 465-496.

Dawson, Todd E., and John S. Pate. "Seasonal water uptake and movement in root systems of Australian phraeatophytic plants of dimorphic root morphology: a stable isotope investigation." Oecologia 107.1 (1996): 13-20.

DeNiro, Michael J., and Samuel Epstein. "Relationship between the oxygen isotope ratios of terrestrial plant cellulose, carbon dioxide, and water." Science 204.4388 (1979): 51-53.

Farquhar, Graham D., and Lucas A. Cernusak. "Ternary effects on the gas exchange of isotopologues of carbon dioxide." Plant, Cell & Environment 35.7 (2012): 1221-1231.

Farquhar, Graham D., Marion H. O'Leary, and Joe A. Berry. "On the relationship between carbon isotope discrimination and the intercellular carbon dioxide concentration in leaves." Functional Plant Biology 9.2 (1982): 121-137.

Farquhar, G. D. "Interpretation of oxygen isotope composition of leaf material." Stable isotopes (1998): 27-62.

Fritts, Harold C. "Dendroclimatology and dendroecology." Quaternary Research 1.4 (1971): 419-449.

Gessler, Arthur, et al. "Stable isotopes in tree rings: towards a mechanistic understanding of isotope fractionation and mixing processes from the leaves to the wood." Tree physiology 34.8 (2014): 796-818.

Helle, Gerhard, and G. H. Schleser. "Beyond CO2-fixation by Rubisco–an interpretation of 13C/12C variations in tree rings from novel intra-seasonal studies on broad-leaf trees." Plant, Cell & Environment 27.3 (2004): 367-380.

Hill, S. A., et al. "Rapid recycling of triose phosphates in oak stem tissue." Plant, Cell & Environment 18.8 (1995): 931-936.

Hughes, Malcolm K. "Dendroclimatology in high-resolution paleoclimatology." Dendroclimatology. Springer, Dordrecht, 2011. 17-34.

Hughes, Malcolm K. "Dendrochronology in climatology–the state of the art." Dendrochronologia 20.1-2 (2002): 95-116.

Kahmen, Ansgar, et al. "Cellulose δ18O is an index of leaf-to-air vapor pressure difference (VPD) in tropical plants." Proceedings of the National Academy of Sciences 108.5 (2011): 1981-1986.

Loader, N. J., and D. L. Hemming. "The stable isotope analysis of pollen as an indicator of terrestrial palaeoenvironmental change: a review of progress and recent developments." Quaternary Science Reviews 23.7-8 (2004): 893-900.

McCarroll, Danny, and Neil J. Loader. "Stable isotopes in tree rings." Quaternary Science Reviews 23.7-8 (2004): 771-801.

Melander, Lars CS, and William Hundley Saunders. Reaction rates of isotopic molecules. John Wiley & Sons, 1980.

Mikola, Peitsa. "Temperature and tree growth near the northern timberline." Tree growth (1962): 265-274.

Park, R., and Samuel Epstein. "Carbon isotope fractionation during photosynthesis." Geochim. et cosmochim. acta 21 (1960).

Roden, John S., Guanghui Lin, and James R. Ehleringer. "A mechanistic model for interpretation of hydrogen and oxygen isotope ratios in tree-ring cellulose." Geochimica et Cosmochimica Acta 64.1 (2000): 21-35.

Saurer, Matthias, et al. "Oxygen isotope analysis of cellulose: an interlaboratory comparison." Analytical Chemistry 70.10 (1998): 2074-2080.

Saurer, Matthias, et al. "Environmental information from stable isotopes in tree rings of Fagus sylvatica." The Impacts of Climate Variability on Forests. Springer, Berlin, Heidelberg, 1998. 241-253.

Scheidegger, Y., et al. "Linking stable oxygen and carbon isotopes with stomatal conductance and photosynthetic capacity: a conceptual model." Oecologia 125.3 (2000): 350-357.

Schleser, Gerhard H., et al. "Isotope signals as climate proxies: the role of transfer functions in the study of terrestrial archives." Quaternary Science Reviews 18.7 (1999): 927-943.

Schweingruber, Fritz Hans. "Modification of the tree-ring structure due to extreme site conditions." Wood structure and environment (2007): 85-126.

Sternberg, Leonel Da SL, Michael J. Deniro, and Rod A. Savidge. "Oxygen isotope exchange between metabolites and water during biochemical reactions leading to cellulose synthesis." Plant Physiology 82.2 (1986): 423-427.

Sternberg, L. da Silveira Lobo. "Oxygen and hydrogen isotope ratios in plant cellulose: mechanisms and applications." Stable isotopes in ecological research. Springer, New York, NY, 1989. 124-141.

Stokes, M. A., and T. L. Smiley. "Introduction to tree-ring dating. University of Chicago." (1968).

Treydte, Kerstin, et al. "The climatic significance of δ13C in subalpine spruces (Lötschental, Swiss Alps) a case study with respect to altitude, exposure and soil moisture." Tellus B 53.5 (2001): 593-611.

Treydte, Kerstin, et al. "Seasonal transfer of oxygen isotopes from precipitation and soil to the tree ring: source water versus needle water enrichment." New Phytologist 202.3 (2014): 772-783.

Chapter 3
The Late Glacial

3. The Late Glacial

3.1 Events from the archives

The Late Glacial has been defined by the onset of a widespread deglaciation in the Northern Hemisphere, following the Last Glacial Maximum (25,000 - 13,000 cal BP). This period was inundated by climate oscillations and cooling events (particularly in the North Atlantic region), culminating in a global warming into the current Holocene epoch. While temperatures began to warm significantly during this period, the deglaciation was interrupted by a series of cool periods in the Northern Hemisphere, including:

1. Aegelsee (Lotter et al. 1992) / the Oldest Dryas (Merkt and Muller 1999) / GI-1d (Rasmussen et al. 2006),
2. Older Dryas (Hughen et al. 1996; Merkt and Muller 1999, Brauer et al. 2000) / GI-1c (Rasmussen et al. 2014)
3. Gerzensee Oscillation (Raden et al. 2012) / Inter-Allerod cool period (Thornalley et al. 2010; Heghen et al. 1996) / GI-1b (Bjork et al. 1993), and
4. The Younger Dryas (Dansgaard 1987; Rach et al. 2014) / GS-1 (Steffensen et al. 2008; Mayle et al. 1999; Rasmussen et al. 2006).

The Aegelsee Oscillation (GI-1d) was a century long period of cooling (Lake Mondsee, NGRIP) or enhanced variability (Lake Ammersee), correlated to reduced tree growth (Friedrich 2001) and local replacement by herbaceous vegetation (Lotter 1992) around 14 000 cal BP. The Older Dryas (GI-1c) was a cool period lasting nearly two centuries in Greenland (Rasmussen et al. 2006), also exemplified as a drop in lacustrine $\delta^{18}O$ (Lauterbach et al. 2011, von Grafenstein et al. 1999). The Gerzensee Oscillation (GI-1b) was a climate dip of similar magnitude, but longer duration, directly preceding the transition to the Younger Dryas. During this oscillation, a large-scale volcanic eruption (Laacher See Eruption) occurred (Schmincke 1999); the exact timing differs between archives, with varve counts estimating 12

880 cal BP (Brauer, 1999) and tree ring data approximating 13 020 cal BP. The most significant climate alteration during the last deglaciation, the Younger Dryas, was a millennial-long rapid cold reversal, characterized by a 4-6°C drop of European temperatures in less than a century (Rasmussen, 2006).

Evidence of such events in the northern hemisphere have been discovered in both Greenland ice core records of air temperature variability ($\delta^{18}O$; Dansgaard, 1987) and lacustrine deposits (varves) of hydrological and biological lake dynamics (U. E. A Lotter, U Siegenthaler, H Birks, 1992), including $\delta^{18}O$ from ostracodes reflecting water temperature variability (cf. Lauterbach et al. 2011). Ice cores record climate on a global and hemispheric scale (Dansgaard 1982), whereas lacustrine deposits provide information focusing on local to regional change.

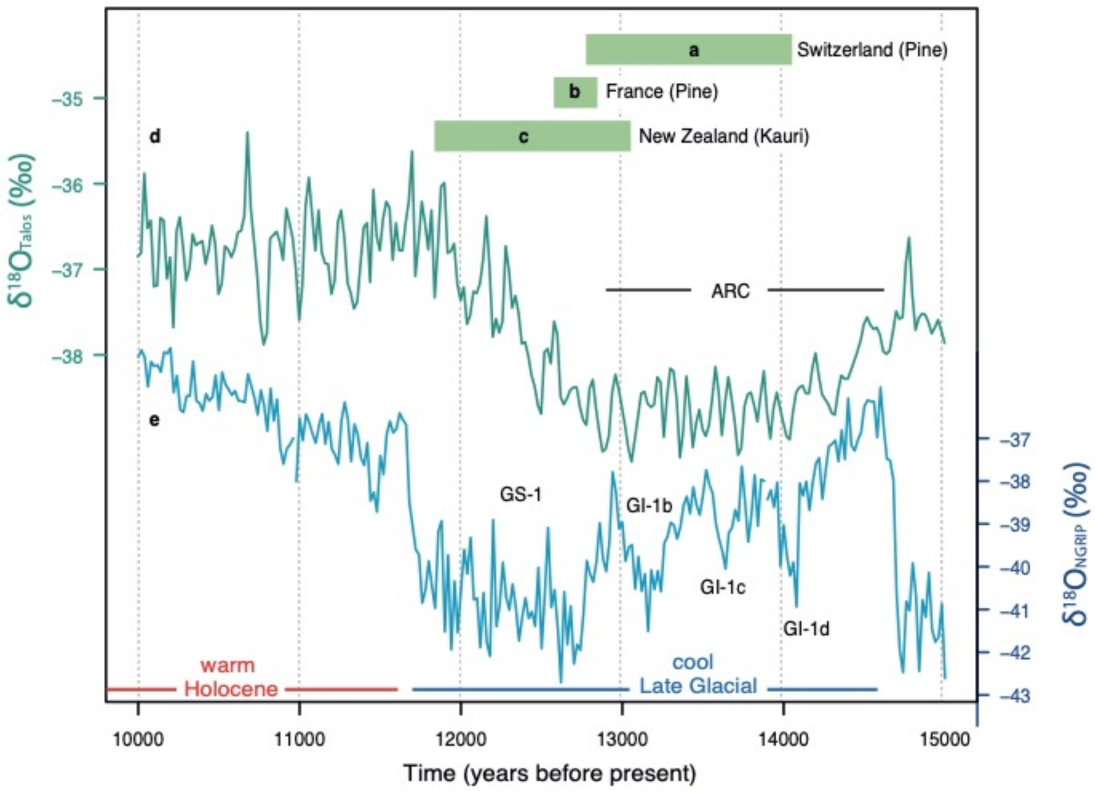

Figure 3.1: An overview of the Late Glacial climate period, exemplified by ice core $\delta^{18}O$ from Antarctica (Talos Dome, Pedro et al. 2011) and Greenland (NGRIP, Rasmussen et al. 2013), both of which are positively correlated to local temperature. Significant Late Glacial climate oscillations in the Northern Hemisphere (GS-1, GI-1b and GI-1c) and Southern Hemisphere (ARC: Antarctic Cold Reversal) are indicated. The tree-ring stable isotope series developed for this thesis are plotted as follows: (a) Switzerland, CH-ISO (Chapter 6), (b) France, Barbiers (Chapter 7) and (c) Kauri, KAU-ISO (Chapter 8).

Due to the particularly high attention to this climate epoch, the different climate oscillations are introduced using a range of terminology within the literature (e.g. Table 1). To circumvent this, Greenland Ice core data has been utilised as the primary age model for Late Glacial climate 'events', developed as the INTIMATE event stratigraphy (Rasmussen et al. 2014) through the synchronisation of volcanic events in three ice core records (NGRIP, GRIP, GISP2).

Greenland (NGRIP)		Austria (Mondsee)		Other equivalent(s)
Terminology	Dates (a b2k)	Terminology	Dates (cal BP)	
GI-1d	14 075 – 13 954 (121 years)	Mo-LG1	13 985 – 13 845 (140 years)	Aegelsee Oscillation[1], Oldest Dryas[2], MK-4[3]
GI-1c$_{1-2}$	13 660 – 13 311 (349 years)	Mo-LG2	13 625 – 13 470 (155 years)	Ammersee[4]
GI-1b	13 311 – 13 099 (212 years)	Mo-LG3	13 125 – 12 835 (290 years)	Inter-Allerød Cold Period[5], Gerzensee Oscillation[6]
onset GS-1	12 896	onset Younger Dryas	12 760	Younger Dryas[7]

Table 3.1: Timing of selected Late Glacial climate events in the Northern Hemisphere from Greenland (NGRIP, Rasmussen et al., 2014) and Austria (Mondsee, Lauterbach et al., 2011). Comparable event terminology from: (1) Lake Gerzensee, Switzerland (Lotter et al., 1992), (2) general pollen zone (Björck et al., 1998), (3) Lake Meerfelder Maar, Germany (Brauer et al., 2000), (4) Lake Ammersee, Germany (von Grafenstein et al., 1999), (5) North Atlantic (Lehman and Keigwin,1992) , (6) Lake Gerzensee, Switzerland (Eicher & Siegenthaler 1976, Lotter et al., 1992) and (7) general pollen zone (Björck et al., 1998)

The Southern Hemisphere did not record the same climate 'events' as the Northern Hemisphere. Instead, Antarctic ice cores demonstrate a gradual warming continuing from the Last Glacial Maximum until the warm Holocene. Embedded in this period is a brief warming pause during the Antarctic Cold Reversal (ACR, 14 700 – 13 000 cal BP; Blunier et al. 1997, Pedro et al. 2011). Hemispheric differences have been recorded during Glacial-Interglacial cycles across the Quaternary period (Crowley 1992, Shackleton et al. 2000). For example. SH warming has led the NH during glacial terminations; due in part to slower melting of NH ice sheets, greatly impacting hemispheric temperatures (Kawamura et al. 2007). Further information on the hemispheric differences can be found in Paper 3 (1.1 - 1.2).

While these climate oscillations are not globally synchronous in nature, signatures of environmental change have frequently been found in different climate proxy records. Yet, it is challenging to compare such events between records that differ in temporal resolution, proxy sensitivity and most importantly, accuracy of dating.

Coarse temporal resolution records (e.g. ocean sediments) may have the potential to record pronounced climate signals spanning thousands of years; yet the intricacies of rapid environmental change, such as extremes, are often concealed within the limited temporal sampling. Thus, investigating the detailed behaviour of climate oscillations on annual, decadal or even centennial time scale requires high-resolution climate proxy records. Only a few high resolution paleoclimate records were available for the LG prior to this thesis - tree-ring widths (Friedrich et al. 2004, extending to 12 325 cal BP), Meerfelder Maar varves (Brauer et al. 2000) and Greenland ice core $\delta^{18}O$ (Steffensen et al. 2008); with the latter two covering the majority of the LG. Whilst Meerfelder Maar represents a very precise, high-resolution record through annual varve counting and tephrochronology, the environmental proxy data (δD) is available at decadal resolution (Rach et al. 2014). On the other hand, North Greenland $\delta^{18}O$ at sub-annual resolution, providing a proxy for local air temperature, also influenced by precipitation seasonality (Steffensen et al. 2008). Such records provide further information about the dynamics of climate change across rapid transitions, often overprinted in lower temporal resolution records.

Multiple environment signatures may be inherent in a single climate record. Therefore, it is vital to decode and eliminate background 'noise' to reveal the dominant environmental variable (or set of interacting variables) being recorded in the region by the particular archive used. This is often done through modern calibration and verification, or by comparing multiple proxies from a single archive.

3.2 Oxygen Isotopes in the Late Glacial

Oxygen isotopes ($\delta^{18}O$) have the potential to record climate variability via the transfer of water through atmosphere, ocean and terrestrial sources -- tracking temperature, atmospheric circulation and precipitation along its way, eventually imprinting signals into natural archives (Table 2).

Archive Type	Proxy	Season	Temporal Resolution	Examples
Ice Cores	Temperature, influenced by precipitation seasonality	Winter	Annual (potential); generally decadal	Steffensen et al. 2008
Lake Carbonates	Temperature	Annual	Annual if laminated; generally decadal	Lauterbach et al. 2011
Speleothems	Temperature, influenced by moisture source, circulation, drip water residence time	Annual	Decadal	Genty et al. 2009

Table 3.2: An overview of different oxygen isotope ($\delta^{18}O$) climate proxy records

Greenland ice core $\delta^{18}O$ data represents one of the foundational proxy records wherein all other paleoclimate records are equated (Steffensen et al. 2008; Rasmussen et al. 2014; Alley et al. 1993). Despite their dating uncertainty, lower latitude and resolution $\delta^{18}O$ records have been event-matched - as both a dating mechanism (Raden et al. 2012) and as a technique to interpret local representation of known Northern Hemisphere climate oscillations (v. Grafenstein et al. 2012; Lauterback et al. 2011). Unfortunately, this often precludes the interpretation of local event timing, rate and magnitude, as $\delta^{18}O$ signatures are highly regional and transient in nature; thus, this event-matching technique has recently been discontinued. Given a suitable, equally resolved and independently dated $\delta^{18}O$ climate record at a lower latitude, the southward propagation of North Atlantic hydroclimatic change could be resolved.

Trees offer an advantageous opportunity to track annual resolution climate using stable isotopes within their cellulose structure, owing to their seasonal growth banding and absolute dating potential (Reimer et al. 2015; Hogg et al. 2016; Reinig et al. 2018; Speer et al. 1971). Despite their advantages, they have been relatively unused in the development of Late Glacial climate reconstructions as subfossil trees are extremely rare.

References (Chapter 3)

Alley, Richard B., et al. "Abrupt increase in Greenland snow accumulation at the end of the Younger Dryas event." Nature 362.6420 (1993): 527-529.

Blunier, Thomas, et al. "Timing of the Antarctic Cold Reversal and the atmospheric CO2 increase with respect to the Younger Dryas event." Geophysical Research Letters 24.21 (1997): 2683-2686.

Brauer, Achim, et al. "AMS radiocarbon and varve chronology from the annually laminated sediment record of Lake Meerfelder Maar, Germany." Radiocarbon 42.3 (2000): 355-368.

Brauer, Achim, Christoph Endres, and Jörg FW Negendank. "Lateglacial calendar year chronology based on annually laminated sediments from Lake Meerfelder Maar, Germany." Quaternary International 61.1 (1999): 17-25.

Crowley, Thomas J. "North Atlantic deep water cools the Southern Hemisphere." Paleoceanography 7.4 (1992): 489-497.

Dansgaard, W. "Ice core evidence of abrupt climatic changes." Abrupt climatic change. Springer, Dordrecht, 1987. 223-233.

Dansgaard, Willi, et al. "A new Greenland deep ice core." Science 218.4579 (1982): 1273-1277.

Eicher, Ulrich, and Ulrich Siegenthaler. "Palynological and oxygen isotope investigations on Late-Glacial sediment cores from Swiss lakes." Boreas 5.2 (1976): 109-117.

Friedrich, Michael, et al. "The 12,460-year Hohenheim oak and pine tree-ring chronology from central Europe—a unique annual record for radiocarbon calibration and paleoenvironment reconstructions." Radiocarbon 46.3 (2004): 1111-1122.

Hogg, Alan, et al. "Decadally resolved lateglacial radiocarbon evidence from New Zealand kauri." Radiocarbon 58.4 (2016).

Hughen, Konrad A., et al. "Rapid climate changes in the tropical Atlantic region during the last deglaciation." Nature 380.6569 (1996): 51-54.
Kawamura, Kenji, et al. "Northern Hemisphere forcing of climatic cycles in Antarctica over the past 360,000 years." Nature 448.7156 (2007): 912-916.

Lauterbach, Stefan, et al. "Environmental responses to Lateglacial climatic fluctuations recorded in the sediments of pre-Alpine Lake Mondsee (northeastern Alps)." Journal of Quaternary Science 26.3 (2011): 253-267.

Lehman, Scott J., and Lloyd D. Keigwin. "Sudden changes in North Atlantic circulation during the last deglaciation." Nature 356.6372 (1992): 757-762.

Eawag, AF Lotter, et al. "Late-glacial climatic oscillations as recorded in Swiss lake sediments." Journal of Quaternary Science 7.3 (1992): 187-204.

Mayle, F. E., et al. "Climate variations in Britain during the Last Glacial–Holocene transition (15.0–11.5 cal ka BP): comparison with the GRIP ice-core record." Journal of the Geological Society 156.2 (1999): 411-423.

Merkt, Josef, and Helmut Müller. "Varve chronology and palynology of the Lateglacial in Northwest Germany from lacustrine sediments of Hämelsee in Lower Saxony." Quaternary International 61.1 (1999): 41-59.

Pedro, J. B., et al. "High-resolution records of the beryllium-10 solar activity proxy in ice from Law Dome, East Antarctica: measurement, reproducibility and principal trends." Past 7 (2011): 707-721.

Rach, Oliver, et al. "Delayed hydrological response to Greenland cooling at the onset of the Younger Dryas in western Europe." Nature Geoscience 7.2 (2014): 109-112.

Rasmussen, Sune Olander, et al. "A new Greenland ice core chronology for the last glacial termination." Journal of Geophysical Research: Atmospheres 111.D6 (2006).

Rasmussen, Sune O., et al. "A stratigraphic framework for abrupt climatic changes during the Last Glacial period based on three synchronized Greenland ice-core records: refining and extending the INTIMATE event stratigraphy." Quaternary Science Reviews 106 (2014): 14-28.

Reimer, Paula et al. "Laboratory Protocols used for AMS Radiocarbon Dating at the 14C Centre" (2015) Scientific Dating Report (no.5)

Reinig, Frederick, et al. "New tree-ring evidence for the Late Glacial period from the northern pre-Alps in eastern Switzerland." Quaternary Science Reviews 186 (2018): 215-224.

Schmincke, Hans-Ulrich, Cornelia Park, and Eduard Harms. "Evolution and environmental impacts of the eruption of Laacher See Volcano (Germany) 12,900 a BP." Quaternary International 61.1 (1999): 61-72.

Shackleton, Nicholas J. "The 100,000-year ice-age cycle identified and found to lag temperature, carbon dioxide, and orbital eccentricity." Science 289.5486 (2000): 1897-1902.

Steffensen, Jørgen Peder, et al. "High-resolution Greenland ice core data show abrupt climate change happens in few years." Science 321.5889 (2008): 680-684.

Thornalley, David JR, Harry Elderfield, and I. Nick McCave. "Intermediate and deep water paleoceanography of the northern North Atlantic over the past 21,000 years." Paleoceanography 25.1 (2010).

von Grafenstein, Ulrich, et al. "A mid-European decadal isotope-climate record from 15,500 to 5000 years BP." Science 284.5420 (1999): 1654-1657.

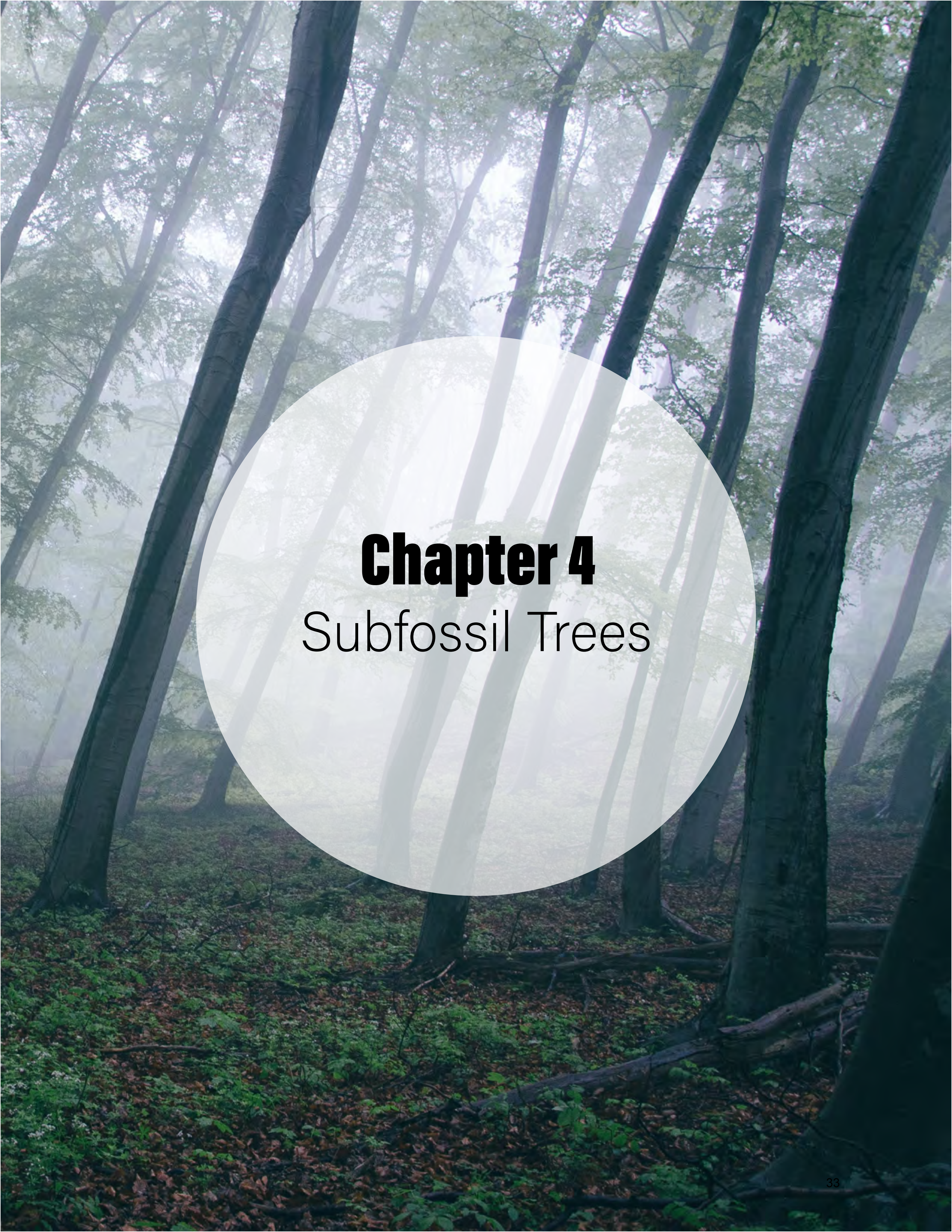

Chapter 4
Subfossil Trees

4. Subfossil forests

4.1 Chronologies in the Holocene and Late Glacial

Annually resolved, absolutely dated (extending to present) tree-ring chronologies exist around the world, generally extending (at best) into the early Holocene (e.g. northern Germany (0-8000 cal BP, Leuschner et al. 2002; Ireland 0-6963 cal BP, Baillie et al. 2009). The longest chronology of this variety consists of southern German and Swiss wood material from the Preboreal Pine Chronology (Friedrich et al. 2004) and the Holocene Oak Chronology (Becker et al. 2003), which is being continuously improved (Hogg et al. 2016; Kaiser et al. 2012; Saurer et al. 2008a), currently extending from present to 12 335 cal BP.

Beyond absolutely dated chronologies, 'floating' tree ring chronologies also exist, which are groups of trees that have been placed in time through radiocarbon dating and thus do not extend to the present. Such chronologies are present in the Late Glacial, including series from Germany (Friedrich et al. 1999, 2000, 2004), southern France (Miramont et al. 2000ab, 2011; Capano et al. 2018), North America (Griggs and Grote, 2016; Leavitt et al., 2006; Panyushkina and Leavitt, 2013, 2007), New Zealand (Hogg et al. 2013, 2016) and Tasmania (Hua et al. 2009; Barbetti et al. 2004). The research in this thesis makes use of three different floating chronologies:

1. The Swiss Late Glacial Master chronology (SWILM) developed by Kaiser et al. (1993, 2012) and Saurer et al. (20008ab) in conjunction with the new Binz forest discovery (Reinig et al. 2018) with pine trees located across the Swiss Plateau, surrounding the city of Zurich (Chapter 4.2.1);
2. The Barbiers chronology developed by Miramont et al. (2000ab, 2011) and Capano et al. (2018) with pine trees discovered in the southern French alps (Chapter 4.2.2);
3. The New Zealand Towai chronology developed by Hogg et al. (2013, 2016) and Palmer et al. (2017) with Kauri trees from peat bogs in North Island (Chapter 4.2.3).

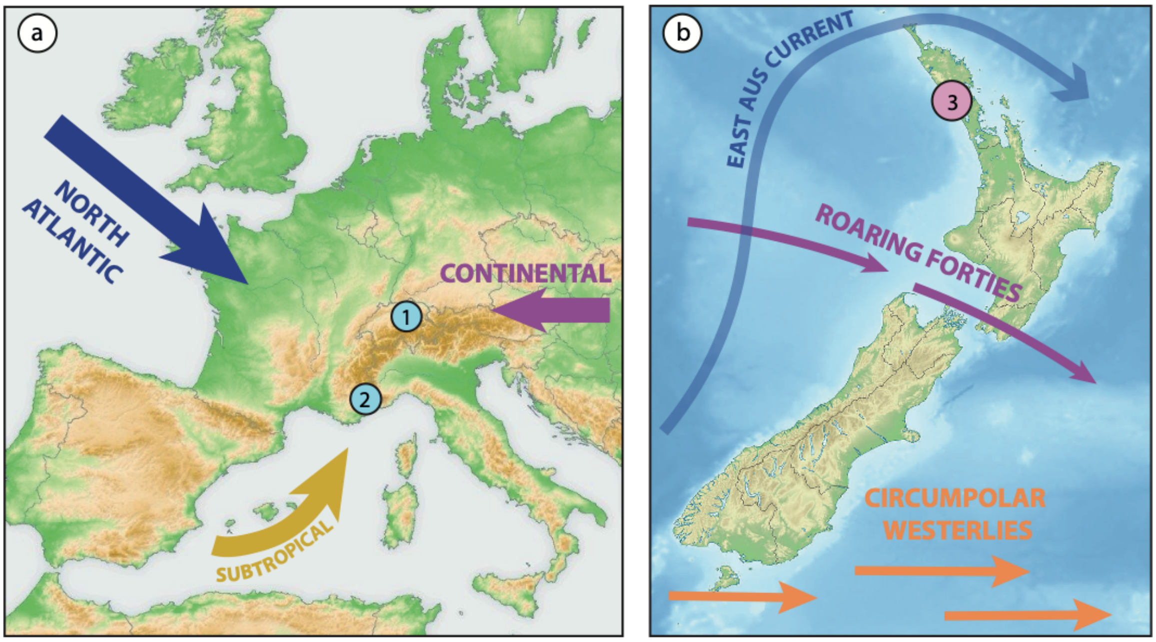

Figure 4.1: Map of tree-ring sites in (a) Europe and (b) New Zealand. The SWILM chronology (1) located in and around Zurich (Switzerland), the Barbiers chronology (2) from the southern French alps, and the New Zealand Towai chronology (3) from North Island.

4.2 Sample sites

4.2.1 The Swiss Plateau

The tree sites (Landikon, Gaenziloo, Binz, Daettnau) are situated at the foothills of the Uetliberg, near Zürich, with a climate characterised by altering humid-oceanic and continental-temperate regimes. Presently, this site has humid continental climate conditions, characterized by strong seasonal variability. During the Late Glacial transition, this variability was more severe inter- and intra- annually (Schaub 2007).

Air masses predominately arrive from the west via the NA (subarctic: low $\delta^{18}O$, high humidity, high standard deviation), following rainout along the slopes of the Jura Mountains. Competing, yet less prominent dry eastern winds (continental: low $\delta^{18}O$, low humidity, low standard deviation) arrive from continental Europe (Kozel and Schotterer 2003; Siegenthaler and Oeschger 1980) as well as humid, warm air masses from the Mediterranean (subtropical: high $\delta^{18}O$, high humidity, low standard deviation) (Wanner et al., 1997). Water isotope signatures in local precipitation are strongly driven by, and thus a signal of, more widespread regional climate variability rather than locally driven fractionation (Kozel and Schotterer 2003).

Acute geomorphological activity from transitioning glaciers carved the land, leaving complex channels and glacial valleys where vegetation propagated (Schaub 2005, 2007, 2008). The instability in climate, and thus hydrological conditions, favoured the preservation of the SWILM samples *in-situ* under an accumulation of saturated sediments.

Figure 4.2: Subfossil pine trees discovered in-situ at a building site near Zurich

4.2.2 The Southern French Alps

In France's Middle Durance region, in the Southern Alps, deposits of Holocene and Late Glacial subfossil trees have been discovered in alluvial sediments along the edges of riverbeds (Miramont et al. 2011). During the Holocene and Late Glacial, sedimentation (and detrital discharge) was high in the region, providing the ideal conditions for the preservation of subfossil forests within flood deposits (Miramont 2004, 2008, 2011). Surrounding sediments are composed of calcareous marl, which readily erode during intense rainfall events (occurring frequently in the region), resulting in the present-day exposure of the subfossil trees *in-situ* (Miramont et al. 2011).

Figure 4.3: Subfossil pine trees discovered at Barbier River (Miramont et al. 2011)

The Middle Durance region is within the temperate zone, mainly influenced by Mediterranean climate - with hot, dry summers and intense storms (and related precipitation) occurring during the autumn and winter. This area is subject to incoming humid, warm winds from the Mediterranean (Le Vent d'Autan; high $\delta^{18}O$, high humidity, low standard deviation) as well as dry air masses, mainly from the North Atlantic (Le Mistral; low $\delta^{18}O$, high humidity, high standard deviation).

4.2.3 North Island New Zealand

A complex mix of maritime air masses modulated by ENSO conditions influences the climate conditions in New Zealand. In the subtropical North Island, where kauri naturally grow presently, conditions are moderately warm and humid (Ecroyd 1982), with rare extreme flooding and frost events in the winter and tropical originating storms in the summer to autumn (NIWA, 2020).

North island is home to an abundance of subfossil kauri trees, found well preserved within lowland peat swamp deposits, extending from the Pleistocene to present. The sites where ancient kauri trees have been discovered are of relic lacustrine, river and coastal origin, where wetland/bog environments meet water bodies. Such sites often contain multiple cohorts of trees, covering thousands of years of growth (Lorrey and Boswijk 2017). In dry years, the stumps are presently exposed from within the sediment as hydrostatic pressure of the soil is eased, pushing the trees to the surface (Lorrey and Boswijk 2017). Those preserved from the Late Glacial generally have thinner tree-ring widths, indicating less optimal growth conditions compared to the current inter-glacial (Odgen et al. 1992). Despite the abundance of Holocene to Late Glacial kauri trees that have been discovered, only one site (Towai farm, North Island) contains trees that grew between 13,000 to 26,000 years before present.

Figure 4.4: Kauri trees exposed from within a bog deposit in New Zealand (photographed by Arno Gasteiger)

References (Chapter 4)

Baillie, Mike GL. "The radiocarbon calibration from an Irish oak perspective." Radiocarbon 51.1 (2009): 361-371.

Barbetti, M., et al. "Radiocarbon variations from the Southern Hemisphere, 10,350–9700 cal BP." Nuclear Instruments and Methods in Physics Research Section B: Beam Interactions with Materials and Atoms 223 (2004): 366-370.

Becker, Bernd. "An 11,000-year German oak and pine dendrochronology for radiocarbon calibration." Radiocarbon 35.1 (1993): 201-213.

Capano, Manuela, et al. "Wood 14 C Dating with AixMICADAS: Methods and Application to Tree-Ring Sequences from the Younger Dryas Event in the Southern French Alps." Radiocarbon 60.1 (2018): 51-74.

Ecroyd, C. E. "Biological flora of New Zealand 8. Agathis australis (D. Don) Lindl.(Araucariaceae) Kauri." New Zealand journal of botany 20.1 (1982): 17-36.

Friedrich, Michael, et al. "The 12,460-year Hohenheim oak and pine tree-ring chronology from central Europe—a unique annual record for radiocarbon calibration and paleoenvironment reconstructions." Radiocarbon 46.3 (2004): 1111-1122.

Friedrich, Michael, et al. "Paleo-environment and radiocarbon calibration as derived from Lateglacial/Early Holocene tree-ring chronologies." Quaternary International 61.1 (1999): 27-39.

Friedrich, Michael, et al. "High-resolution climate signals in the Bølling–Allerød Interstadial (Greenland Interstadial 1) as reflected in European tree-ring chronologies compared to marine varves and ice-core records." Quaternary Science Reviews 20.11 (2001): 1223-1232.

Griggs, Carol, and Todd Grote. "The Younger Dryas to Early Holocene tree-ring radiocarbon, paleoecological and paleohydrological record for the Bell Creek Site, Lake Ontario Lowlands, New York State, USA."

Hogg, Alan, et al. "Decadally resolved lateglacial radiocarbon evidence from New Zealand kauri." Radiocarbon 58.4 (2016).

Hogg, Alan G., et al. "SHCal13 Southern Hemisphere calibration, 0–50,000 years cal BP." Radiocarbon 55.4 (2013): 1889-1903.

Hua, Quan. "Radiocarbon: a chronological tool for the recent past." Quaternary Geochronology 4.5 (2009): 378-390.

Kaiser, Klaus Felix, et al. "Challenging process to make the Lateglacial tree-ring chronologies from Europe absolute–an inventory." Quaternary Science Reviews 36 (2012): 78-90.

Kaiser, K. F. "Beitr age zur Klimageschichte vom Hochglazial bis ins fr uhe Holoz an, rekonstruiert mit Jahrringen und Molluskenschalen aus verschiedenen Vereisungsgebieten." Eidgen. ossische Forschungsanstalt f. ur Wald, Schnee und Landschaft. Birmensdorf, Ziegler Druck-und Verlags-AG, Winterthur (1993): 203.

R. Kozel, Schuerch, M., and U. Schotterer. The Swiss National Network for the Observation of Isotopes in the Water Cycle (NISOT)-10-year experience of operation. No. IAEA-CN--104. 2003.

Leavitt, Steven W., et al. "Climate in the Great Lakes region between 14,000 and 4000 years ago from isotopic composition of conifer wood." Radiocarbon 48.2 (2006): 205-217.

Leuschner, Hanns Hubert, et al. "Subfossil European bog oaks: population dynamics and long-term growth depressions as indicators of changes in the Holocene hydro-regime and climate." The Holocene 12.6 (2002): 695-706.

Lorrey, Andrew M., et al. "The scientific value and potential of New Zealand swamp kauri." Quaternary Science Reviews 183 (2018): 124-139.

Miramont, Cécile, et al. "Le cycle de sédimentation «postglaciaire principal» des bassins marneux subalpins: état des lieux." Méditerranée 102.1 (2004): 71-84.

Miramont, C., et al. "Subfossil tree deposits in the Middle Durance (Southern Alps, France): environmental changes from Alleröd to Atlantic." Radiocarbon 42.3 (2000): 423-435.

Miramont, Cécile. "Evolution temporelle de la dynamique érosive et sédimentaire dans les Alpes du sud: l'exemple des bassins de" terres noires" et de la Durance." Forêt méditerranéenne (2000).

Miramont, Cécile, et al. "L’étalonnage du temps du radiocarbone par les cernes d’arbres. L’apport des séries dendrochronologiques du gisement de bois subfossiles du torrent des barbiers (Alpes françaises du sud)." Quaternaire. Revue de l'Association française pour l'étude du Quaternaire 22.3 (2011): 261-271.

NIWA New Zealand Climate Date (https://niwa.co.nz/education-and-training/schools/resources/climate/overview) 2020

Ogden, John, et al. "The late Quaternary history of kauri (Agathis australis) in New Zealand and its climatic significance." Journal of biogeography (1992): 611-622.

Palmer, Jonathan, et al. "Changes in El Nino-Southern Oscillation (ENSO) conditions during the Younger Dryas revealed by New Zealand tree-rings." EGUGA (2017): 6717.

Panyushkina, Irina P., and Steven W. Leavitt. "Ancient boreal forests under the environmental instability of the glacial to postglacial transition in the Great Lakes region (14 000–11 000 years BP)." Canadian Journal of Forest Research 43.11 (2013): 1032-1039.

Panyushkina, Irina P., and Steven W. Leavitt. "Insights into Late Pleistocene-early Holocene Paleoecology from fossil wood around the Great Lakes region." Wisconsin Geological and Natural History Survey Open-File Report 1 (2007).

Reinig, Frederick, et al. "New tree-ring evidence for the Late Glacial period from the northern pre-Alps in eastern Switzerland." Quaternary Science Reviews 186 (2018): 215-224.

Saurer, M., et al. "An investigation of the common signal in tree ring stable isotope chronologies at temperate sites." Journal of Geophysical Research: Biogeosciences 113.G4 (2008).

Schaub, Matthias. Lateglacial environmental conditions on the Swiss Plateau: a multi-proxy approach using tree rings and sediment-based proxies. Diss. University of Zurich, 2007.

Schaub, Matthias, et al. "Extension of the Swiss Lateglacial tree-ring chronologies." Dendrochronologia 23.1 (2005): 11-18.

Schaub, Matthias, et al. "Environmental change during the Allerød and Younger Dryas reconstructed from Swiss tree-ring data." Boreas 37.1 (2008): 74-86.

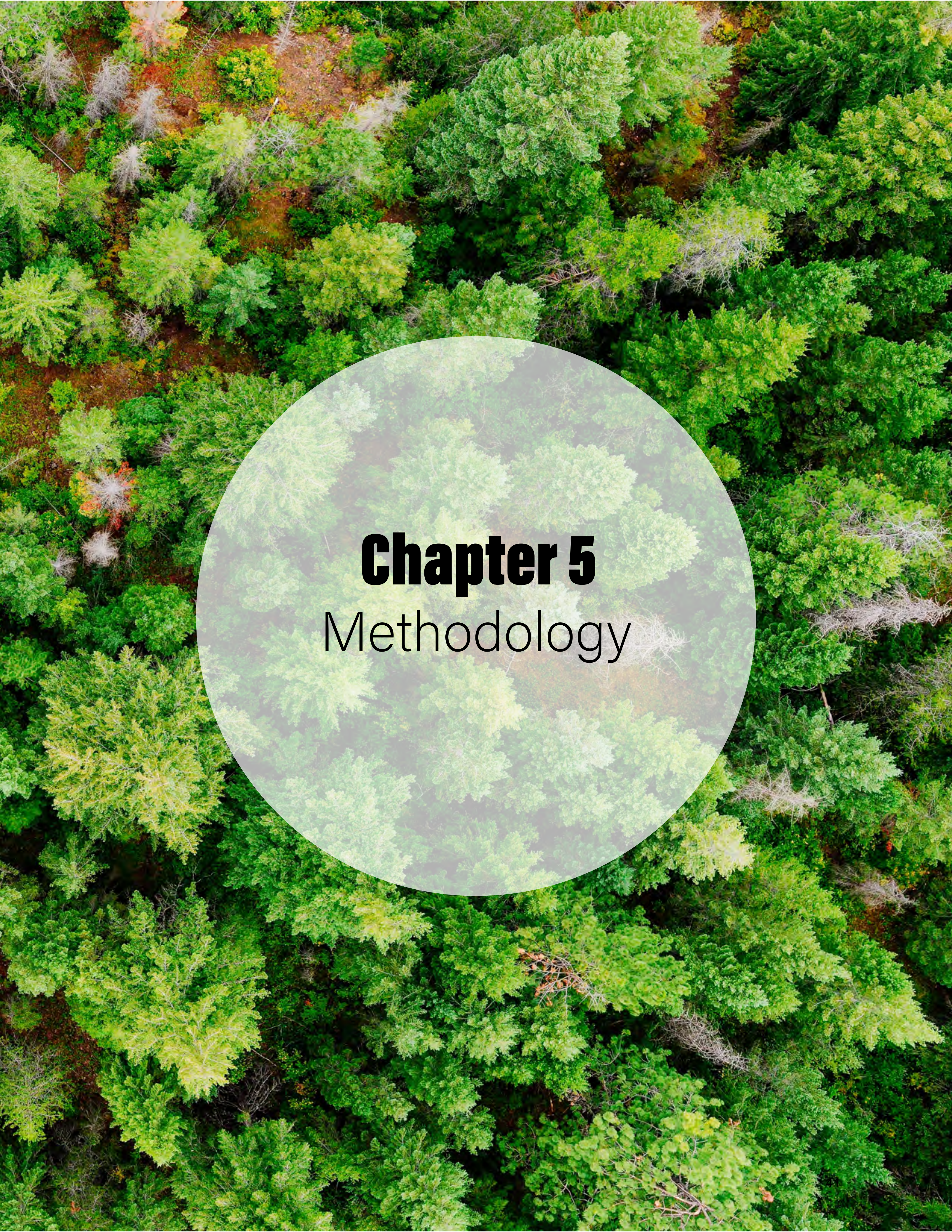

Chapter 5
Methodology

5. Methodology

5.1 Dendrochronology and radiocarbon dating

The floating tree chronologies (SWILM, Barbiers, Towai) utilised for this research were predominantly dated - through classical dendrochronological techniques in conjunction with radiocarbon dating - prior to the start of the project. The Binz material discovered in 2016 (n_{trees} = 253), however, was dated as part of this research (Reinig et al. 2018, Reinig et al. 2020, Sookdeo et al. 2020).

After the Binz sample excavation, stumps were dried, disks were cut (at least 3 from each sample). and subsequently sanded to reveal the growth rings (Reinig et al. 2018). Tree-ring widths were measured on multiple radii per disk using TSAPWin and a measuring table fitted with a LinTab device (Rinn et al. 1996) at the Swiss Federal Research Institute WSL (Birmensdorf, Switzerland).

Resulting tree-ring widths were initially cross-dated between trees using visual and statistical methods (e.g. Baillie and Pilcher, 1973). High resolution 14C measurements were performed at the Laboratory of Ion Beam Physics (ETH-Zurich, Switzerland) using a high-precision ^{14}C Accelerator Mass Spectrometer (AMS; Sookdeo et al. 2020), providing precise tree ages calibrated along the IntCal13 calibration curve (±20 to 25-year error of 1-sigma; Reimer et al., 2013).

5.2 Sample selection and stable isotope chronology development

A subset of samples was chosen from each chronology (SWILM, Barbiers, Towai) in an effort to develop stable isotope datasets with 4-5 tree overlaps through time. This is the quantity predicted to be required for tree-ring stable isotope records to produce an adequate population signal. The (expressed) population signal statistically quantifies the degree to which the (finite) subset of trees record the same environmental signal; how well the data reflects what would be produced from an infinite number of trees in the region (Wigley et al., 1984).

A subset of 27 trees were chosen from the SWILM chronology in an effort to cover the majority of the Late Glacial into the Younger Dryas onset (Publication 1: Pauly et al. 2020); beyond which ^{14}C dating remains challenging (Reinig et al. 2019). In some cases, tree-rings were difficult to decipher under a light microscope and therefore required anatomical techniques to develop adequate data (Reinig et al. 2018); such trees were avoided. Additionally, many samples exhibited reaction wood and could not be used; compressed wood has relatively low cellulose content (and high lignin content), which could impact cellulose extraction efficiency and eventually stable isotopes measurements (e.g. Walia et al. 2010). In those remaining trees, many demonstrated various states of decay, the highest of which were avoided where possible. This was particularly the case along the outer edge of the tree disks, and therefore often only part of a disk could be used. Given these considerations, the stable isotope series were generally much shorter in length than the maximum tree ring width chronologies and the ideal sample replication (4-5 trees) was not possible for the entire
chronology.

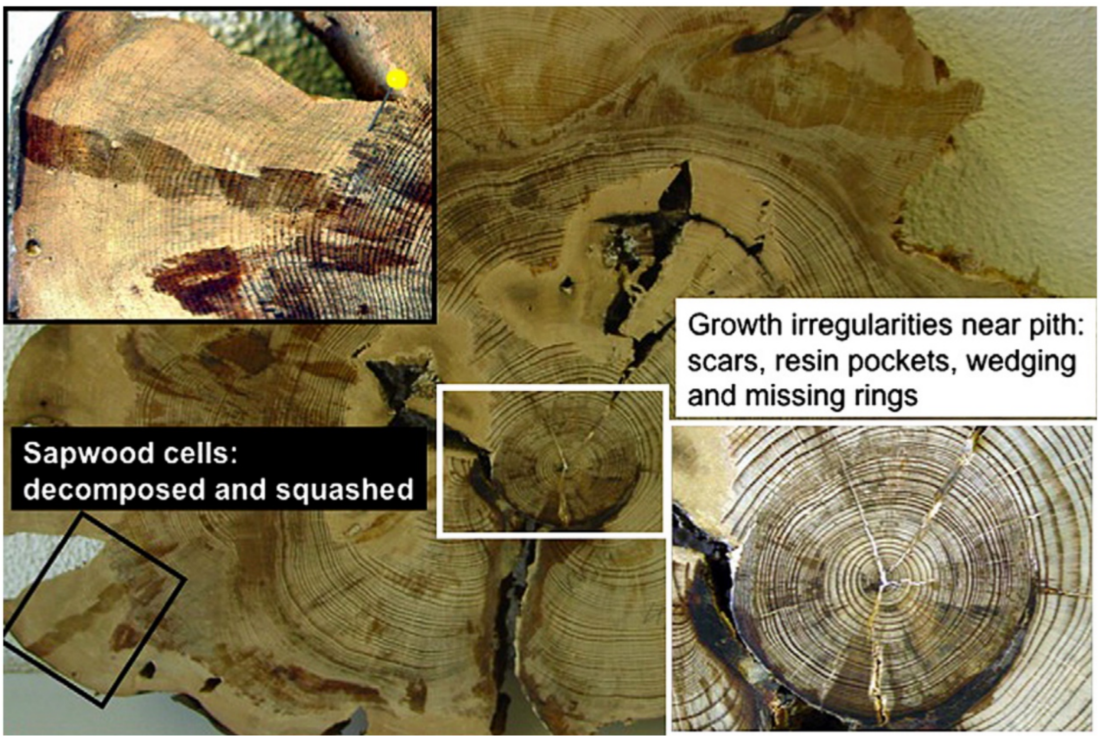

Figure 5.1: Examples of preservation challenges associated with subfossil trees from Zurich (Kaiser et al. 2012)

The Barbiers chronology is relatively limited in the number of samples covering the Late Glacial, therefore a subset of trees (n_{trees} = 7) growing across the Younger Dryas onset were chosen, covering ~12 900 - 12 600 cal BP (Publication 2: Pauly et al. 2018). These trees represent a period of high accuracy in 14C dating (Capano et al. 2018), when distinct IntCal13 wiggles permit precise placement.

The kauri tree subset from Towai was previously measured at decadal resolution (Kaplick et al. 2013; n_{trees} = 5) but was not yet published. This was extended in this thesis through the measurement of annual resolution (n_{trees} = 1) during a period of interest (Publication 3: Pauly et al. 2020).

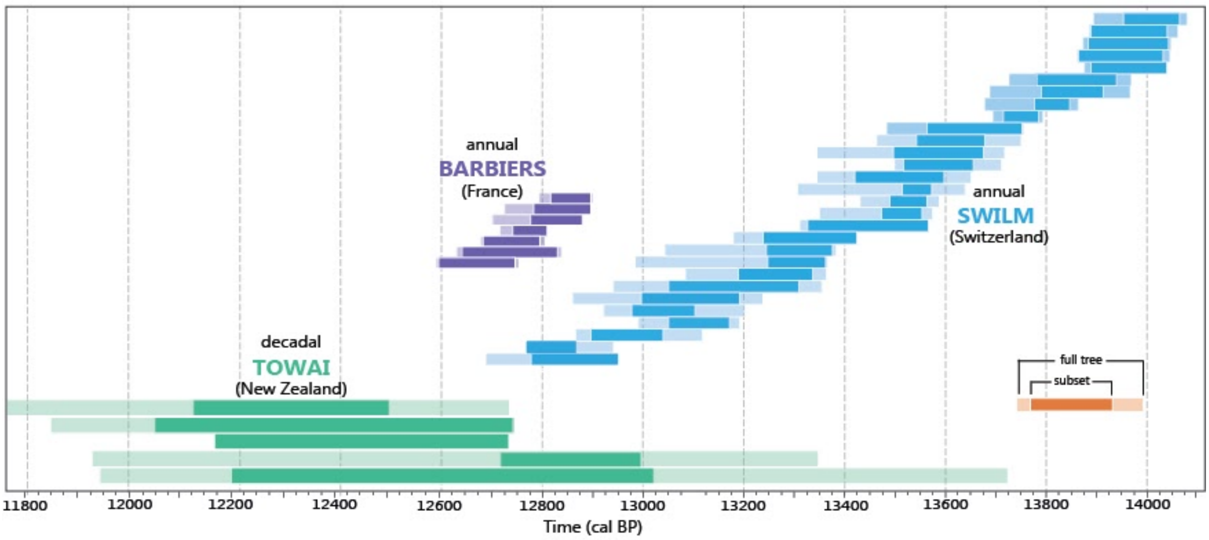

Figure 5.2: A gantt plot of the sample subsets from three sites (Towai, Barbiers and SWILM) used for stable isotope analysis in this thesis. Each bar represents an individual tree, with the full length (from tree-ring widths) and subset length (for stable isotope analysis) indicated.

The wood material from Barbiers and Towai was generally of very good quality compared to the SWILM material, with very little evidence of (visual) decay.

5.3 Cellulose extraction and stable isotope measurement

Radial cross-sections were cut using a high precision saw (Buehler Isomet 5000) from each tree disk (~10-15mm width, length from bark to pith). Sample transects were chosen from the tree disk based on their regular ring boundaries and low quantities of scars, resin ducts and missing rings.

In preparation for cellulose extraction, two different ring preparation methods were tested: (1) Individual rings from each cross-section were cut using a manual scalpel under a light microscope, and (2) Thin sections (~5mm depth x 10-20mm width x 50-100mm length) were cut from the radial sections, containing 10-50 rings (depending on ring widths). In the first method, individual rings were extracted using one of two devices: (1) Filter Bag Drum Tower (FBDT: Helle et al. 2020) or (2) Modified Büchner Funnels fitted in custom PTFE-devices (polytetrafluoroethylene) developed at GFZ (Wieloch et al. 2011). For the second method, the thin sections (wood laths) were extracted using special containers fitted with a series of PTFE punching sheets (Schollaen et al. 2017). The individual ring method was preferred when the rings were relatively thin (<3mm) and/or the wood was delicate and/or the ring boundaries were difficult to decipher under a light microscope.

The Jayme-Wise-method (Loader et al. 1997; Green 1963) of cellulose chemical extraction was used for the subfossil trees in this research, it is the most prevalent of the three extraction methods used in the literature. The specific chemical method was used:

1. Initial Alkaline Extraction with NaOH (5%) at 60°C for a total of 4 hours, exchanging solution after 2 hours
2. Washing samples with water
3. Chlorination with $NaClO_2$ (7.5%, to pH of 4-5) for a total of 37-30 hours, exchanging solution every 8 hours
4. Washing samples with HCl (1%) followed by deionized water until pH neutrality is achieved

The initial removal of extractives (Step 1) is particularly important for pine trees due to the resinous nature of the wood.

The Brendel Method (Anchukaitis et al. 2008; Dodd et al. 2008; English et al. 2011; Gaudinski et al. 2005) was not used as it requires a reaction temperature of 120°C (near the boiling point of the extraction devices used) and prefers finely ground wood samples. On the other hand, the Jayme-Wise method specifies a reaction temperature of only 60-70°C, demonstrates consistent results across inter-laboratory comparisons (Boettger et al. 2007) and has been proven for structurally complex wood samples (e.g. mummified wood; Hook et al. 2015). Further considerations for cellulose extraction can be found in Schollean et al. (2017) and Helle et al. (2020).

Following extraction, the samples were cooled (~ -10°C) and homogenized with an ultrasonic node (in a customised fitted-cabinet) and then freeze-dried for 48 hours. Samples were then weighed and packed into silver capsules (ø3.3x4mm) for stable isotope measurement (Delta V, Thermofisher Scientific Bremen; coupled with TC/EA HT at 1400°C). Measurements were then calibrated against international and lab-internal reference material (IAEA-CH3, IAEA-CH6 and Sigma-Aldrich Alpha-Cellulose) using two reference standards with widespread isotopic compositions for a single-point normalisation (Paul, Skrzypek, and Forizs 2007). Final isotope ratios are given in δ value, relative to VSMOW (δ18O) and VPDB (δ13C), with replication reproducibility of ±0.3‰ (δ18O) and ±0.15‰ (δ13C).

5.4 Model calculations in the aboreal system

Based on dual-isotope theory, signals of sourcewater $\delta^{18}O$ ($\delta^{18}O_{sw}$) from tree-ring cellulose stable isotopes can be estimated from tree-ring cellulose stable oxygen ($\delta^{18}O_{cel}$) and carbon ($\delta^{13}C_{sw}$); with the latter being used as a proxy for vpdLA in a simplified model expression formerly derived by Saurer et al. 1997:

$\delta^{18}O_{sw} = \delta^{18}O_{cel} + (\varepsilon k + \varepsilon e) * vpdLA * (1- p) * (1 - e - P)/P + \varepsilon_{cel}$ (modified)

If the factors (1 - p) and (1 - e - P)/P are combined and denoted as 'dampening factor' ƒ, the equation above can be given as:

$\delta^{18}O_{sw} = \delta^{18}O_{cel} + ƒ(\varepsilon k + \varepsilon e) * vpdLA + \varepsilon_{cel}$

This equation was rearranged and modified as per Anderson et al. (2002) by Pauly et al. (2018) to calculate sourcewater from Late Glacial trees in southern France, used in this thesis:

$\delta^{18}O*_{SW\text{-}tree} = \delta^{18}O_{cel} – (1 – f)(1 – vpdLA) (\varepsilon e + \varepsilon k) – \varepsilon_{biochem}$ (Anderson et al. 2002)

εe, εk and εbiochem are constants, equivalent to 28‰ (Majoube, 1971), 28‰ (Buhay & Edwards, 1995) and 27‰ (DeNiro & Epstein, 1979,1981; Sternberg 1989), respectively. The related dampening factor (f) and relative humidity (rH) were calculated from the equations below.

The 'dampening factor' ƒ, combines the Peclet effect (1 - e - P)/P at leaf level and the isotopic exchange ($1-p_{ex}p_x$) between xylem water and cellulose precursors during cellulose polymerization in the trunk.

$f = (1-p_{ex}p_x)$ (Barbour 2007; Saurer et al. 2012)

$\delta^{13}C = (a)rH + (b)T – 6.0$ (Edwards et al. 2000)

The $p_{ex}p_x$ parameter represents the ratio of oxygen which can be exchanged during tree-ring cellulose development (p_{ex}) and the proportion of sourcewater within the synthesising cell (p_x). A range of 0.3 – 0.5 was calculated as per Barbour (2007).

The leaf-level $\delta^{18}O$ (due to vapour pressure) was derived by subtracting the environmental ($\delta^{18}O*_{SW\text{-}tree}$) signal from the total tree cellulose $\delta^{18}O$:

$\Delta\delta^{18}O_{cel\text{-}SW} = \delta^{18}O_{cel} - \delta^{18}O*_{SW\text{-}tree}$ (Publication 2: Pauly et al. 2018)

While all water transported and contained within trees carries the $\delta^{18}O$ signature of the soil water taken up by the roots, $\delta^{18}O$ of leaf-water ($\delta^{18}O_L$) is modified by another process. Evapotranspiration from leaf to air $\delta^{18}O_L$ is generally enriched in ^{18}O (i.e. $\delta^{18}O_L > \delta^{18}O_{SW}$), because the heavier water vapor has a lower vapor pressure than lighter water vapour and because the heavier variety diffuses more slowly than the lighter variety (i.e. when water evaporates from the leaf, heavier molecules tend to be left behind). Hence, the ^{18}O enrichment of leaf-water usually rises with increasing evapotranspiration (e.g. Sheshshayee et al., 2005), following increasing leaf-to-air vpd or decreasing air rH (e.g. Helliker and Ehleringer, 2002).

The $\delta^{18}O$ value of cellulose is about 27‰ (± 4‰), higher than that of the water (Epstein et al. 1977; Deniro and Epstein 1981). However, within the leaves the ^{18}O enrichment at the sites of evaporation (stomata) diffuses back towards the xylem, while the actual flow of water is opposed, i.e. from the xylem to the evaporation sites. This means that as transpiration increases the average leaf ^{18}O enrichment becomes increasingly depleted and is known as Péclet effect (Farquhar and Lloyd 1993); adding some nonlinearity to the positive relationship between transpiration rate and 18O enrichment of leaf-water.

Due to the implications outlined above, the climate signal in tree ring $\delta^{18}O$ is usually weaker than in the $\delta^{18}O$ of precipitation (Saurer et al. 2012). Nonetheless, $\delta^{18}O$ of the soil water is still found the dominating factor determining $\delta^{18}O$ of tree-ring cellulose because the effect of ^{18}O-evaporative enrichment in the leaves is being dampened due to isotopic exchange (ranging between 30-50%; Barbour, 2007) with tree stem water during cellulose biosynthesis (e.g. Sternberg 2009; Treydte et al. 2014).

References (Chapter 5)

Anchukaitis, Kevin J., et al. "Consequences of a rapid cellulose extraction technique for oxygen isotope and radiocarbon analyses." Analytical Chemistry 80.6 (2008): 2035-2041.

Anderson, W. T., et al. "Model evaluation for reconstructing the oxygen isotopic composition in precipitation from tree ring cellulose over the last century." Chemical Geology 182.2-4 (2002): 121-137.

Baillie, Michael GL, and Jonathan R. Pilcher. "A simple crossdating program for tree-ring research." (1973).

Barbour, Margaret M. "Stable oxygen isotope composition of plant tissue: a review." Functional Plant Biology 34.2 (2007): 83-94.

Boettger, Tatjana, et al. "Wood cellulose preparation methods and mass spectrometric analyses of δ13C, δ18O, and nonexchangeable δ2H values in cellulose, sugar, and starch: an interlaboratory comparison." Analytical Chemistry 79.12 (2007): 4603-4612.

Buhay, William M., and Thomas WD Edwards. "Climate in southwestern Ontario, Canada, between AD 1610 and 1885 inferred from oxygen and hydrogen isotopic measurements of wood cellulose from trees in different hydrologic settings." Quaternary Research 44.3 (1995): 438-446.

Capano, Manuela, et al. "Wood 14 C Dating with AixMICADAS: Methods and Application to Tree-Ring Sequences from the Younger Dryas Event in the Southern French Alps." Radiocarbon 60.1 (2018): 51-74.

DeNiro, Michael J., and Samuel Epstein. "Relationship between the oxygen isotope ratios of terrestrial plant cellulose, carbon dioxide, and water." Science 204.4388 (1979): 51-53.

DeNiro, Michael J., and Samuel Epstein. "Isotopic composition of cellulose from aquatic organisms." Geochimica et Cosmochimica Acta 45.10 (1981): 1885-1894.

Dodd, Justin P., et al. "Robotic micromilling of tree-rings: a new tool for obtaining subseasonal environmental isotope records." chemical geology 252.1-2 (2008): 21-30.

Edwards, T. W. D., et al. "δ13C response surface resolves humidity and temperature signals in trees." Geochimica et Cosmochimica Acta 64.2 (2000): 161-167.

English, Nathan B., et al. "The effects of α-cellulose extraction and blue-stain fungus on retrospective studies of carbon and oxygen isotope variation in live and dead trees." Rapid Communications in Mass Spectrometry 25.20 (2011): 3083-3090.

Epstein, Samuel, Peter Thompson, and Crayton J. Yapp. "Oxygen and hydrogen isotopic ratios in plant cellulose." Science 198.4323 (1977): 1209-1215.

Farquhar, Graham D., and Jon Lloyd. "Carbon and oxygen isotope effects in the exchange of carbon dioxide between terrestrial plants and the atmosphere." Stable isotopes and plant carbon-water relations. Academic Press, 1993. 47-70.

Gaudinski, Julia B., et al. "Comparative analysis of cellulose preparation techniques for use with 13C, 14C, and 18O isotopic measurements." Analytical Chemistry 77.22 (2005): 7212-7224.

Green, John W. "Wood cellulose." Methods in carbohydrate chemistry (1963): 9-12.

Helliker, Brent R., and James R. Ehleringer. "Differential 18O enrichment of leaf cellulose in C3 versus C4 grasses." Functional Plant Biology 29.4 (2002): 435-442.

Hook, Benjamin A., et al. "Extraction of α-cellulose from mummified wood for stable isotopic analysis." Chemical Geology 405 (2015): 19-27.

Kaiser, Klaus Felix, et al. "Challenging process to make the Lateglacial tree-ring chronologies from Europe absolute–an inventory." Quaternary Science Reviews 36 (2012): 78-90.

Kaplick, Julia. „Water and Carbon Relations in New Zealand Kauri Forest” PhD Thesis (2013), The University of Auckland

Loader, N. J., et al. "An improved technique for the batch processing of small wholewood samples to α-cellulose." Chemical Geology 136.3-4 (1997): 313-317.

Majoube, Michel. "Fractionnement en oxygène 18 et en deutérium entre l’eau et sa vapeur." Journal de Chimie Physique 68 (1971): 1423-1436.

Paul, Debajyoti, Grzegorz Skrzypek, and István Fórizs. "Normalization of measured stable isotopic compositions to isotope reference scales–a review." Rapid Communications in Mass Spectrometry: An International Journal Devoted to the Rapid Dissemination of Up-to-the-Minute Research in Mass Spectrometry 21.18 (2007): 3006-3014.

Reimer, Paula J., et al. "IntCal13 and Marine13 radiocarbon age calibration curves 0–50,000 years cal BP." Radiocarbon 55.4 (2013): 1869-1887.

Reinig, Frederick, et al. "New tree-ring evidence for the Late Glacial period from the northern pre-Alps in eastern Switzerland." Quaternary Science Reviews 186 (2018): 215-224.

Reinig, Frederick, et al. "Introducing anatomical techniques to subfossil wood." Dendrochronologia 52 (2018): 146-151.

Rinn, F. "TSAP-Win. Time series analysis and presentation for dendrochronology and 409 related applications." User reference (2003).

Saurer, Matthias, et al. "Stable carbon isotopes in tree rings of beech: climatic versus site-related influences." Trees 11.5 (1997): 291-297.

Saurer, Matthias, et al. "Influence of atmospheric circulation patterns on the oxygen isotope ratio of tree rings in the Alpine region." Journal of Geophysical Research: Atmospheres 117.D5 (2012).

Sheshshayee, M. S., et al. "Oxygen isotope enrichment (Δ18O) as a measure of time-averaged transpiration rate." Journal of Experimental Botany 56.422 (2005): 3033-3039.

Sookdeo A., Kromer B., Adolphi F., Beer J., Brehm N., et al. 2020. "Tree-ring radiocarbon reveals reduced solar activity during Younger Dryas cooling. " (2020, Submitted)

Sternberg, L. da Silveira Lobo. "Oxygen and hydrogen isotope ratios in plant cellulose: mechanisms and applications." Stable isotopes in ecological research. Springer, New York, NY, 1989. 124-141.

Sternberg, Leonel da Silveira Lobo O'Reilly. "Oxygen stable isotope ratios of tree-ring cellulose: The next phase of understanding." New Phytologist 181.3 (2009): 553-562.

Treydte, Kerstin, et al. "Seasonal transfer of oxygen isotopes from precipitation and soil to the tree ring: source water versus needle water enrichment." New Phytologist 202.3 (2014): 772-783.

Walia, Ankit, Robert D. Guy, and Barry White. "Carbon isotope discrimination in western hemlock and its relationship to mineral nutrition and growth." Tree physiology 30.6 (2010): 728-740.

Wigley, Thomas ML, Keith R. Briffa, and Phillip D. Jones. "On the average value of correlated time series, with applications in dendroclimatology and hydrometeorology." Journal of climate and Applied Meteorology 23.2 (1984): 201-213.

CHAPTER 6

Paper 1

An annual-resolution stable isotope record from Swiss subfossil pine trees growing in the Late Glacial

An annual-resolution stable isotope record from Swiss subfossil pine trees growing in the Late Glacial

Maren Pauly[1,2,3], Gerhard Helle[1,2], Ulf Büntgen[4,5,6], Lukas Wacker[7], Kerstin Treydte[5], Frederick Reinig[5], Chris Turney[8], Daniel Nievergelt[5], Bernd Kromer[9], Michael Friedrich[10], Adam Sookdeo[7,11], Ingo Heinrich[1], Frank Riedel[2], Daniel Balting[1,12], Achim Brauer[1,13]

https://doi.org/10.1016/j.quascirev.2020.106550

1. GFZ German Research Centre for Geosciences, Section 43 'Climate Dynamics and Landscape Evolution' (Potsdam, Germany)

2. Free University of Berlin, Department of Earth Sciences, Section of Palaeontology (Berlin, Germany)

3. Bath Spa University, School of Science (Bath, United Kingdom)

4. University of Cambridge, Department of Geography (Cambridge, United Kingdom)

5. Swiss Federal Institute for Forest, Snow and Landscape Research WSL, Dendrosciences Group (Birmensdorf, Switzerland)

6. Global Change Research Centre and Masaryk University (Brno, Czech Republic)

7. ETH Zürich, Department of Physics, Ion Beam Physics Laboratory (Zürich, Switzerland)

8. University of New South Wales, Chronos ^{14}Carbon-Cycle Facility Changing, and Earth Research Centre, School of Biological, Earth and Environmental Sciences (Sydney, Australia)

9. University of Heidelberg, Institute of Environmental Physics (Heidelberg, Germany)

10. University of Hohenheim, Institute of Botany (Stuttgart, Germany)

11. University of New South Wales, Chronos ^{14}Carbon-Cycle Facility (Sydney, Australia)

12. Alfred Wegener Institute, Climate Sciences/Paleo-climate Dynamics (Bremerhaven, Germany)

13. University of Potsdam, Institute for Earth and Environmental Sciences (Potsdam, Germany)

CHAPTER 7

Paper 2

Subfossil trees suggest enhanced Mediterannean hydroclimate variability at the onset of the Younger Dryas

Subfossil trees suggest enhanced Mediterranean hydroclimate variability at the onset of the Younger Dryas

Maren Pauly[1,2], Gerhard Helle[1,2], Cecile Miramont[3], Ulf Büntgen[4-6], Kerstin Treydte[5], Frederick Reinig[5], Frédéric Guibal[7], Olivier Sivan[7], Ingo Heinrich[1], Frank Riedel[2], Bernd Kromer[8], Daniel Balanzategui[1], Adam Sookdeo[9], Lukas Wacker[9], Achim Brauer[1,10]

1. GFZ German Research Centre for Geosciences, Section 5.2 Climate Dynamics and Landscape Evolution, Potsdam, Germany

2. Free University Berlin, Department of Earth Sciences, Section of Palaeontology, Berlin, Germany

3. Aix Marseille Univ, Avignon Université, CNRS, IRD, IMBE, Mediterranean Institute of Marine and Terrestrial Biodiversity and Ecology, Aix-en-Provence, France.

4. University of Cambridge, Department of Geography, Cambridge, United Kingdom

5. Swiss Federal Institute for Forest, Snow and Landscape Research WSL, Dendrosciences, Birmensdorf, Switzerland

6. Global Change Research Centre and Masaryk University, Brno, Czech Republic

7. French National Institute for Preventive Archaeological Research, Venelles, France

8. University of Heidelberg, Institute of Environmental Physics, Heidelberg, Germany

9. ETH Zürich, Ion Beam Physics, Zürich, Switzerland

10. University of Potsdam, Institute for Earth and Environmental Science, Potsdam, Germany

Abstract

Nearly 13,000 years ago, the warming trend into the Holocene was sharply interrupted by a reversal to near glacial conditions. Climatic causes and ecological consequences of the Younger Dryas (YD) have been extensively studied, however proxy archives from the Mediterranean basin capturing this period are scarce and do not provide annual resolution. Here, we report a hydroclimatic reconstruction from stable isotopes ($\delta^{18}O$, $\delta^{13}C$) in subfossil pines from southern France. Growing before and during the transition period into the YD (12 900–12 600 cal BP), the trees provide an annually resolved, continuous sequence of atmospheric change. Isotopic signature of tree sourcewater ($\delta^{18}O_{sw}$) and estimates of relative air humidity were reconstructed as a proxy for variations in air mass origin and precipitation regime. We find a distinct increase in inter-annual variability of sourcewater isotopes ($\delta^{18}O_{sw}$), with three major downturn phases of increasing magnitude beginning at 12 740 cal BP. The observed variation most likely results from an amplified intensity of North Atlantic (low $\delta^{18}O_{sw}$) versus Mediterranean (high $\delta^{18}O_{sw}$) precipitation. This marked pattern of climate variability is not seen in records from higher latitudes and is likely a consequence of atmospheric circulation oscillations at the margin of the southward moving polar front.

7.1 Introduction: the Younger Dryas in Europe

During the abrupt and intense climate change from the Allerød warm phase to the YD cold reversal in the North Hemisphere (ca. 12 700–11 600 cal BP; Brauer et al. 2014; Dansgaard, 1987) sea-ice production and drifting enhanced (Not & Hillaire-Marcel, 2012), alpine glaciers advanced (Ivy-Ochs 2006), storm intensity strengthened (Brauer et al. 2008), and a reorganization of the atmosphere (Steffensen et al. 2008; Alley 2007) may have occurred. Greenland ice core data (NGRIP) reveal temperature drops of 10–15 °C with simultaneous reductions in snow accumulation and amplifications in atmospheric dust within less than a decade (Steffensen et al. 2008; Alley et al. 1993). During the rapid cooling, lake sediment records across Europe signal intensified wind stress, aridity and detrital input, alongside drastic ecological changes (Brauer et al. 2008; Lotter et al. 1992; Lücker & Brauer 2004).

The results are spatially heterogeneous in terms of hydrological change, as other European lake records find more humid conditions and/or increased quantity and intensity of precipitation (associated with higher lake levels in certain cases; Peyron et al. 2005; Ammann et al. 2000). Model simulations constrained by proxy data indicate no single factor could cause the observed YD cold reversal, but rather a complex combination of weakened Atlantic meridional overturning circulation (AMOC), altered atmospheric circulation patterns, and moderate negative radiative forcing as most plausible driving factors (Renssen et al. 2015). Nevertheless, mechanisms of climate variability in the North Atlantic region remain under intense debate (Alley et al. 1993), even for the most recent past (Vecchi et al. 2017).

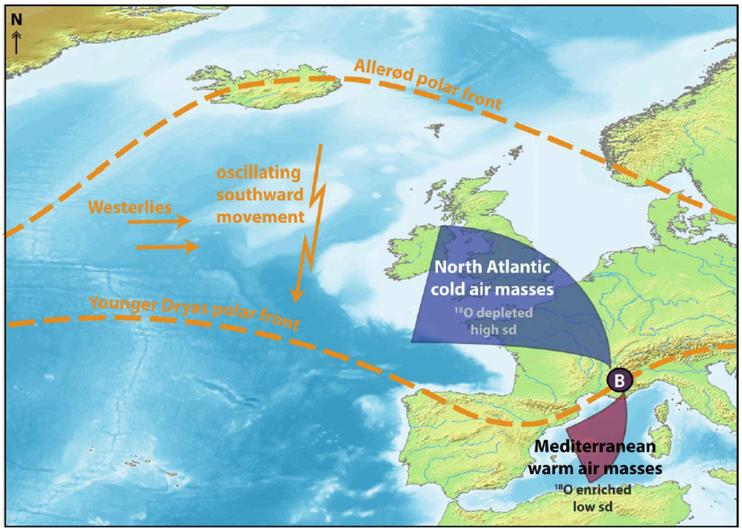

Figure 7.1 Influences of air mass conversions and the oscillating polar front on Barbiers during the Late Glacial: Map indicating position of Barbiers (B) in conjunction with hypothesized polar front variability (from Allerød to Younger Dryas; Hua et al. 2013; Brauer et al. 1999) and influential air masses (North Atlantic vs. Mediterranean; Celle-Jeanton et al. 2001). Map produced in Illustrator, using a Wikimedia Commons public domain base map from DEMIS Mapserver (https://commons.wikimedia.org/wiki/File:WorldMap-B_non-Frame.png).

In the Mediterranean, climate information on the YD from terrestrial records is scarce. Distinct change is evident in speleothem $\delta^{18}O$ (Chauvet cave; Genty et al. 2005), although a significantly less pronounced drop in summer temperatures (July) than at mid-latitudes has been reported (Heiri et al. 2014). Today, the Mediterranean climate is characterized by hot dry summers, and relatively mild (depending on orography)-humid winters (Figure S7.1). Model simulations specify that this summer-dry/winter-wet regime also persisted at the Last Glacial Maximum (LGM) when climate-forcing mechanisms were substantially different (Prentice et al. 1992). Thus, we assume that this general feature of seasonality was active during the Allerød/YD transition and in particular cold season precipitation, snow storage, and subsequent spring melt provided the water source for the studied trees.

7.2 Subfossil trees from southern France

The study site is located in the western Mediterranean on the foothills of the southern French Alps (Barbiers region: 44°21′11″N, 5°49′50″E, Fig. S7.2; Miramont et al. 2011). The steeply sloped valley of Barbiers shows evidence of highly unstable geomorphological conditions, where the subfossil trees were discovered enclosed (and thus well-preserved) within an alluvial sediment deposit, caused by multiple flooding events (Miramont et al. 2011). The region surrounding Barbiers is situated within a transitional climatic zone that is influenced by warm Mediterranean, cool Atlantic and mixing of air masses from both origins. Generally, precipitation from North Atlantic air masses is characterized by rather low, but highly variable $\delta^{18}O$ values, whereas vapour produced over the Mediterranean Sea carries a higher $\delta^{18}O$ signature with low variance (Celle-Jeanton et al. 2001). During the YD, when the Polar Front migrated south (Fig. 7.1), the interaction and mixing of these air masses was conceivably more intense and frequent in southern France. Although evident at the global scale (Kaiser et al.

2012), Mediterranean oxygen isotopes of precipitation ($\delta^{18}O_{precip}$) do not show strong relationships to local surface temperatures, as they are more strongly influenced by origin of moist air masses, transport lengths, rainout histories and amount of precipitation (Celle-Jeanton et al. 2001). Hence, $\delta^{18}O_{precip}$ at Barbiers predominantly signals changes in the relative contribution of precipitation from air masses of the two different origins (Fig. 7.1), an assumption that provides the theoretical basis for the Polar Front interpretation in this study.

Here we present carbon and oxygen isotope chronologies from tree-ring cellulose ($\delta 13C_{cell}$, $\delta^{18}O_{cell}$) used to develop the first annually resolved, biochemical climate proxy for reconstructing the abrupt cooling transition to the YD in the Mediterranean, thereby extending the latitudinal transect of annually-resolved records southward from Greenland (Steffensen et al. 2008) and western Germany (Brauer et al. 2008). The records were built using a subset of seven well preserved trees from a floating tree ring-width chronology (Miramont et al. 2011; Capano et al. 2017), of relatively low replication (9 trees) as sub-fossil trees growing during the Allerød/YD transition remain elusive (Reinig et al. 2018). The individual trees of the chronology have relatively shortaverage lifespans between 95–210 years, indicative of the highly variable and unstable site conditions. Despite the short-lived trees, none of the known ontogenetic effects related to age or tree height (Helama et al. 2015; Hogg et al. 2016) were evident in the stable isotope data (Fig. S7.5). Tree-ring width patterns are in some cases concurrent with tree burying in this region (abrupt growth decrease; Miramont et al. 2011) and thus may not record a clear climate signal, particularly in consideration of the low sample replication.

7.3 Methods

7.3.1 Sampling, chronology development and radiocarbon dating

Subfossil pine trunks (*Pinus sylvestris L.*, n_{trees} = 18: 16 in-situ, 2 uprooted) were collected adjacent to the Barbiers riverbed in southeastern France (44°21′11″N, 5°49′50″E, Figure S7.2) from an alluvial deposit spread across three tributaries on the southern foothills of Saint-Genis Mountain (Miramont et al. 2011; Miramont et al. 2000). Cross-sectional disks were cut and their surfaces were polished using various sandpapers (80 to 1200 grit sizes) to assist with tree-ring identification. Tree-ring width was measured on numerous tracks per disk using a LINTAB measuring table combined with TSAP-Win software. Samples were initially radiocarbon dated at low-resolution (Miramont et al. 2011; Miramont et al. 2000), within 1σ ^{14}C error range, and tree-ring width series of all trees were cross-dated visually and statistically (TSAP-Win) to build two initial floating chronologies (BarbA n_{trees} = 6, BarbB n_{trees} = 3, Fig. S7.3ab; Miramont et al. 2011); 9 additional trees discovered (younger and older than BarbA and BarbB) could not be cross-dated and thus were not included in the chronologies. Subsequently, the chronologies were radiocarbon dated with high-resolution ^{14}C analyses performed at CEREGE (Centre de Recherche et d'Enseignement de Géosciences de l'Environnement) Aix-Marseille University (Capano et al. 2017). The new high-resolution radiocarbon (^{14}C) dates of a two-tree sequence (210 years: Barb-12, Barb-17, Fig. S7.3) were measured using every 3rd ring within each tree (Capano et al. 2017); previous ^{14}C dating (to build BarbA and BarbB) was based on 10-year blocks (Miramont et al. 2011; Miramont et al. 2000). The new sequence (used to connect BarbA and BarbB into a single chronology) was wiggle matched with the decadal Kauri (Hogg et al. 2016) and YDB (Hua et al. 2013) chronologies using visual tuning. This analysis permitted the inclusion of Barb-17 and Barb-5 (both initially BarbB) into the BarbA chronology, where initial tree placement results18 required secondary confirmation, as there was more than one statistically plausible cross-dated position. A sequence age of 12 836 to 12 594 cal BP was found for the Barb12-Barb17 sequence, thus allowing the connection of the two tree-ring width chronologies into one (Capano et al. 2017) and placing the entire floating dendroisotope chronology (this study) at 12 906 to 12 594 cal BP (Figure S7.3).

Chronological synchronization between the three annually resolved data sets from Greenland (NGRIP; Steffensen et al. 2008), western Germany (Meerfelder Maar; Brauer et al. 1999) and southern France (Barbiers, this study) was completed using (1) volcanic tie points (Vedde Ash; Lane et al. 2012) and (2) radiocarbon wiggle matching (Capano et al. 2017). Meerfelder Maar is renowned for its high chronological precision, with continuous annually laminated sediments from the Late Glacial to the Holocene and three tephra layers (isochrons) in the Holocene (Ulmener Maar Tephra, 11 000 varve BP; Brauer et al. 1999; Zolitschka, et al. 1995), Younger Dryas (Vedde Ash, 12 140 varve BP; Lane et al. 2012) and Allerod (Laacher See Tephra, 12 880 varve BP; Brauer et al. 1999). Direct evidence from the Vedde volcanic eruption (Vedde Ash = VA) has also been conclusively discovered in NGRIP40, providing a tie point to synchronize the two annual records. Based on these assumptions, the NGRIP VA (12 171 ± 144 b2k) has been matched to Meerfelder Maar VA (12 140 ± 40 varve BP; Lane et al. 2015), with a shift of 19 years (12 190 b2k) applied to the data utilized in this study. Since the dendroisotope record at Barbiers is older than the Vedde eruption and shows no direct evidence of the Laacher See eruption (i.e. local volcanic ash in-situ), it was independently placed on the calendar scale based on results by Capano et al. (2017). The known dates of Meerfelder Maar tephra isochrones and Barbiers trees permit the estimation of absolute ages, allowing a robust connection between the three proxy archives and thus a regional inter-site comparison of climatic events.

7.3.2 Stable Isotope Analysis

A subset of samples (n = 7, 12 906–12 594 cal BP, Fig. S7.3) with high preservation and clear tree ring boundaries was selected for stable isotope analysis. One track on each tree disk was cut from pith to bark with a conventional band saw and then radially sliced into 1–1.5 mm width 'thick' sections (modified Isomet 5000 precision saw, Buehler, Esslingen, Germany). Individual annual rings were separated by hand using a scalpel blade for cellulose extraction. Holocellulose was extracted from wholewood using the two step base-acid method (Wieloch et al. 2011; Schollaen et al. 2017): sodium hydroxide for resin and extractives removal followed by acidified sodium chlorite to eliminate lignins. Following extraction, samples were washed thoroughly with milli-Q water, homogenized (ultrasonic sonode device for Eppendorf sample vials) and then freeze-dried for 48 hours. Resultant homogenized cellulose was weighed and packed in silver (tin) capsules for stable oxygen (carbon) analysis. Measurements were completed on an Isotope Ratio Mass Spectrometer Delta V, ThermoFisher Scientific, Bremen, Germany with TC/ EA HT pyrolysis device for $\delta^{18}O$ determination (Isotope Ratio Mass Spectrometer ISOPRIME coupled online to a Carlo Erba NA1500 Elemental Analyzer for δ13C). The samples analyzed are referenced to standard materials from the International Atomic Energy Agency (IAEA-C3, IAEA-CH6, IAEA-601 and IAEA-602), and checked with secondary standards from Sigma-Aldrich Chemie GmbH, Munich, Germany (Sigma Alpha-Cellulose and Sigma Sucrose) using a two-point normalization method (Debajyoti et al. 2007). Sample replication resulted in a reproducibility of better than ±0.1‰ for δ13Ccell values and ±0.3‰ for $\delta^{18}O_{cell}$ values. The isotope ratios are given in the δ-notation, relative to the standards V-PDB for $\delta^{13}C$ and V-SMOW for $\delta^{18}O$ (Figure S7.4).

7.3.2 Climate proxy calculations

Proxy reconstruction calculations of local sourcewater ($\delta^{18}O_{SW}$) and relative humidity. Local sourcewater $\delta^{18}O$ signature ($\delta^{18*}O_{SW}$, Fig. 1b) was calculated based on the model of Anderson et al. (2002):

$$\delta_{sw} = \delta^{18}O_{cell} - (1 - f)(1 - rH)(\varepsilon_e + \varepsilon_k) - \varepsilon_{biochem} \tag{1}$$

The dampening factor (f) was calculated as per Equation 2[45] and relative humidity from Equation 3[46]:

$$f = -1.47rH + 0.03T + 0.11TRX + 0.62 \tag{2}$$

$$\delta^{13}C_{cell} = (-0.17)rH + (-0.15)T - 6.0 \tag{3}$$

Temperature (T) was derived from annual NGRIP ice core δ18O (Steffensen et al. 2008; calibration of T = $\delta^{18}O$ + 3‰; Johnsen et al. 2001), with latitudinal (+50 °C) and growing season (+8 °C) corrections and the Tree Ring Index (TRX) was calculated for individual trees and then averaged into the mean chronology. Constants of $\varepsilon_{biochem}$ = 27‰ (DeNiro et al. 1981, 1979; Sternberg et al. 1989), ε_e = 28‰(Majoube 1971) and ε_k = 28‰ (Buhay & Edwards 1995) were used. The statistical influence of NGRIP $\delta^{18}O$ (as a predictor for temperature) on the modelled sourcewater has been approximated to test the impact of chronological error. Regression models were used to calculate the relative importance of multiple input variables ($\delta^{18}O_{NGRIP}$, $\delta^{18}O_{cell}$, $\delta^{13}C_{cell}$, tree ring width: Figure 7.1, S7.4) on the modelled sourcewater output. The calculated linear model coefficients of the dendrodata ($\delta^{18}O_{cell}$, $\delta^{13}C_{cell}$, tree-ring width) were two orders of magnitude higher (0.674, −0.539 and 0.393, respectively) than NGRIP data (−0.006), proving the dual-isotope model output is stable within dating uncertainties. These results are logical as $\delta^{18}O_{cell}$ is mainly a measure of local sourcewater variability, influenced by stomata conductance (also recorded in $\delta13C_{cell}$), which is driven by relative humidity and thus temperature (inherent in tree ring widths). The resultant $\delta^{18*}O_{SW}$ was subtracted from $\delta^{18}O_{cell}$

to extract the proportion of $\delta^{18}O_{cell}$ changes due to changes in (leaf level) vapour pressure ($\Delta\delta^{18}O_{cell\text{-}SW}$) over sourcewater; utilized in a dual-isotope modelling approach (Capano et al. 2017) to infer periods of high and low humidity, by comparing decadal-scale trajectories (+/−) of $\Delta\delta^{18}O_{cell\text{-}SW}$ and $\delta^{13}C$ (Figure S7.4).

Inter-annual $\delta^{18}O_{cell}$ variability (Fig. 7.2d, Δ‰) was calculated by subtracting current year $\delta^{18}O_{cell}$ (‰) from previous year $\delta^{18}O_{cell}$ (‰) to calculate ‰ difference per year of each individual tree. These values were then converted to absolute differences and subsequently averaged to produce a mean curve (Δ‰). Change point analysis was completed using an R package ('changepoint'; Killick et al. 2014) to find the position of multiple change points within the modelled sourcewater time series ($\delta^{18*}O_{SW}$) according to mean and variability; with four and one change points found, respectively (Table S7.2).

7.4 Discussion

The entire underlying cross-dated tree-ring series (9 trees) was positioned on the absolute time scale by ^{14}C wiggle matching with Kauri tree-ring data proposed by Capano et al. 2017 (Methods, Fig. S7.2). Our reconstructions (7 trees) date 12 906–12 594 cal BP and cover 312 years (Fig. 2). In a multi-parameter approach, tree ring-width, $\delta^{18}O_{cell}$ and $\delta^{13}C_{cell}$ (Fig. S7.3) were utilized in combination with NGRIP $\delta^{18}O$-derived annually resolved temperature (Steffensen et al. 2008) to (a) reconstruct local sourcewater $\delta^{18}O$ ($\delta^{18*}O_{SW}$, predominately reflecting oxygen isotopes of precipitation; Figure 7.2b and (b) to estimate relative humidity, both based on leaf-level dual-isotope theory (Barnard et al. 2012; Scheidegger 2000; Figure 7.2a and S7.4, Methods). Annual NGRIP $\delta^{18}O$ was positioned by synchronization to annual (varved) Meerfelder Maar lake sediment records (via the Vedde Ash Tephra), hence the

Barbiers tree-ring chronology was positioned on the absolute time scale independently (Methods, Fig. S7.2; Capano et al. 2017).

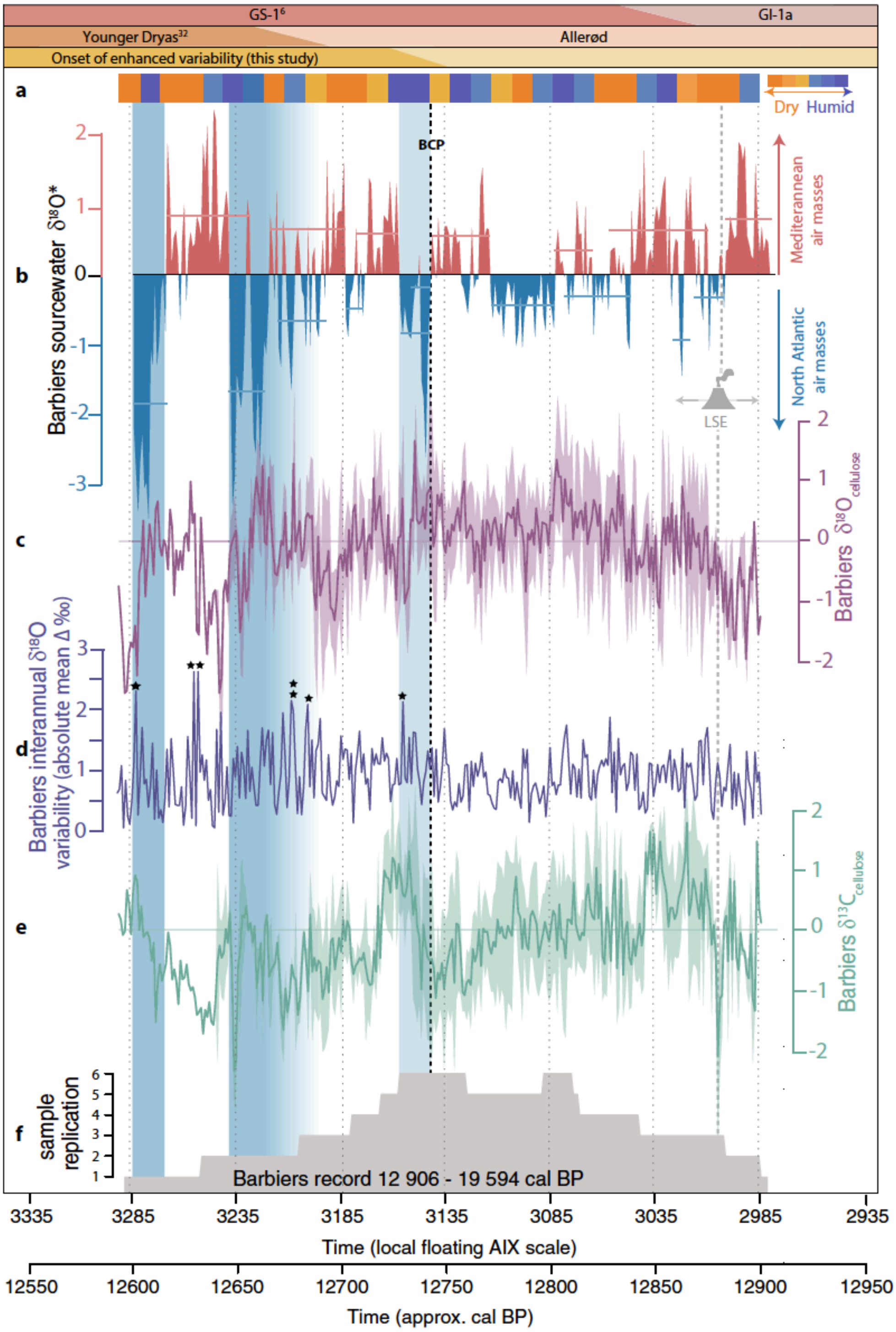

Figure 7.2. Barbiers tree-ring stable isotopes and palaeoclimate proxy records: (a) dual-isotope model recording dry vs. humid phases (10-year steps), derived from stable carbon and oxygen isotope ratios (Capano et al. 2017); (b) modelled Barbiers sourcewater $\delta^{18}O$ (‰ vs. VSMOW, z-scored, see Methods); mean z-scored tree cellulose (c) $\delta^{18}O$ (‰ vs. VSMOW), (d) inter-annual variability thereof (mean absolute change, ‰ – asterisks designate extremes of >2‰), (e) $\delta^{13}C$ (‰ vs. VPDB) and (f) sample replication. Laacher See Eruption (LSE; Rach et al. 2014; Brauer et al. 2008) indicated with 40- year dating error. Blue shaded areas highlight periods of extreme sourcewater depletion during the period of enhanced inter-annual variability (Barbiers Change Point, BCP).

During the first few decades of the Barbiers record (12 906 to 12 865 cal BP), the trees show increases in $\delta^{18}O_{cell}$, with stable or increasing $\delta^{13}C_{cell}$ and isotopically-heavy (modelled) sourcewater (Figure 7.2bce) – indicative of the Late Glacial climate improvement following the Gerzensee Oscillation (Switzerland; Lotter et al. 1992), GI-1b (Greenland; Björck et al. 1998) or Mo-LG3 (Austria; Lauterbach et al. 2011). Embedded in this transition period from humid/cooler to drier/warmer conditions is a sharp, short-lived (5-year) decline in $\delta^{13}C_{cell}$ (ntrees = 2), concurrent yet less pronounced increase in $\delta^{18}O_{cell}$ (n_{trees} = 1) corresponding with the timing of the Laacher See volcanic eruption (LSE) within dating uncertainties (Fig. 7.2: LSE, Fig. 7.3: LST, 12 880 ± 40 cal BP, Meerfelder Maar; Rach et al. 2014). This volcanic eruption likely produced a stratospheric volcanic plume capable of reaching southern France (Engels et al. 2015), resulting in reduced solar radiation (from increased atmospheric opacity), with the potential to induce a short-term reduction in photosynthetic efficiency and/or stomatal conductance, as reflected in the $\delta^{13}C_{cell}$ record.

The tree-ring isotope records continue relatively constantly for the next 160 years (12 865 to 12 740 cal BP), until an increase in inter-annual variability of $\delta^{18}O_{cell}$ (+0.2‰ absolute, Fig. 7.2d) and $\delta^{18*}O_{SW}$ (0.87‰ to 2.13‰, Fig. 7.2b, Table S7.2) coincides with an enhanced magnitude and frequency of extreme years (doubling of events with >3.0‰ inter-annual difference), particularly in pulses of isotopically light sourcewater (values exceeding 2 standard deviations beyond the mean, Fig. 7.2b, Table S7.1) occurring from 12 740 cal BP; hereafter referred to as the Barbiers Change Point (BCP). The influence of sample replication on changes in variability of the mean time series was tested using two segments with equally low sample replication (2 trees) pre- (12 906 – 12 883 cal BP) and post- (12 680 – 12 642 cal BP) BCP. This analysis yielded average absolute inter-annual variabilities of 0.61‰ and 1.24‰, respectively; proving low sample replication is likely not a cause of the increase, yet is still a limitation in the dataset. Despite the initial significant, short-lived sourcewater depletion at the BCP boundary, change point analysis (Methods) suggests five distinct $\delta^{18*}O_{SW}$ change phases; the first in variability (12 702 cal BP) and the following four in mean (>0.5‰: 12 664, 12 646, 12 616, 12 608 cal BP) (Table S7.2). This provides further evidence that the transformation to extreme conditions (BCP) occurred within an overall switch to new conditions according to the mean chronology.

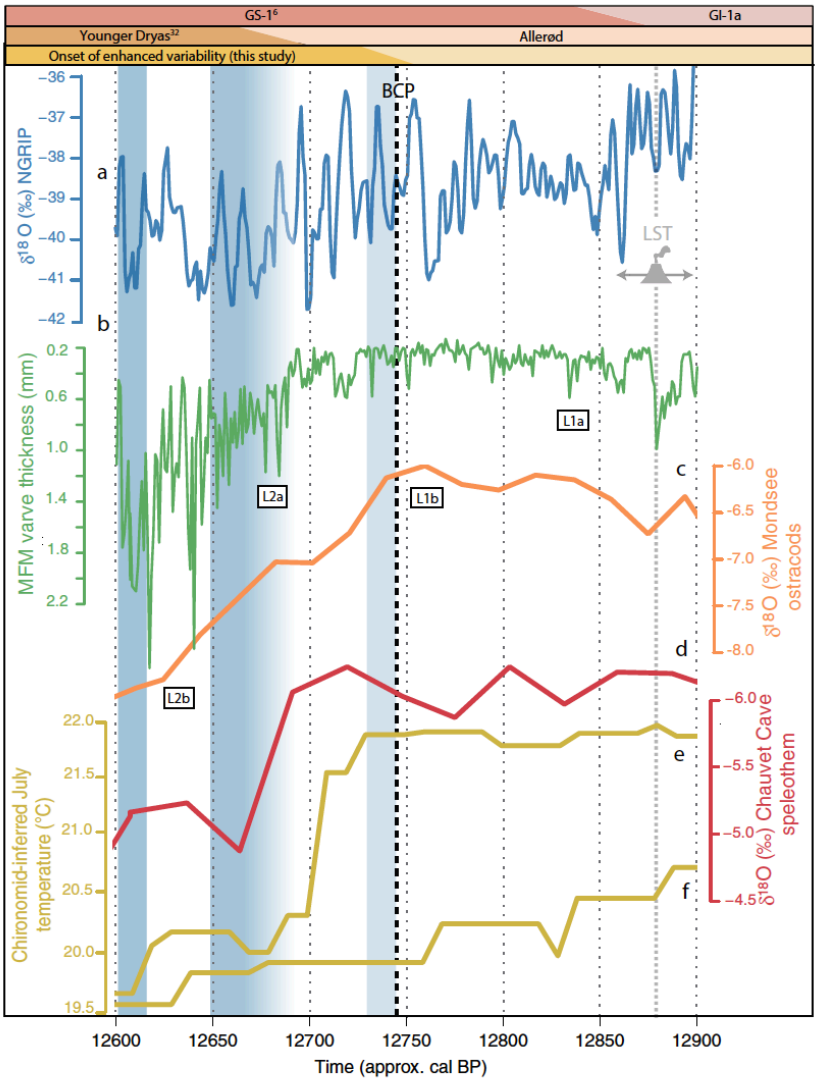

Figure 7.3. Selected palaeoclimate proxy records in the Northern Hemisphere: (a) NGRIP $\delta^{18}O$ (‰ vs. VSMOW; Steffensen et al. 2008); Meerfelder Maar (b) varve thickness (Brauer et al. 2008); (c) Mondsee ostracod $\delta^{18}O$ (‰ vs. VPDB; Lauterbach et al. 2011); (d) Chauvet Cave speleothem $\delta^{18}O$ (‰ vs. VPDB; Genty et al. 2006), chironomid inferred July air temperatures (Heiri et al. 2015) in (e) the Alpine region and (f) southwest Europe. Position of Laacher See Tephra (LST, 12 880 ± 40 varve years BP; Rach et al. 2014) and event timing of GS-1 onset at NGRIP (deuterium excess), Meerfelder Maar (L1a: aquatic lipid biomarkers, L2a: varve thickness), Mondsee (L1b: ostracod $\delta^{18}O$, L2b: increased NAP). Blue shaded areas indicate periods of extremely depleted modelled sourcewater $\delta^{18}O$ values at Barbiers (this study). See Figure S7.6 for map of selected records.

We argue that the conversion of air masses formed at mid- and high- latitudes (Fig. 7.1) with those from the Mediterranean intensified in southern France at the onset of the YD (BCP), along the margin of the southward moving polar front; producing more intense cold season storms from both origins (enhanced $\delta^{18*}O_{SW}$ variability) and more frequent and/or more intense precipitation events (progressively increasing magnitude of negative $\delta^{18*}O_{SW}$ excursions) originating from North Atlantic air masses. The positive $\delta^{18*}O_{SW}$ excursions after the BCP (particularly between 12640–12615 cal BP, Table S7.2) may be related to more frequent Mediterranean tropical-like cyclones (MTLCs), that are fostered by strong vertical temperature gradients between the sea surface and high troposphere. Together with a general southward shift of cold season lows over mid latitudes, more frequent upper atmospheric cold intrusions meeting warm and moist low-pressure systems over the western Mediterranean Sea is likely, increasing the number of MTLCs and worsening of the growing conditions (storm and flood damage) for the trees at Barbiers. However, these positive excursions are, however, lower amplitude than the negative excursions associated with increased polar outbreak and cold extremes (Tables S7.1, S7.2). At 12 593 cal BP a final local tree die-off occurs, conceivably reflecting the reduction in Pinus forests and expansion of shrub vegetation found across Europe (Lotter et al 1992; Lauterbach et al. 2011). This corroborates with evidence of reduced competition and forest thinning from the overall negative lifespan trend in $\delta^{13}C_{cell}$ (ntrees = 5, Fig. S7.5) and an increase in photosynthetic efficiency ($\delta^{13}C_{cell}$) of the last remaining tree.

In central Europe, two-step sequential YD transitions have been identified in annually laminated records from Meerfelder Maar (Rach et al. 2014; Engels et al. 2016; Fig. 7.3: L1a, L2a) and Mondsee (Fig. 7.3: L1b, L2b; Fig. S7.6; Lauterbach et al. 2011). The initial transition step (decline of lipid biomarker δD (L1a) and calcite $\delta^{18}O$ (L1b), respectively) has been attributed to the onset of decreasing temperatures. Whereas the second step was interpreted as a consequence of enhanced storminess and aridity, as seen in sediment regime expressed as varve micro-faces change (Brauer et al. 2008) and vegetation alterations and a lake level drop: increased varve thickness at Meerfelder Maar (L2a) and reduced calcite precipitation/increased flux of allochthonous sediments at Mondsee (L2b). This is contradictory to results at Barbiers, where the climate change was not one-directional (i.e. continuous alteration in atmospheric regime to glacial conditions), but rather bi-directional with enhanced extremes in both humidity and precipitation. Along these lines, the continuous speleothem growth at Chauvet Cave (130 km from Barbiers, Fig. S7.6) across the onset of the YD is in contrast with speleothems located at higher latitudes (i.e. Villars Cave), which show reduced growth or hiatus (Genty et al. 2006) signalling persistent low relative humidity during the YD cold reversal (as found at Meerfelder Maar; Engels et al. 2016).

From BCP onwards, drops in Barbiers $\delta^{18*}O_{SW}$ are simultaneous with deuterium excess in the NGRIP record (Steffensen et al. 2008), a proxy for North Atlantic moisture-source evaporative conditions. In contrast, the $\delta^{18*}O_{SW}$ upswing phases at Barbiers are not recorded in the North Atlantic, Meerfelder Maar or Mondsee, hinting that they are an expression of a locally specific climate anomaly (i.e. phases of intensified precipitation (e.g. MTLCs) originating from the Mediterranean Sea). Together, evidence of a latitudinal discrepancy in the Mediterranean becomes clear, where increased magnitude/frequency of precipitation events (this study) and relatively high humidity (Genty et al. 2006) were prevalent rather than enhanced aridity as often recorded north of the Alps (Lauterbach et al. 2011; Rach et al. 2014).

The temperature decline elucidating the cold reversal (L1a, L2a, GS-1) is still evident (yet more gradual) in lower latitude (Mediterranean-influenced) speleothem (Genty et al. 2006) and sediment core (Peyron et al. 2005; Cacho et al. 2011) records, and thus likely at Barbiers (though this is intertwined within the $\delta^{18*}O_{SW}$ signal). When considering the mean Barbiers tree $\delta^{18}O_{cell}$ record alone, a general decline of 2‰ is evident from 12 740 cal BP onward. Since this represents a complex signal of paired sourcewater and physiological dynamics, it is only through the proxy climate reconstruction (sourcewater and relative humidity) that this signal can be interpreted in detail as a complex signal of air mass origin, transportation, conversion and resultant storm tracks, rather than simply deduced as a stable drop in temperature. The contrasting sourcewater signature of strengthened MTLCs (enriched $\delta^{18*}O_{SW}$) versus the higher frequency of polar outbreaks (depleted $\delta^{18*}O_{SW}$) in the Mediterranean may explain the delayed and/or lower amplitude YD cooling traced in available sediment records within the region (Peyron et al. 2005; Genty et al. 2006; Cacho et al. 2001); the coarse resolution of which would dampen the signal of enhanced inter-annual variability in both directions. Further, the highly resolved Meerfelder Maar data recorded a brief, decadal oscillation in varve facies and pollen preceding this distinct YD transition (Engels et al. 2016), underscoring the importance of high-resolution records in reconstructing incremental/progressive change during climate instability and change, as seen in the step-wise oscillatory nature of hydroclimate variability in southern France at Barbiers.

7.5 Conclusions

The isotope data presented here suggest the importance of the careful consideration of spatial disparities when comparing multiple records of past rapid climate oscillations across a vast region, as slight latitudinal differences can coerce divergent feedback mechanisms associated with complex atmospheric and oceanic circulation changes. This study provides new insight into the behaviour of sub-fossil trees from annually-resolved stable isotope data during the intense climate change of the Late Glacial, and proves the potential of combined tree-ring parameters (ring-width, stable carbon and oxygen isotopes) in reconstructing local hydrological dynamics resulting from changing atmospheric circulation. We find further evidence to support the theorized southern movement of the polar front (Broecker et al. 2003; Brauer et al. 2008), expressed as an enhanced amplitude and frequency of winter storms and extreme events at Barbiers during the onset of a widespread and probably more capricious than previously thought reversal to the near glacial conditions of the YD.

7.6 References

1. Brauer, A. et al. 2014 “The importance of independent chronology in integrating records of past climate change for the 60 e 8 ka INTIMATE time interval”. Quaternary Science Reviews. 106.

2. Dansgaard, W. 1987 “Ice core evidence of abrupt climatic change”. Abrupt Clim. Chang. 223–224.

3. Not, C. & Hillaire-Marcel, C. 2012 “Enhanced sea-ice export from the Arctic during the Younger Dryas”. Nat. Commun. 3, 647.

4. Ivy-Ochs, S. et al. 2006 “The timing of glacier advances in the northern European Alps based on surface exposure dating with cosmogenic 10Be, 26Al, 36Cl, and 21Ne”. Geol. Soc. Am. Spec. Pap. 415, 43–60.

5. Brauer, A., Haug, G. H., Dulski, P., Sigman, D. M. & Negendank, J. F. W. 2008 “An abrupt wind shift in western Europe at the onset of the Younger Dryas cold period”. Nat. Geosci. 1, 520–523.

6. Steffensen, J. P. et al. 2008 “High-Resolution Greenland Ice Core Data Show AbruptClimate Change Happens in Few Years”. Science (80-.). 321, 680–683.

7. Alley, R. B. 2007 “Wally Was Right: Predictive Ability of the North Atlantic ‘Conveyor Belt’ Hypothesis for Abrupt Climate Change”. Annu. Rev. Earth Planet. Sci. 35, 241–272.

8. Alley, R. B. et al. 1993 “Abrupt increase in Greenland snow accumulation at the end of the Younger Dryas event”. Nature 362, 527–529.

9. Lotter, A. F., Eicher, U., Siegenthaler, U. & Birks, H. J. B. 1992 “Late-glacial climate oscillations as recorded in Swiss lake sediments”. J. Quat. Sci. 7, 187–204.

10. Lücke, A. & Brauer, A. 2004 “Biogeochemical and micro-facial fingerprints of ecosystem response to rapid Late Glacial climatic changes in varved sediments of Meerfelder Maar (Germany)”. Palaeogeogr. Palaeoclimatol. Palaeoecol. 211, 139–155.

11. Peyron, O. et al. 2005 “Late-Glacial climatic changes in Eastern France (Lake Lautrey) from pollen, lake-levels, and chironomids”. Quat. Res. 64, 197–211.

12. Ammann, B. et al. 2000 “Quantification of biotic responses to rapid climatic changes around the Younger Dryas - A synthesis”. Palaeogeography, Palaeoclimatology, Palaeoecology 159.

13. Renssen, H. et al. 2015 “Multiple causes of the Younger Dryas cold period”. Nat. Geosci. 8, 946–949.

14. Vecchi, G., Delworth, T. & Booth, B. 2017 “Climate science: Origins of Atlantic decadal swings”. Nature 548, 284–285.

15. Genty, D. et al. 2006 “Timing and dynamics of the last deglaciation from European and North African $\delta^{13}C$ stalagmite profiles-comparison with Chinese and South Hemisphere stalagmites”. Quat. Sci. Rev. 25, 2118–2142.

16. Heiri, O. et al. 2014 “Validation of climate model-inferred regional temperature change for late-glacial Europe”. Nat. Commun. 5, 4914.

17. Prentice, C., Guiot, J. & Harrison, S. 1992 “Mediterrannean vegetation, lake levels and palaeoclimate at the Last Glacial Maximum”. Nature 357, 57–59.

18. Miramont, C. et al. 2011 “Radiocarbon time scale calibration using tree rings. Contribution of french subfossil tree-ring chronologies at Barbiers River (Southern French Alps)”. Quaternaire 22, 261–271.

19. Celle-Jeanton, H., Travi, Y. & Blavoux, B. 2001 "Isotopic typology of the precipitation in the Western Mediterrenean region at the three different time scales". Geophys. Res. Lett. 28, 1215–1218.

20. Kaiser, K. F. et al. 2012 "Challenging process to make the Lateglacial tree-ring chronologies from Europe absolute - an inventory". Quat. Sci. Rev. 36, 78–90.

21. Capano, M. et al. 2017 "Wood 14C dating with AixMICADAS: methods and application to tree-ring sequences from the Younger Dryas event in the southern French Alps". Radiocarbon.

22. Reinig, F. et al. 2018 "New tree-ring evidence for the Late Glacial period from the northern pre-Alps in eastern Switzerland". Quat. Sci. Rev. 186, 215–224.

23. Helama, S., Arppe, L., Timonen, M., Mielikäinen, K. & Oinonen, M. 2015 "Age-related trends in subfossil tree-ring δ13C data". Chem. Geol. 416, 28–35.

24. Brienen, R. J. W. et al. 2017 "Tree height strongly affects estimates of water-use efficiency responses to climate and CO2 using isotopes". Nat. Commun. 8, 288.

25. Hogg, A. et al. 2016 "Decadally Resolved Lateglacial Radiocarbon Evidence from New Zealand Kauri". Radiocarbon 58, 709–733.

26. Barnard, H. R., Brooks, J. R. & Bond, B. J. 2012 "Applying the dual-isotope conceptual model to interpret physiological trends under uncontrolled conditions". Tree Physiol. 32, 1183–1198.

27. Scheidegger, Y., Saurer, M., Bahn, M. & Siegwolf, R. 2000 "Linking Stable Oxygen and Carbon Isotopes with Stomatal Conductance and Photosynthetic Capacity: A Conceptual Model". Oecologia 125, 350–357.

28. Björck, S. et al. 1998 "An event stratigraphy for the last termination in the North Atlantic region based on the Greenland ice-core record: a proposal by the INTIMATE group". J. Quat. Sci. 13, 283–292.

29. Lauterbach, S. et al. 2011 "Environmental responses to Lateglacial climatic fluctuations recorded in the sediments of pre-Alpine Lake Mondsee (northeastern Alps)". J. Quat. Sci. 26, 253–267.

30. Rach, O., Brauer, A., Wilkes, H. & Sachse, D. 2014 "Delayed hydrological response to Greenland cooling at the onset of the Younger Dryas in western Europe". Nat. Geosci. 7, 109–112.

31. Engels, S., Van Geel, B., Buddelmeijer, N. & Brauer, A. 2015 "High-resolution palynological evidence for vegetation response to the Laacher See eruption from the varved record of Meerfelder Maar (Germany) and other central European records". Rev. Palaeobot. Palynol. 221, 160–170.

32. Engels, S. et al. 2016 "Subdecadal-scale vegetation responses to a previously unknown late-Allerød climate fluctuation and Younger Dryas cooling at Lake Meerfelder Maar (Germany)". J. Quat. Sci. 31, 741–752.

33. Cacho, I. et al. 2001 "Variability in the western Mediterranean Sea surface temperature during the last 25,000 years and its connection with the Northern Hemisphere climatic changes". Paleooceanography 16, 40–52.

34. Broecker, W. S. 2003 "Does the trigger for abrupt climate change reside in the ocean or in the atmosphere?" Science 300, 1519–22.

35. Miramont, C., Sivan, O., Rosique, T., Edouard, B. & Jorda, M. 2000 "Subfossil tree deposits in the Middle Durance (southern Alps, France): Environmental changes from Allerod to Atlantic". Radiocarbon 47, 115–134.

36. Hua, Q., Barbetti, M. & Rakowski, A. 2013 "Atmospheric radiocarbon for the period 1950–2010". Radiocarbon 55, 2059–2072 .

37. Brauer, A., Endres, C. & Negendank, J. F. W. 1999 "Lateglacial calendar year chronology based on annually laminated sediments from Lake Meerfelder Maar, Germany”. Quat. Int. 61, 17–25.

38. Lane, C. et al. 2012 “Was the 12.1ka Icelandic Vedde Ash one of a kind?” J. Quat. Sci. 27, 141–149.

39. Zolitschka, B., Negendank, J. F. W. & Lottermoser, B. G. 1995 “Sedimentological proof and dating of the early Holocene volcanic eruption of Ulmener Maar (Vulkaneifel, Germany)”. Geol. Rundschau 84, 213–219.

40. Mortensen, A., Bigler, M., Grönvold, K., Steffensen, J. P. & Johnsen, S. J. 2005 “Volcanic ash layers from the Last Glacial Termination in the NGRIP ice core”. J. Quat. Sci. 20, 209–219.

41. Lane, C. et al. 2015 “The Late Quaternary tephrostratigraphy of annually laminated sediments from Meerfelder Maar, Germany”. Quat. Sci. Rev. 122, 192–206.

42. Wieloch, T., Helle, G., Heinrich, I., Voigt, M. & Schyma, P. 2011 “A novel device for batch-wise isolation of??-cellulose from small-amount wholewood samples”. Dendrochronologia 29, 115–117.

43. Schollaen, K. et al. 2017 “A guideline for sample preparation in modern tree-ring stable isotope research”. Dendrochronologia 44, 133–145.

44. Debajyoti, P., Skrzypek, G. & Forizs, I. 2007 “Normalization of measured stable isotopic compositions to isotope reference scales – a review”. Rapid Commun. Mass Spectrom. 21, 3006–2014.

45. Anderson, W. T., Bernasconi, S. M., McKenzie, J. A., Saurer, M. & Schweingruber, F. 2002 “Model evaluation for reconstructing the oxygen isotopic composition in precipitation from tree ring cellulose over the last century” RID E-5394-2010. Chem. Geol. 182, 121–137.

46. Edwards, T. W. D. et al. 2000 “d13C response surface resolves humidity and temperature”. Geochim. Cosmochim. Acta 64, 161–167.

47. Johnsen, S. J. et al. 2001 “Oxygen isotope and palaeotemperature records from six Greenland ice-core stations: Camp Century, Dye-3, GRIP, GISP2, Renland and NorthGRIP”. J. Quat. Sci. 16, 299–307.

48. DeNiro, M. J. & Epstein, S. 1981 “Isotopic composition of cellulose from aquatic organisms”. Geochim. Cosmochim. Acta 45, 1885–1894.

49. DeNiro, M. J. & Epstein, S. 1979 “Relationship Between the Oxygen Isotope Ratios of Terrestrial”. Science (80-.). 204, 51–53.

50. Sternberg, L. da S. L. 1989 “Oxygen and Hydrogen Isotope Ratios in PlantCellulose: Mechanisms and Applications”. in Stable Isotopes in Ecological Research 124–141.

51. Majoube, M. 1971 “Fractionnement en oxyge’ne 18 et en deuté rium entre l’eau et sa vapeur“. J. Chim. Phys. 68, 1423–1436.

52. Buhay, W. M. & Edwards, T. W. D. 1995 “Climate in southwestern Ontario, Canada, between AD 1610 and 1885 inferred from oxygen and hydrogen isotopic measurements of wood cellulose from trees in different hydrologic settings”. Quaternary Research 44, 438–446.

53. Killick, R. & Eckley, I. 2014 “changepoint: An R Package for Changepoint Analysis”. J. Stat. Softw. 58, 1–19.

7.7 Supplementary Material

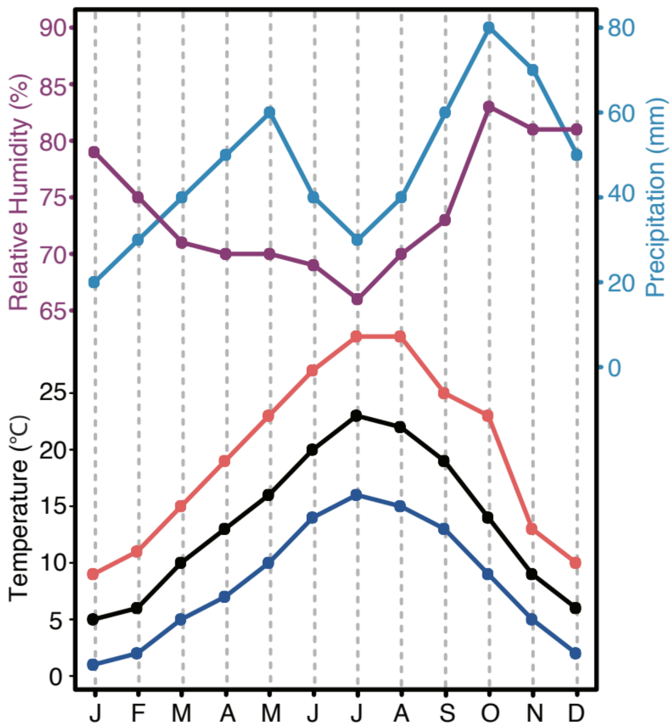

S7.1 Present day climate indices: annual variability in relative humidity, precipitation, and temperature (red = high, black = average, blue = low) at nearby climate station (Avignon, France).

a	BARB-4	BARB-5	BARB-7	BARB-12	BARB-13	BARB-14	BARB-17
BARB-4	- / 0	2.9 / 95	2.1 / 107	5.7 / 139	4.5 / 87	4.5 / 156	1.4 / 55
BARB-5	2.9 / 95	- / 0	4.0 / 92	3.2 / 95	1.1 / 17	0.1 / 86	2.0 / 40
BARB-7	2.1 / 107	4.0 / 92	- / 0	3.9 / 131	0.5 / 14	0.5 / 83	0.7 / 79
BARB-12	5.7 / 139	3.2 / 95	3.9 / 131	- / 0	2.4 / 46	3.0 / 115	3.8 / 126
BARB-13	4.5 / 87	1.1 / 17	0.5 / 14	2.4 / 46	- / 0	8.4 / 104	- / 0
BARB-14	4.5 / 156	0.1 / 86	0.5 / 83	3.0 / 115	8.4 / 104	- / 0	0.1 / 31
BARB-17	1.4 / 55	2.0 / 40	0.7 / 79	3.8 / 126	- / 0	0.1 / 31	- / 0

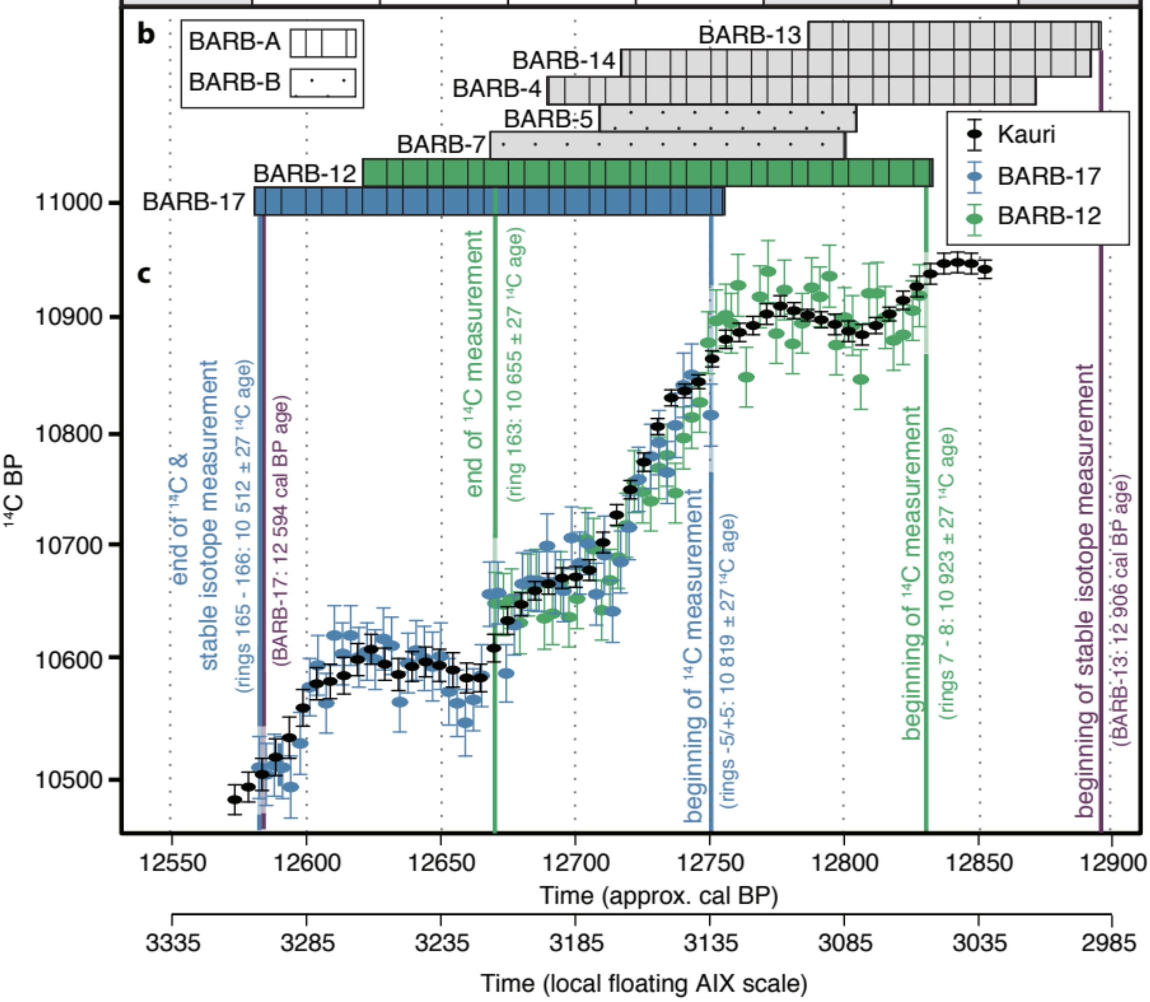

Figure S7.2. Cross-dating and radiocarbon wiggle matching of Barbiers trees: (a) Statistical cross-dating of seven Barbiers trees utilized for the dendroisotope record (this study), based on results from Reinig et al. 2018 and Hogg et al. 2016. (T-Value with Baillie-Pilcher-Standardization / number of overlapping years); (b) overlap of individual trees from two tree chronologies (BarbA, BarbB; Reinig et al. 2018); (c) trees wiggle matched with Southern Hemisphere (Kauri) decadal radiocarbon calibration curve (Brienen et al. 2017) using high resolution ^{14}C measurements from a two-tree sequence (Barb 12 & Barb 17, as per Hogg et al. 2016); Kauri ^{14}C ages corrected for the inter-hemispheric gradient (57 ^{14}C years subtracted).

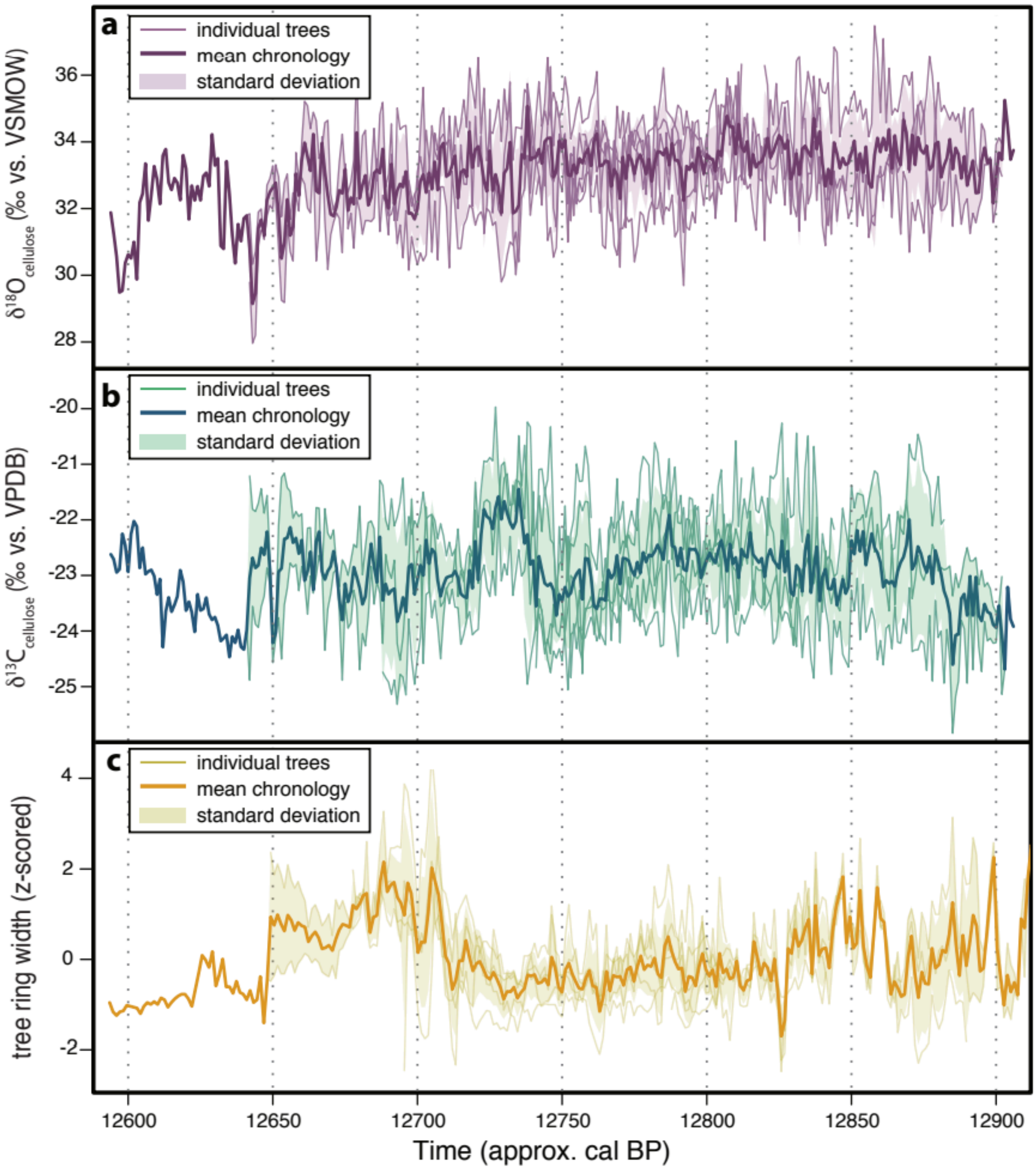

Figure S7.3. Tree-ring parameters of Barbiers trees: (a) oxygen ($\delta^{18}O_{cell}$ ‰ vs. VSMOW) and (b) carbon ($\delta^{13}C_{cell}$ ‰ vs. VPDB), measured at the GFZ Helmholtz Centre Potsdam, Section 5.2 Climate Dynamics and Landscape Evolution and (c) tree-ring widths (z-scored), measured at CEREGE, Aix-Marseille University.

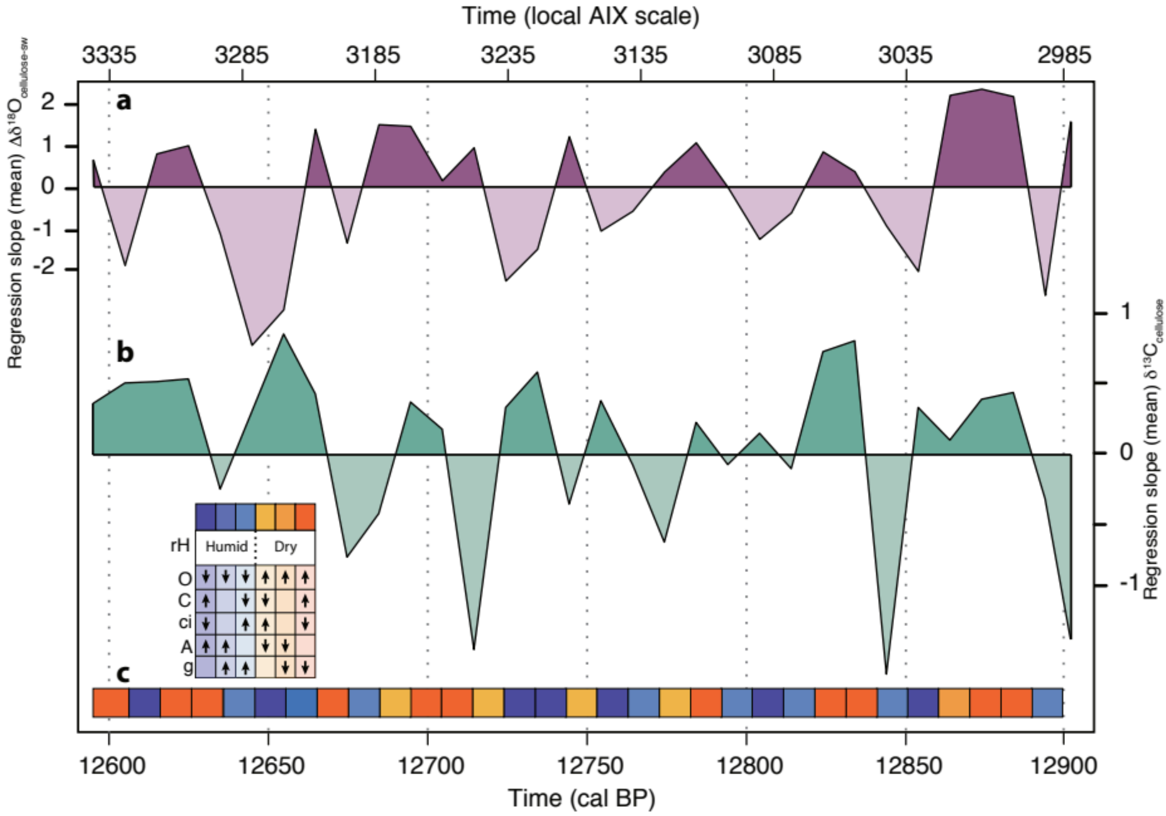

Figure S7.4. Dual-isotope modelling results of Barbiers trees: Decadal regression slopes from mean (a) $\delta^{18}O$ (stomata-driven $\delta^{18}O$ signal: $\Delta\delta^{18}O = \delta^{18}O_{cellulose} - \delta^{18}O_{sw}$) and (b) $\Delta\delta^{13}C$ records. Resultant $\Delta\delta^{18}O$-$\delta^{13}C$ scenarios plotted (c). Table inset: relative humidity (rH) and CO2 leaf partial pressure (Ci) derived from $\delta^{18}O$ (O) and $\delta^{13}C$ (C) trajectory (a,b), respectively. Maximum photosynthesis (A) and stomatal conductance (g) change output based on aforementioned parameters.

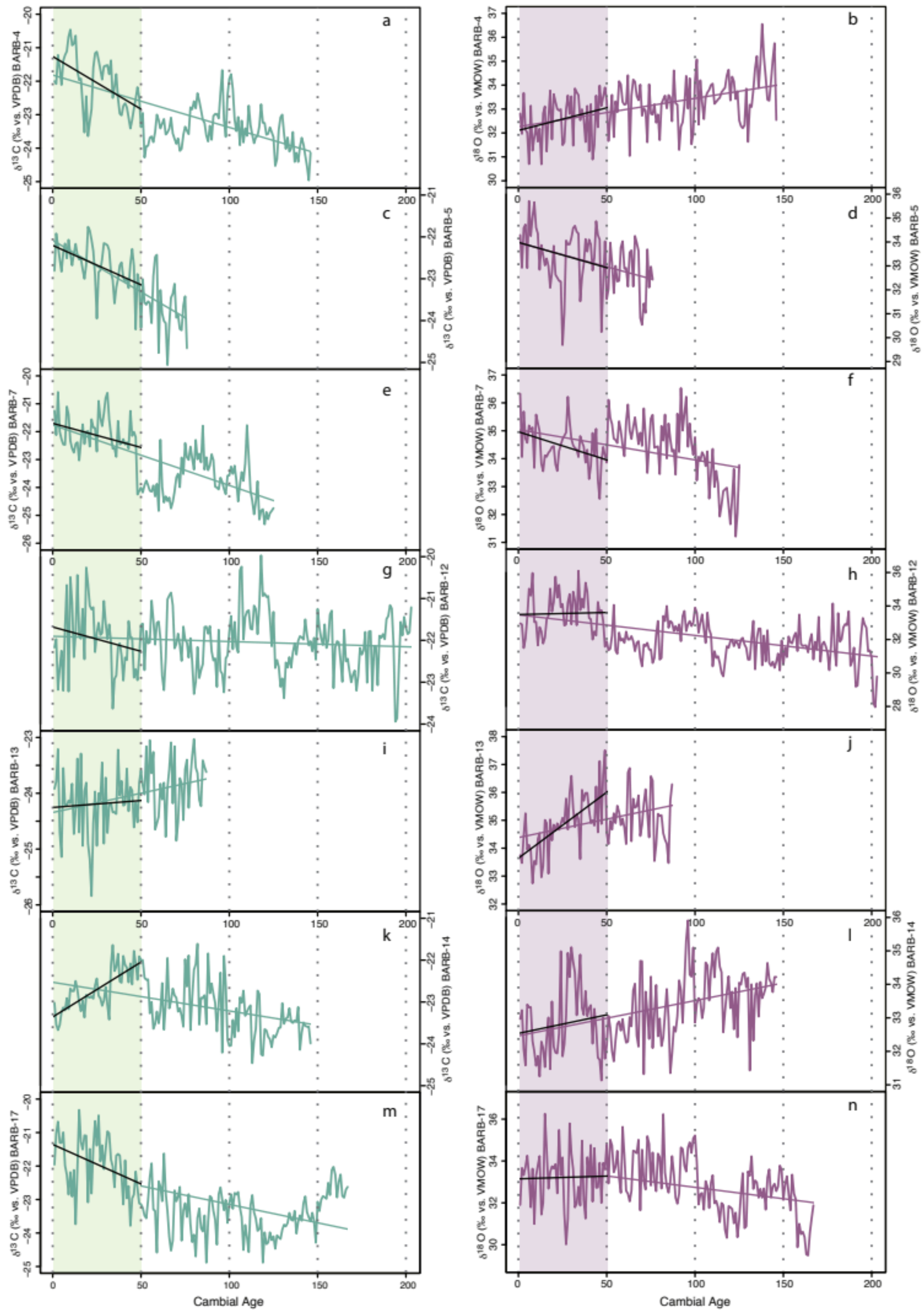

Figure S7.5. Individual dendroisotope records of Barbiers River trees: Age trends in carbon (green, ‰ vs. VPDB) and oxygen (purple, ‰ vs. VSMOW) isotopes from (a,b) BARB-4, (c,d) BARB-5, (e,f) BARB-7, (g,h) BARB-12, (i,j) BARB-13, (j,l) BARB-14, (m,n) BARB-17 for first 50 years (juvenile years, black lines) and full tree (green/purple lines). Innermost rings (at most 10) may be missing due to preservation issues.

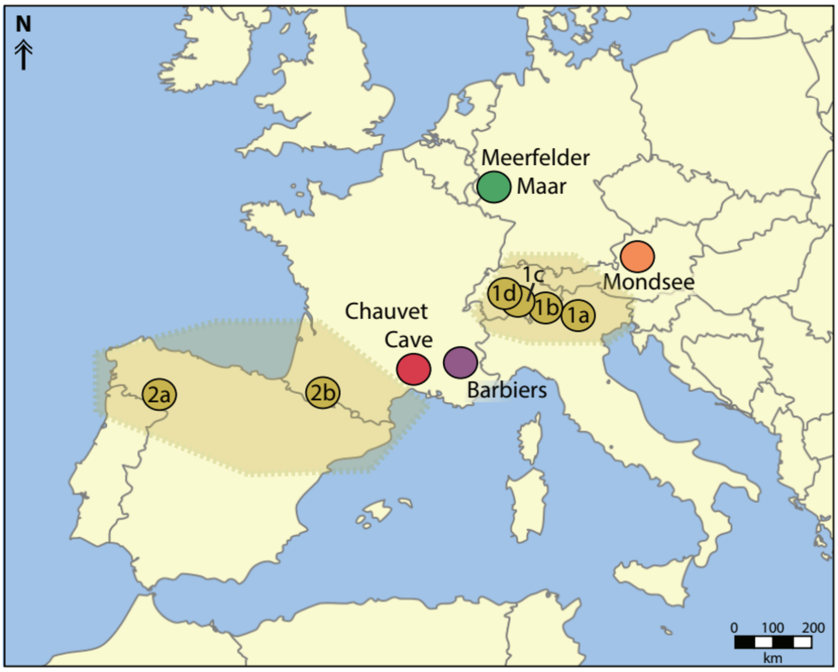

Figure S7.6. Location of selected palaeoclimate proxy records within Europe: Barbiers subfossil trees (this study), Chauvet Cave speleothems (Genty et al. 2006), Mondsee (Lauterbach et al. 2011) and Meerfelder Maar (Rach et al. 2014) indicated. Locations of chironomid-inferred July temperatures (Heiri et al. 2014) in the Alpine Region (1a: Lago di Lavarone, 1b: Maloja Riegel, 1c: Foppe, 1d: Hinterburgsee) and southwest Europe (2a: Laguna de la Roya, 2b: Ech). Highlighted areas for each temperature proxy region shows the estimated spatial area represented by the stacked record.

Time range	Average ‰ sourcewater	Number of years
12 740 – 12 738 cal BP	-3.3‰	3
12 662 – 12 658 cal BP	-3.6‰	5
12 653 – 12647 cal BP	-3.4‰	7
12 640 – 12639 + 12 636 cal BP	+2.6‰	3
12 608 – 12 601 cal BP	-4.6‰	8

Table S7.1: Periods of enhanced sourcewater depletion (-) and enrichment (+), with values greater than 2 standard deviations beyond the chronology mean.

Change Points	
mean	12 664 cal BP
	12 646 cal BP
	12 616 cal BP
	12 608 cal BP
variability	12 702 cal BP

Table S7.2: Change points defined in the sourcewater time series according to mean and variability using 'changepoint' R package (Killick R and Eckley IA, 2014).

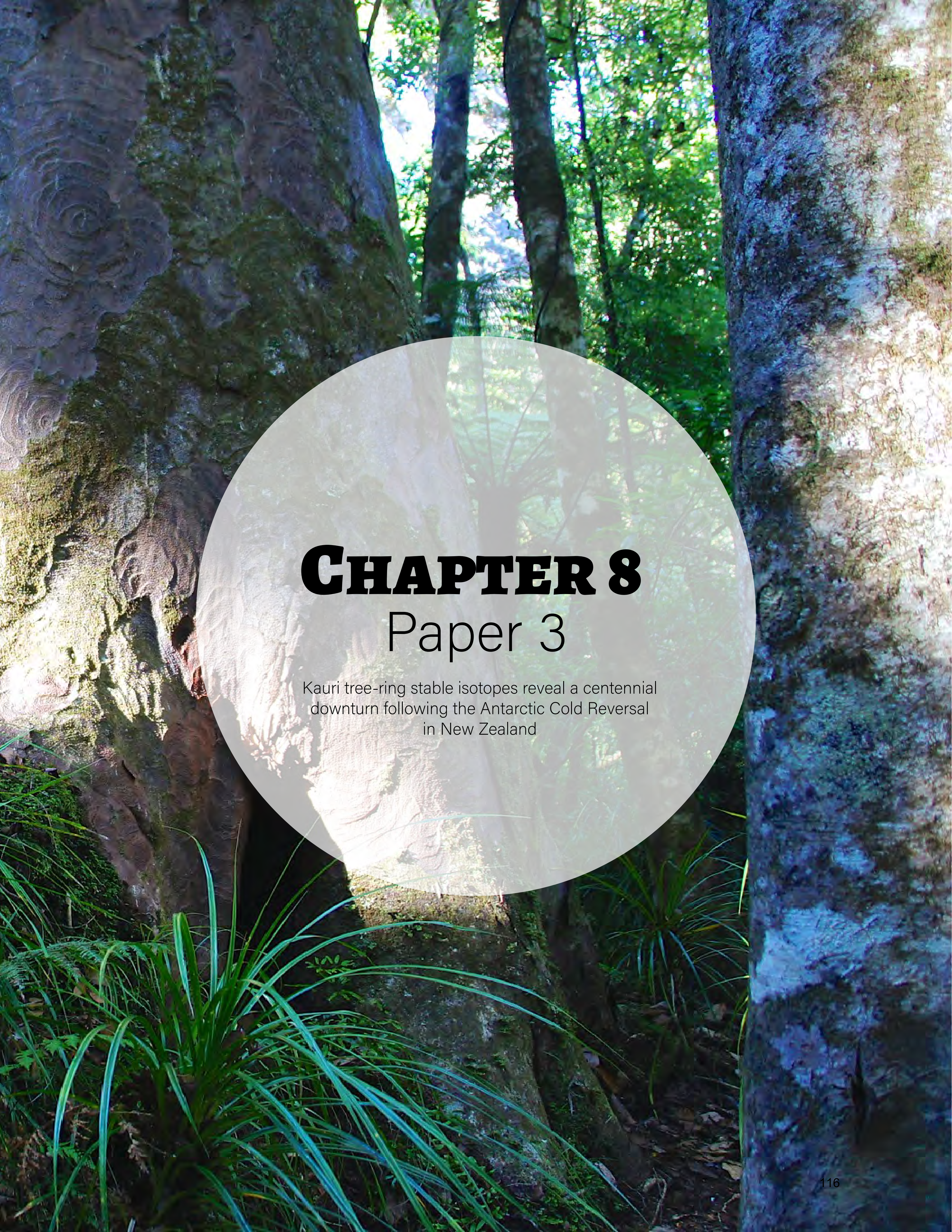

Chapter 8

Paper 3

Kauri tree-ring stable isotopes reveal a centennial downturn following the Antarctic Cold Reversal in New Zealand

Kauri tree-ring stable isotopes reveal a centennial climate downturn following the Antarctic Cold Reversal in New Zealand

Maren Pauly[1,2,3], Chris Turney[4], J Palmer[4], Ulf Büntgen[5,6], Achim Brauer[1], Gerhard Helle[1,2]

1. GFZ German Research Centre for Geosciences, Section 43 'Climate Dynamics and Landscape Evolution' (Potsdam, Germany)

2. Free University of Berlin, Department of Earth Sciences, Section of Palaeontology (Berlin, Germany)

3. Bath Spa University, School of Science (Bath, United Kingdom)

4. University of New South Wales, Palaeontology, Geobiology and Earth Archives Research Centre (PANGEA), School of Biological, Earth and Environmental Sciences (Sydney, Australia)

5. University of Cambridge, Department of Geography, Cambridge, United Kingdom

6. Global Change Research Centre and Masaryk University, Brno, Czech Republic

Abstract

The dynamics of the Late Glacial (LG) have been demonstrated by numerous records from the Northern Hemisphere (NH) and far fewer from the Southern Hemisphere (SH). SH paleoclimate records reveal a general warming trend, interrupted by a deglaciation pause (ACR: Antarctic Cold Reversal, ~14,700 – 13,000 cal BP). Here we present decadal tree-ring stable isotope chronologies ($\delta^{18}O$, $\delta^{13}C$) from New Zealand (NZ) subfossil kauri trees (n=6) covering the post-ACR millennium from 13 020 – 11 850 cal BP. We find a distinct, simultaneous downturn (~12 625 – 12 375 cal BP) in all tree-ring proxies paralleling regional tree growth declines, suggesting a widespread climate deterioration. This downturn was characterised by sustained high precipitation, low temperatures and high relative humidity in NZ with incoming weather fronts from the South Ocean. Despite these promising results, questions remain about what drove the Kauri Downturn and how the hydroclimatic conditions were altered during this time period.

8.1. Introduction

8.1.1 The Late Glacial

Significant attention in paleoclimate research has focussed on the transitional period between the last glaciation and the current Holocene interglacial, known at the Late Glacial (~14,700 – 11,600 cal BP). In the Northern Hemisphere (NH), the gradual warming was interrupted by numerous fast transitions to cold episodes of various lengths. The most prominent millennium-long cold reversal to near glacial conditions is evidenced in Greenland ice core δ18O and deuterium excess (GS-1; Figure 8.1h). This led to significant palynological changes in continental Europe characterizing the so-called Younger Dryas period (YD) (Brauer et al. 2000; Steffensen et al. 2008; Rach et al. 2014). The Southern Hemisphere (SH) however tells a very different story, with the gradual warming continuing until the warm Holocene, with the exception of a brief warming pause during the Antarctic Cold Reversal (ACR, ~14,700 to 13,000 cal BP; Blunier et al. 1997; Pedro et al. 2011; WAIS 2015) (Figure 8.1g) and various decadal oscillations demonstrated in New Zealand (NZ) records (Barrell et al. 2013). Similar hemispheric divergences have been discovered over long-term Glacial-Interglacial cycles across the Quaternary period (Crowley 1992), evidenced as SH warming leading the NH during glacial terminations; due in part to slower melting of NH ice sheets, greatly impacting hemispheric temperatures (Kawamura et al. 2007).

The abrupt NH cold reversal (Younger Dryas onset / beginning of GS-1) at the end of the Late Glacial has been hypothesised to be a result of weakening of the Atlantic meridional overturning circulation (AMOC; Carlson and Clark 2012; Renssen et al., 2015); an Atlantic ocean current system characterised by a northward flow of tropical surface warm waters, which cool and sink in the North Atlantic and eventually reroute back south along the coast of North

America. AMOC weakening can occur as a result of freshening of the North Atlantic (due to ice melt), decelerating the thermosaline-modulated oceanic circulation system. Such weakening would theoretically block warm tropical waters from entering the North Atlantic allowing for reestablishment of sea ice (and GS-1/YD glacial conditions), while concurrently impeding cool deep-water upwelling in the south Atlantic causing SH warming and thus a bipolar divergence in climate. Changes in AMOC activity are hypothesised to be further compounded in the SH by shifts in the southern westerly wind belt and associated ocean currents as the Intertropical Convergence Zone (ITCZ) oscillated across latitudes (Denton et al., 2010). Thus, climate change induced by variations in AMOC and related ocean circulation can lead to a complex and divergent set of conditions between regions and hemispheres (Figure 8.1), also demonstrated in the coupled atmosphere-ocean general circulation model, TraCE-21ka (Supplementary Figure 8.1); referred to as the the "bipolar seesaw" (Stocker et al. 1998).

Figure 8.1. A high-resolution view of the Late Glacial in the Southern Hemisphere. Decadal z-scored chronology (KAU-ISO) of (**a**) $\delta^{13}C_{cell}$ and (b) $\delta^{18}O_{cell}$ and with standard deviation shaded (n_{trees} = 6); (**c**) tree-ring width of full Towai chronology (Palmer et al. 2017) subsetted tolength of KAU-ISO (13 020 - 11 850 cal BP). Kauri downturn (KD) shaded. (**d**) Bars represent individual kauri trees used in this study, with the full length of individual trees in light blue and decadal stable isotope (KAU-ISO) subset in dark blue. (**e**) Lake Hayes sediment record of Ca/Ti (Hinojosa et al. 2019); (**f**) Speleothem $\delta^{13}C$ from New Zealand (Whittaker et al. 2008); (**g**) Antarctic (Talos Dome; Pedro et al. 2011) and (**h**) Greenland (NGRIP, Rasmussen et al. 2013) ice core $\delta^{18}O$ during the Late Glacial with the Antarctic Cold Reversal (ACR) and Greenland Stadial 1 (GS-1; equivalent to the pollen defined Younger Dryas) indicated. Climate stages according to (**i**) Kaigo Bog stratigraphy (Newnham & Lowe 2000; Hajdas 2006), including the Late-glacial mild episode (NZce-4), the Late-glacial cool episode (NZce-3), the Pre-Holocene amelioration (NZce-2) and theHolocene Inter-glacial (NZce-1); Time according to GICC05 (years before 1950).

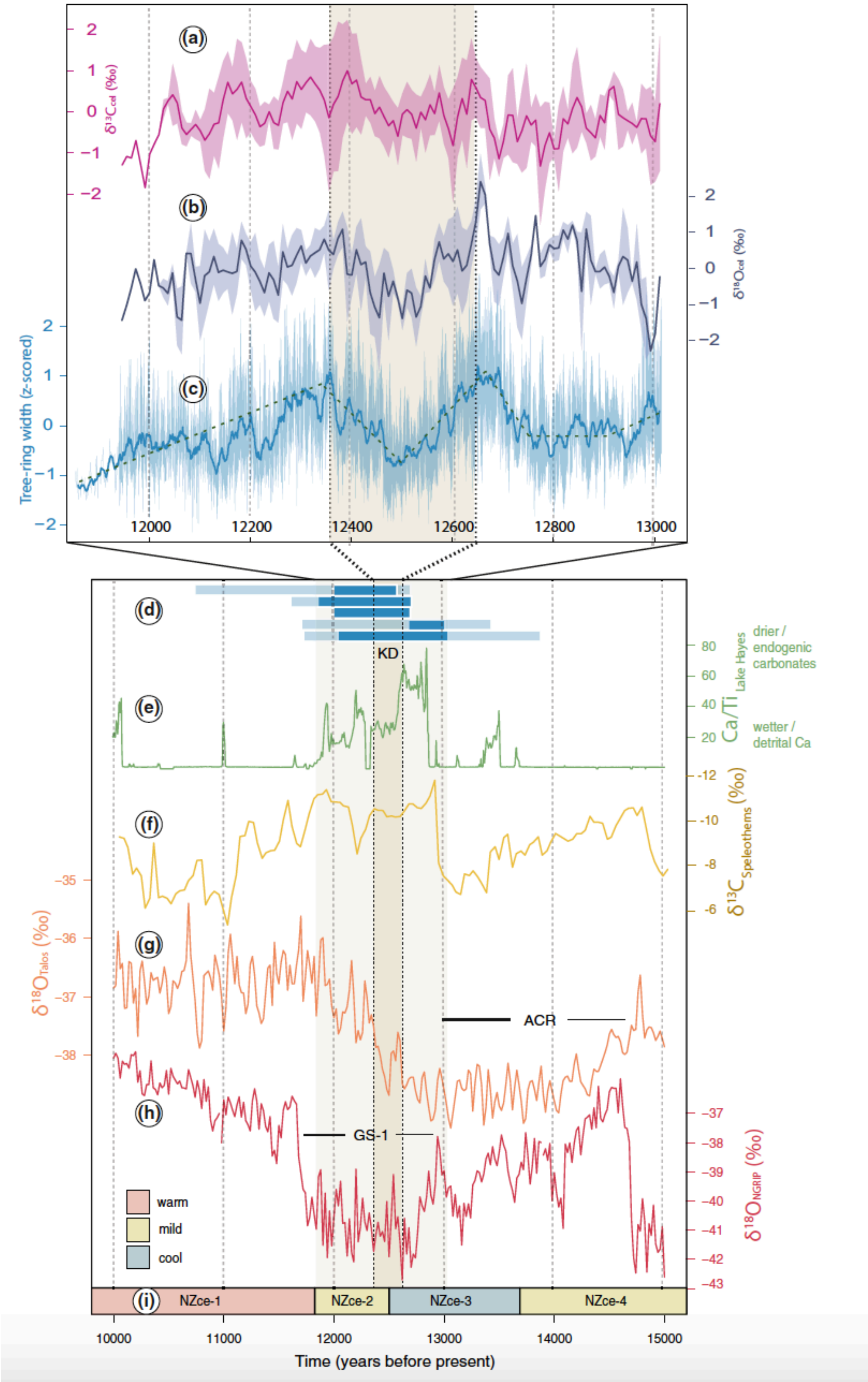
(a)
(b)
(c)
(d)
(e)
(f)
(g)
(h)
(i)
δ13Ccel (‰)
δ18Ocel (‰)
Tree-ring width (z-scored)
KD
Ca/Ti Lake Hayes
drier / endogenic carbonates
wetter / detrital Ca
δ13C Speleothems (‰)
δ18O Talos (‰)
ACR
GS-1
δ18O NGRIP (‰)
warm
mild
cool
NZce-1
NZce-2
NZce-3
NZce-4
Time (years before present)

8.1.2 LG climate downturns. Southern vs. Northern hemisphere

While the triggers of LG cold episodes are still under debate, numerous climate records in the NH have been established to understand the impact and regionality of cold episodes across the Late Glacial. These records (Lauterbach et al. 2011; von Grafenstein et al. 1999; Brauer et al. 2000; Merkt & Muller 1999) demonstrate long-term and low frequency temperature variability similar to Greenland ice cores (Steffensen et al. 2008; Rasmussen et al. 2014), with some regional differences in the rate, magnitude and timing of climate events (e.g. Pauly et al., 2018; Rach et al. 2014). Conversely, the southern hemisphere has far fewer paleoclimate records available covering this interesting climate period, with only a handful of relevantly high (decadal) temporal resolution (e.g. Hajdas et al., 2006; De Deckker et al., 2012, etc; Figure 8.1). During the YD phase, when the NH plunged into cold conditions, Antarctica experienced a warming trend. Antarctic ice core $\delta^{18}O$ (e.g. Pedro et al. 2011), reconstructed Southern Ocean sea surface temperature (Correge et al., 2004) and New Zealand glacier retreat (Kaplan et al., 2010) argue for steadily increasing temperatures between ~12 900 – 11 800 cal BP in the SH. Southern Australia ocean core data suggests this warm phase was regionally modulated by an oscillating Subtropical Front (STF), permitting a millennial flickering of the Leeuwin Current (LC) strength across southern Australia past Tasmania (De Deckker et al. 2012). This STF activity ultimately impacted regional temperature and precipitation patterns during distinct phases. During one such interval (~12 500 – 12 380 cal BP), Tasmanian huon pine (Lagarostrobus franklinii) and New Zealand kauri (Agathis australis) trees show significant centennial-long growth depressions (Hua et al., 2009; Palmer et al., 2016; Figure 8.1c) which may be related to a changed state of the mid-latitude Southern Ocean and related El Niño-Southern Oscillation (ENSO) activity (Palmer et al. 2016). Locally, this interval parallels a conversion from a dry ACR to relatively wet conditions at Lake Hayes in South Island NZ (Hinojosa et al. 2019; Figure 8.1e). In North Island, this short period represents a transition from the late-glacial cool episode (NZce-3) to the pre-Holocene amelioration (NZce-2) according to Kaipo bog stratigraphy (Figure 8.1i; Newnham & Lowe 2000; Hajdas 2006; Barrell et al. 2013) as well as wet, cool conditions recorded in Ruakuri Cave speleothems during Heinrich Event 0 (Whittaker et al. 2008; Figure 8.1f). Regionally, a short-term depletion in Talos ice core $\delta^{18}O$ (Figure 8.1g; ~12 580 – 12 380 cal BP), and Law ice core $\delta^{18}O$ (Pedro et al. 2011; ~12 540 – 12 320 cal BP) may provide hints of the climate deterioration in Eastern Antarctica; although it generally appears to be independent of the Atlantic and West Antarctic regions, with no significant signal visible in Western Antarctica (EDML, Siple and Bryd ice cores; Pedro et al. 2011). Palmer et al. (2016) hypothesised this tree growth downturn was followed by a strengthening of ENSO expression in the region and/or solar variability. However, due to the limited climate records existing over this period and the limited age control of New Zealand records, the climatological characteristics of this centennial-duration event remain under debate.

8.1.3 Kauri trees as a climate archive

New Zealand kauri (Figure 8.2ab) trees are southern hemisphere conifers which can grow for multiple millennia (Palmer et al., 2016) and thrive in warm-temperate lowlands regions. Due to their long lifespan, annual rings and sensitivity to summer climate indices, Kauri trees are an important bioarchive. Studies include living kauri trees (Fowler et al., 2004; Ogden and Ahmed 1989), archaeological timber (Boswijk et al., 2006), as well as ancient material (e.g. Lorrey and Ogden, 2005; Turney et al., 2010; Palmer et al., 2016) dating as far as 60,000 years before present. Tree-ring width chronologies of kauri have demonstrated a connection with ENSO activity in modern times (Fowler et al., 2007, 2000) as well as during the Holocene (Fowler et al., 2012) and the Late Glacial (Palmer et al., 2016).

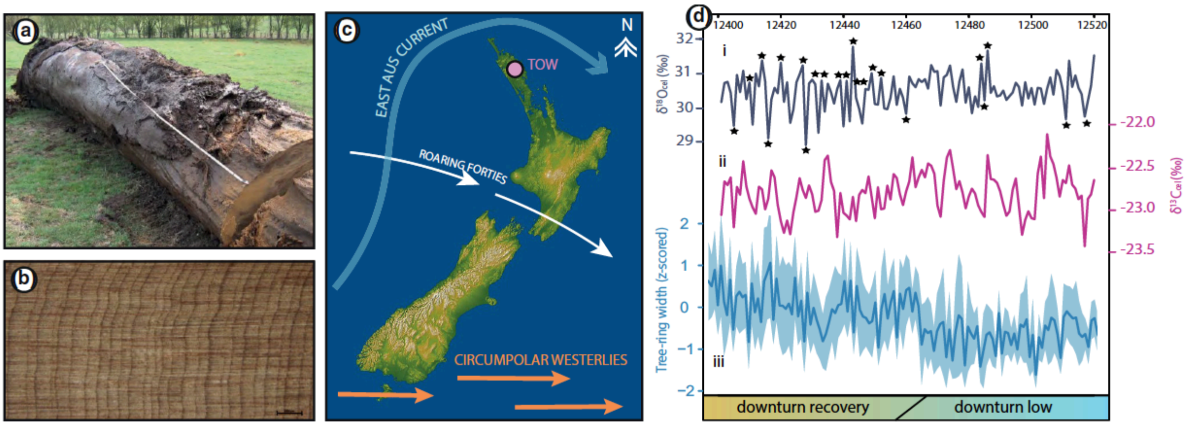

Figure 8.2. Kauri tree characteristics, site and annual variability. (**a**) Stump of kauri tree found on Towai farm; (**b**) close-up of individual tree-rings; (**c**) climate situation in New Zealand with site location (TOW) indicated; (**d**) annual (**i**) $\delta^{18}O_{cell}$ (**ii**) $\delta^{13}C_{cell}$ (**iii**) and tree-ring width (z-scored) of a single tree during the latter half of the Kauri Downturn; stars represent annual variability >1‰.

The sensitivity of kauri to summer season (November – February; NDJF) hydroclimate indices have been further explored through stable isotope analysis of modern kauri cellulose (e.g. Lorrey et al., 2016; Brookman 2014; Text S8.7). Brookman (2014) demonstrated the concurrent sensitivity of $\delta^{18}O$ and $\delta^{13}C$ from kauri tree-ring cellulose ($\delta 13C_{cell}$, $\delta^{18}O^{cell}$) to various climate parameters in the summer, including positive correlations to mean temperature (r_o = 0.70, r_c = 0.89), solar radiation (r_o = 0.64, r_c = 0.89) and soil moisture (r_o = 0.71, r_c = 0.84), as well as negative correlations to rainfall (r_o = -0.33, r_c = -0.22) and relative humidity (r_o = -0.41, r_c = -0.65). Lorrey et al. (2016; 2018) also found a correlation between $\delta^{18}O_{cell}$ and the SOI indicating that kauri $\delta^{18}O_{cell}$ may be a useful proxy of past ENSO conditions. While both $\delta^{18}O_{cell}$ and $\delta^{13}C_{cell}$ in kauri tend to be similarly sensitive to the abovementioned climate variables, age-related offsets as well as divergences in microclimate conditions can introduce complexities into the $\delta^{13}C_{cell}$ record (Brookman 2014) as described in other Late Glacial records (Pauly et al. 2020).

By using kauri tree-ring stable isotopes, we aim to investigate the hydroclimate state of North Island during the post-ACR millennium (13 020 – 11 850 cal BP) and identify the radiation of ocean-atmospheric dynamics and expression of ENSO in the SH by exploring connections amidst other regional records. Using a dual stable isotope modelling approach, we analyse $\delta^{18}O$ and $\delta^{13}C$ to interpret the growing season climate conditions present before, during and after a distinct growth depression (~12 625 – 12 375 cal BP, Figure 8.1c).

8.2. Methods

8.2.1 Subfossil kauri chronology

Here we present a dual stable isotope chronology (carbon and oxygen) developed from tree-ring cellulose extracted from subfossil trees discovered near Towai in Northland, New Zealand (35°30.3930S, 174°10.3760E; Figure 8.2c; Text S8.8). A subset of trees (n_{trees} = 6) has been chosen (based on a minimum required to develop a strong climate signal from $\delta^{18}O_{cell}$; Lorrey et al. 2016) from a floating tree-ring chronology (Towai), which covers 13 134 – 11 694 cal BP (n_{trees} = 37, 1σ error of ±7 years; Hogg et al., 2016).

This period spans the Greenland Isotope defined GS-1 (Rasmussen et al., 2014) and pollen defined NH Younger Dryas (e.g. Björck et al. 1998), immediately following the SH Antarctic Cold Reversal (ACR) (Figure 8.1) and spanning the SH 'Late-glacial cool episode' into the 'pre-Holocene amelioration (Barrell et al. 2013) defined by NZ bog pollen (Newnham and Lowe, 2000; Hajdas et al. 2006; Lowe et al. 2008, 2013).

The stable isotope chronology (KAU-ISO) is of decadal resolution with a sample replication of 4-6 trees for the majority of the chronology (56%; 670 years), with some periods having a replication of 3 trees (28%; 280 years) and even less with a replication of 1-2 (15%; 160 years) (Figure 8.1d). The subset of trees were chosen for this work as an initial investigation into the potential to reconstruct climate during the Late Glacial with kauri trees.

The tree-ring width chronology (Palmer et al., 2016) with which this dendroisotope data was developed, hypothesised a connection between a distinct growth depression (~12 625 – 12 375 cal BP) and subsequent increased intensity in ENSO activity. Trees used here were growing before, during and after this peculiar 250 year-long growth depression (Palmer et al., 2016), which we aim to further explore in this study.

8.2.2 Cellulose extraction and stable isotope analysis

Cellulose was extracted from wholewood material of 10-year blocks of tree rings (Wieloch et al. 2011; Schollaen et al. 2017) from individual trees covering 13 020 – 11 850 cal BP, which is a subset of the Towai tree-ring chronology. Annual stable isotopes were also measured from an individual tree, covering mid-point of the growth depression, between 12 520 – 12 400 cal BP (Figure 8.2d). The samples were homogenized and freeze-dried prior to being weighed and packed (silver capsules (ø3.3x4mm) for stable isotope measurement (Delta V, Thermofisher Scientific Bremen; coupled with TC/EA HT at 1400°C). The measurements were not pooled between trees, only within the 10-year blocks. Results were compared against international and lab-internal reference material (IAEA-CH3, IAEA-CH6 and Sigma-Aldrich Alpha-Cellulose) using two reference standards with widespread isotopic compositions for a single-point normalisation (Paul, Skrzypek, and Forizs 2007). Final isotope ratios are given in δ value, relative to VSMOW ($\delta^{18}O$) and VPDB ($\delta^{13}C$), with replication reproducibility of ±0.3‰ ($\delta^{18}O$) and ±0.15‰ ($\delta^{13}C$).

8.2.3 TraCE-21ka climate model outputs

The time interval covered by KAU-ISO was investigated using TraCE-21ka, a coupled atmosphere-ocean general circulation model - which simulates global climate evolution between the Late Glacial Maximum (LGM: 21,000 years before present) to modern times - using the Community Climate System Model version 3 (CCSM3). Three periods of time were examined: (1) Pre-downturn (12 800 cal BP), (2) Kauri Downturn (12 500 cal BP), and (3) Post-downturn (12 200 cal BP), and four climate variables: annual (1) relative humidity, (2) precipitation, (3) temperature, and (4) sea level pressure. The modelling was completed over the SH summer season (November - February), when kauri trees exhibit growth (Ecroyd 1982). Climate model outputs were visualised using PaleoView v1.5.1 with a user defined geographic region (covering Australia, New Zealand and a portion of the Southern Ocean) and changes relative to 10,000 cal BP.

8.3. Results

8.3.1 Stable isotope & tree-ring chronologies

8.3.1.1 Decadal stable isotope record

Stable oxygen ($\delta^{18}O_{cell}$) and carbon ($\delta^{13}C_{cell}$) records of tree-ring cellulose average ~30.6‰ and ~ -22.0‰ with ranges of 4.3‰ (28.3 to 32.6‰) and 3.8‰ (-20.3 to -24.1‰) and inter-decadal variability of 0.66‰ and 0.37‰, respectively. Inter-tree correlation for $\delta^{18}O_{cell}$ and $\delta^{13}C_{cell}$ is not consistent; ranging between -0.76 to +0.88 for $\delta^{18}O_{cell}$ and -0.44 to +0.80 for $\delta^{13}C_{cell}$ (Table S8.1, Figure S8.2).

Decadal mean $\delta^{18}O_{cell}$ and $\delta^{13}C_{cell}$ records were developed from the individual tree-ring records with an average standard deviation of 0.89 for δ18Ocel and 0.70 for $\delta^{13}C_{cell}$. Correlations between mean $\delta^{18}O_{cell}$ and $\delta^{13}C_{cell}$ are strongly positive during much of the dataset, with 38% of the dataset demonstrating correlation coefficients above +0.4, a high of +0.82 and absolute average of 0.36 (Figure S8.2).

During the first 350 years of the chronology (~13 000 - 12 650 cal BP), mean $\delta^{18}O_{cell}$ exhibits an increasing trend with a peak at ~12 650 - 12 640 cal BP (Figure 8.1b), while mean $\delta^{13}C_{cell}$ demonstrates a plateau within a relatively negative anomaly with a similar (albeit less extreme) peak at 12 640 cal BP (Figure 8.1a). Similar to the previously reported tree-ring width downturn (Palmer et al. 2016; Figure 8.1c), $\delta^{18}O_{cell}$ and $\delta^{13}C_{cell}$ from KAU-ISO show concurrent and significant depletions between approximately 12 630 – 12 380 cal BP. This set of depletions begin with a peak (maximum of the entire sequence for $\delta^{18}O_{cell}$) around 12 630 cal BP, followed by a steady decline, with deepest point centred ~12 450 cal BP. This event sequence will hereafter be referred to as the "Kauri Depression" (KD). All tree-ring parameters (width, $\delta^{18}O_{cell}$, $\delta^{13}C_{cell}$) recover, peaking at ~12 380 cal BP and then continue slow decline until the end of the chronology at 11 850 cal BP.

Mean inter-tree correlations for $\delta^{18}O_{cell}$ are higher during the downturn (average = 0.22, range = -0.07 to +0.55), compared with pre- and post- downturn; $average_{pre}$ = -0.23, $range_{pre}$ = -0.76 to +0.07, $average_{post}$ = +0.07, $range_{post}$ = -0.22 to +0.28. Conversely, inter-tree correlations for δ13Ccel are equivalent pre- and during downturn ($average_{pre}$ = 0.13, $range_{pre}$ = -0.44 to +0.80, $average_{downturn}$ = 0.13, $range_{downturn}$ =-0.26 to +0.48, respectively) and relatively higher post-downturn (average = +0.28, range$_{post}$ = -0.27 to +0.64). Slightly higher inter-tree correlations have been found modern kauri stable isotope chronologies of $\delta^{18}O_{cell}$ and $\delta^{13}C_{cell}$, with a correlation of 0.21-0.64 for $\delta^{18}O_{cell}$ (Brookman 2014, Lorrey et al. 2016) and 0.35 for $\delta^{13}C_{cell}$ (Brookman 2014).

8.3.1.2 Annual stable isotope record

Dual isotopes of a single tree were analysed covering the latter half of the KD (12 520 – 12 400 cal BP) to provide information on the inter-annual variability of $\delta^{18}O_{cell}$ and $\delta^{13}C_{cell}$ during this climate "event" (Table S2). This tree displayed a range of $\delta^{18}O_{cell}$ values of only 2.9‰ (28.9 to 31.8‰), which is much more limited than modern kauri $\delta^{18}O_{cell}$ values which demonstrate an 8‰ range (28.8 to 36.8‰) according to Brookman (2014). Based on similarities between the absolute values of the isotopic records, tree species and location, we assume similar seasonal trends identified in Brookman (2014) would also impact the annual dataset presented in this study.

8.3.2 Climate Model

Whilst precipitation and relative humidity can be estimated from the kauri records in this study, information on temperature and sea level pressure, as well as spatial trends of all parameters, were further investigated using Paleoview software to visualise TRaCE21ka data. The TRaCE21ka model outputs confirm that a phase of high relative humidity and high precipitation in SH summer (NDJF) occurred in NZ during the downturn (~12 500 cal BP) compared to pre- and post- downturn (12 800 cal BP and 12 200 cal BP, respectively), matching the results of KAU-ISO.

8.4. Discussion

8.4.1 Stable isotope chronologies

The decadal stable isotope chronologies (KAU-ISO, 13 020 – 11 850 cal BP) from kauri tree-rings reflected similar means and ranges compared to modern studies (Brookman 2014). Inter-tree correlations varied throughout the record (Figure S8.1), potentially due to the pooling of decadal tree-rings within individual trees; pooling has been shown to hide bias of individual trees which deviate from the population signal (Liñán et al. 2011). Trees showed more significant correlations between individual trees for δ13Ccel measurements over $\delta^{18}O_{cell}$, in contrast to other subfossil (Pauly et al. 2018, 2020) stable isotope studies, which generally show stronger population signals in $\delta^{18}O_{cell}$ data. Despite individual tree differences, mean $\delta^{18}O_{cell}$ and $\delta^{13}C_{cell}$ demonstrate strong correlations (38% of chronology >0.4; Figure S8.2), reflecting a set of interdependent variables within the climate system and similar long-term trends.

Annual values of $\delta^{18}O_{cell}$ tend to be more enriched (mean = 30.5‰) than concurrent decadal $\delta^{18}O_{cell}$ values (mean = 29.7‰). This is likely due to the temporal bundling of depleted rainfall (low $\delta^{18}O$) conditions as a result of persistent, widespread and low frequency (decadal) atmospheric oscillations occurring over the climate downturn. Similar statistics have been reported in relation to modern rainfall extremes and related long-term climate modes in the region (e.g. Aryal et al., 2009; Grimm and Tedeschi 2009; Willems 2013).

8.4.2 Climate downturn conditions in New Zealand

The simultaneous downturn (KD) in multiple tree-ring proxies (tree-ring width, $\delta^{18}O_{sw,}$ $\delta^{18}O_{cel}$ and $\delta^{13}C_{cell}$) from our kauri chronology suggests that they are all sensitive to the variability of a single (or set of interacting) climate parameters. Based on modern intra-annual calibrations of the kauri trees from NZ (Brookman 2014), we suspect a decline in growing season temperature, concurrent with an increase in relative humidity and change in precipitation source are responsible for this downturn within the tree-ring and stable isotope signals.

Inter-tree correlations for $\delta^{18}O_{cell}$ are highest during KD (Figure S8.2) compared to drier and warmer pre- and post- KD periods. Previous studies of Late Glacial subfossil trees (Pauly et al. 2018, 2020) have demonstrated stronger inter-tree $\delta^{18}O_{cell}$ correlations during phases of anomalously low $\delta^{18}O_{cell}$ (assumed to be higher precipitation and/or precipitation from a depleted source), likely due to the reduced influence of stomata-driven fractionation on $\delta^{18}O_{cell}$ (Pauly et al. 2020). Indeed, the $\delta^{13}C_{cell}$ demonstrates the lowest inter-tree correlation during the humid KD, suggesting the trees are less sensitive to stomata dynamics controlling $\delta^{13}C_{cell}$ over this interval. Whilst we assume atmospheric conditions are the main driver in kauri stable isotope variability, we cannot rule out groundwater as being another factor modulating sourcewater uptake.

At annual resolution, during the deepest depression in the tree-ring data, $\delta^{18}O_{cell}$ shows low inter-annual variability (12 520 – 12 450 cal BP, Figure 8.2d) and low tree-ring growth. Trees then show an abrupt increase in growth and the inter-annual variability of $\delta^{18}O_{cell}$ increases considerably (12 450 – 12 400 cal BP), with instances of inter-annual $\delta^{18}O$ changes >1‰ increasing by more than 3-fold. Modern NZ precipitation exhibits extremes every ~2.9 years (Ummenhofer and England, 2007), whereas data in this study show KD extremes at a rate 1 every 12 years and recovery extremes of 1 in every 3-4 years (Figure 2d). Within the Late Glacial context, dendroisotope records from southern France have revealed similar increases in inter-annual tree-ring $\delta^{18}O$ (+0.2‰ absolute) as a result of the oscillating movement of the polar front at the onset of the Younger Dryas (Pauly et al. 2018).

The similar variability exhibited in modern and ancient kauri tree $\delta^{18}O_{cell}$ and lack of annual or decadal $\delta^{18}O_{cell}$ extremes during the downturn argue against intermittent, flooding as a driver of the depressed tree growth in the region. Furthermore, the tree proxy records do not contain any evidence of flood conditions, which would result in a cessation of growth (rather than a growth depression) as trees would be unable to take up water in anoxic, flooded conditions (Schöngart et al., 2002). Such circumstances have resulted in the destruction of other kauri forests and shortened tree lifespans, leading to swamp preservation of kauri stumps throughout Northland and the Waikato lowlands following extreme storm events (e.g. Green et al. 1985; Ogden et al. 1992; Boswijk et al. 2005). In the case of the kauri in this study, they continued to grow following the depression.

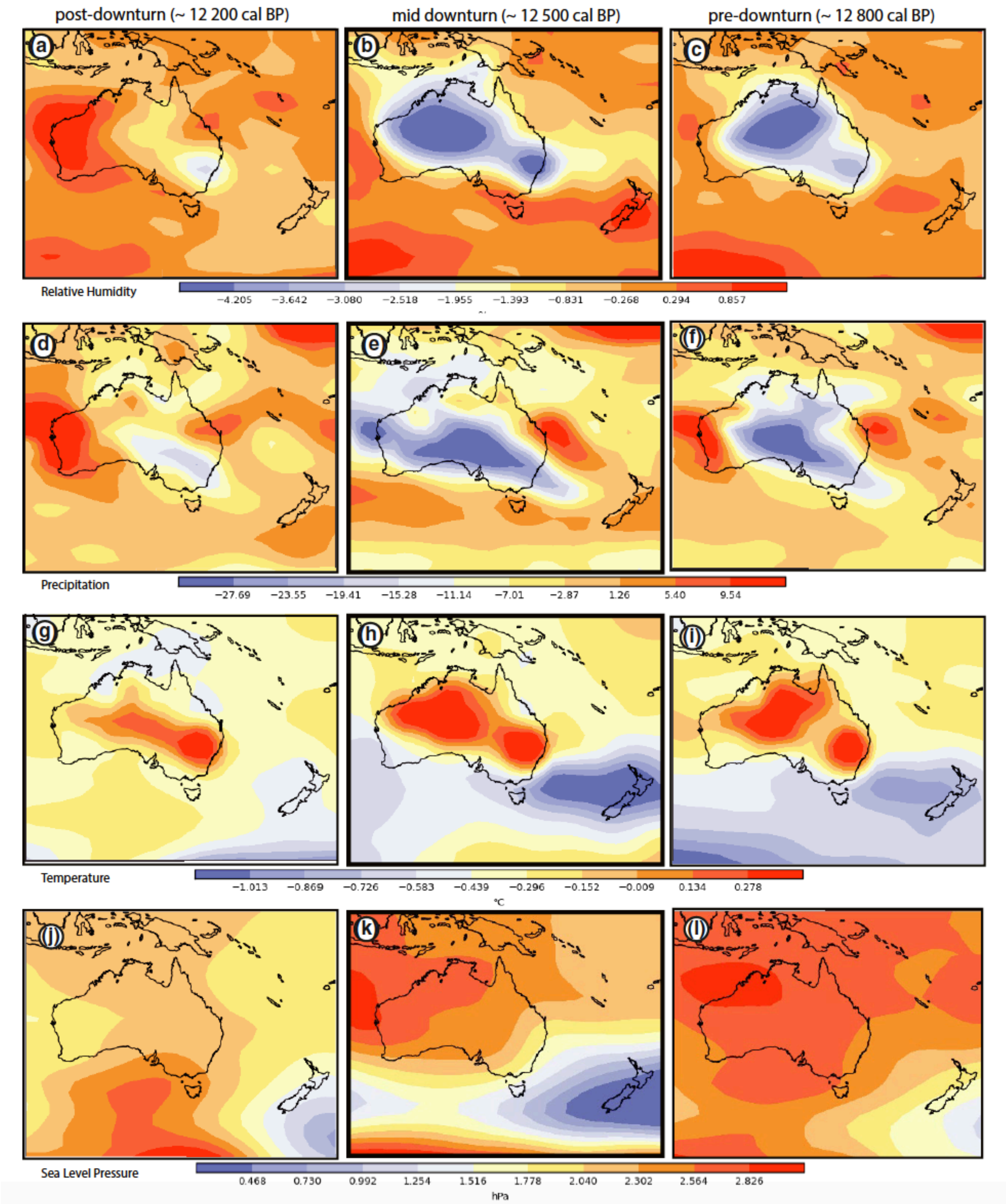

Figure 8.3. The Late Glacial in the South Pacific demonstrated by coupled atmosphere-ocean general circulation TraCE-21ka. (**a-c**) relative humidity, (**d-f**) precipitation, (**g-i**) temperature and (**j-l**) sea level pressure in three periods: pre-downturn (12 800 cal BP), mid-downturn (12 500 cal BP) and post-downturn (12 200 cal BP).

8.4.3 Combining climate model outputs with dual-isotope theory

Kauri trees thrive in cool and dry summer conditions; yet the trees in this study reveal a prolonged period of unfavourable conditions (moist, cool summers) for kauri growth. Such basic hydroclimate conditions from a modern perspective would be equivalent to a phase of increased La Niña frequency (cold phase of ENSO). However, the climate model (TrACE21ka, Figure 8.3) output during the downturn offers additional climate variables, providing strong evidence against a prolonged phase of La Niña activity (Table S8.3).

Kauri tree-rings show reduced growth (low tree-ring width) with high humidity (depleted $\delta^{18}O_{cell}$ and $\delta^{13}C_{cell}$) and increased precipitation (depleted $\delta^{18}O_{cell}$ and $\delta^{13}C_{cell}$) during the downturn based on dual-isotope theory (Scheidegger et al. 2000). The TRaCE21ka model provides additional evidence of low temperatures and low sea level pressure conditions being prevalent during the downturn. Together, the model outputs and KAU-ISO reconstructions support the theory of a regional-scale climate deterioration (Palmer et al. 2016).

The model-predicted low sea level pressure, increased southerly airflow (via incoming air masses) and cooler temperatures spanning the downturn are uncharacteristic of La Niña, leaving the period without a clear modern analogue. Rather, it is more likely that sustained low-pressure conditions (Figure 3k) occurred in New Zealand over the downturn. Areas of low pressure (depressions) in the region would lead to high precipitation, low temperatures and high relative humidity compared to pre- and post- downturn periods, as evidenced in Figure 8.3. In particular, weather fronts from the South Ocean (Antarctica) would bring about isotopically depleted rain, creating the continuous depletion in $\delta^{18}O_{cell}$, reflecting sourcewater.

Mean $\delta^{18}O_{cell}$ and $\delta^{13}C_{cell}$ show higher correlations (Figure S8.2) during and after the downturn compared to before, signifying that the interacting climate variables (temperature, relative humidity and precipitation) are picked up more strongly in the kauri trees during the extreme climate interval compared to the preceding average conditions. Pauly et al. (2020) showed stronger dual isotope correlations in subfossil trees during wetter conditions (higher precipitation, higher humidity) in the NH due to reduced leaf level fractionation (^{18}O enrichment) resulting from partial stomata closure. We expect similar results here as the pre-downturn period represents average dry conditions in NZ compared to cooler, wetter conditions during and following KD (as recorded in KAU-ISO and TRaCE21ka).

Modern hydroclimate models suggest that anomalous wet years across New Zealand correspond to below average sea surface temperatures and low sea level pressure across and south of New Zealand (latitude 30-60º band; Ummenhofer and England 2007), similar to the downturn model output. These conditions have been shown to occur as a result of an alteration in atmospheric circulation, with equatorial shifts in and weakening of the westerlies as well an increase in incoming (south eastern) polar winds (Ummenhofer and England 2007). Given the similarity between these modern model results and those from this study (in terms of temperature, sea level pressure and precipitation), we hypothesise the downturn was a result of a similar change in atmospheric circulation. As downturn subsided, westerlies would have theoretically strengthened and moved poleward, warming the 30-60º latitude band region.

8.4.4 Proxy landscape during the Late Glacial

8.4.4.1 Proxy records in New Zealand

During KD, coral records in the South Pacific reveal a period of relatively low SST (Corrège et al., 2004), concurrent with a flickering of the Leeuwin Current (De Deckker et al. 2008) impacting flow of westerlies across NZ. Furthermore, a sediment record Lake Hayes in southisland NZ (Hinojosa et al. 2019) recorded a short-term drop in Ca/Ti around 12 500 cal BP (Figure 1e), representing an increase in detrital input and relatively humid/wet conditions (decreased evapouration); compared to the generally dry conditions during the post ACR interval locally (12 900 – 11 600 cal BP).

This period of cool, wet conditions occurs at the transition between the local "Late-glacial cool episode" (NZce-3; 13 740 – 12 550 cal BP) and the "pre-Holocene amelioration" (NZce-2; 12 550 – 11 880 cal BP), according to NZ INTIMATE climate event stratigraphy (Barrell et al. 2013; Figure 8.1i), as described across North Island (Lowe et al., 2008, 2013). Synchronous downward trends in pollen and SST at the onset of NZce-2 - reconstructed from an east Tasmanian Sea core (MD06-2991) and Okarito Bog, respectively - suggest an ocean-atmosphere coupling of conditions occurred in the region (Ryan 2017).

A short-lived, mild depletion in Antarctic ice core $\delta^{18}O$ (Figure 8.1g) is evident at the time of the KD – particularly in east Antarctic (e.g. Law and Talos; Pedro et al. 2011) – but is difficult to tie to NZ proxy records due to potential dating uncertainties, coarse (multi-decadal) temporal resolution as well as the fact that the proxies record different seasons. Given the more complex climate parameters influencing NZ (e.g. polar and subtropical air masses, zonal westerlies) compared to Antarctica, one would expect a higher quantity of climate oscillations occurring in this region compared to those recorded in Antarctic ice cores (Barrell et al. 2013). While a general climate transition between the cool Late-glacial and warm Holocene is clear from the available NZ records, the KAU-ISO record suggests this climate conversion involved a significant and prolonged (multi-centennial) hydroclimate shift in NZ. However, the climate drivers and high-resolution dynamics of this interval are difficult to interpret.

8.4.4.2 Ocean-atmosphere teleconnections

An atmospheric $\Delta^{14}C$ rise in the SH has been associated with the onset of the Younger Dryas (increased ^{14}C at ~12 740 cal BP; Hua et al. 2009). This is followed by a few centuries of high variability, including a short-lived peak at ~12 600, concurrent with the onset of KD. Hua et al. (2009) hypothesised that the lack of uniformity between SH terrestrial (Hua et al. 2009), Pacific (Edwards et al. 1993; Bard et al. 1998, 2004; Burr et al. 1998, 2004) and Atlantic (Hughen et al. 2004; Fairbanks et al. 2005) $\Delta^{14}C$ datasets during the early YD peak imply this period initiated as a result of ocean circulation changes rather than ^{14}C (solar) production rate. This delayed peak in tree-ring $\Delta^{14}C$ (compared to marine $\Delta^{14}C$; Hua et al. 2009) is concurrent with the KD onset (this study and Palmer et al. 2016), suggesting the ocean circulation changes may have driven this climate deterioration recorded in kauri trees on land. This theory is corroborated by the modelled incoming polar winds and related drops sea surface temperature (Figure 8.3).

Whilst ^{10}Be-modelled $\Delta^{14}C$ (representing atmospheric $\Delta^{14}C$ unaltered by ocean reservoirs; Hua et al. 2009) underestimates tree-ring $\Delta^{14}C$ at the onset of the YD, it closely follows tree-ring $\Delta^{14}C$ along the KD timeline a couple centuries later (~12 600 – 12 400 cal BP). This hints that either (1) solar variability and/or (2) the release of ^{14}C-depleted oceanic CO_2 from the Southern Ocean (Marchitto et al. 2007), likely acted to sustain the climate downturn in New Zealand after the initial (global) ocean circulation trigger, similar to solar variability modulated climate during the Little Ice Age (Grey et al. 2010 and references therein). While the available SH atmospheric CO_2 records from ice cores (e.g. Marcott et al. 2014) are of low temporal resolution (multi-decadal) during this interval, they do indicate an increase following the Antarctic Cold Reversal plateau, substantiating the CO_2 release theory. Furthermore, other studies have suggested that climate deteriorations may be amplified through anomalous sea surface temperatures, thereby driving persistent atmospheric circulation states lasting for decades to centuries (van Geel et al. 2003).

8.5. Conclusions

The subfossil kauri tree-ring width and stable isotopes, in addition to climate model outputs from this study provide further evidence of spring/summer hydroclimate conditions during the YD/GS-1 in the SH, complementing the previously constructed kauri tree-ring width record (Palmer et al. 2016). While the millennial-length Younger Dryas cold reversal is not strongly demonstrated in SH paleoclimate records, variability in tree-ring ^{14}C (Hua et al. 2009) and the Kauri Downturn (this study and Palmer et al. 2016) imply that ocean circulation changes triggered a shorter climate deterioration lasting for at least two and a half centuries (~12 625 – 12 375 cal BP) over this time interval. Such conditions are generally reflected in regional lake and ocean sediment records, albeit at lower temporal resolution. Despite these promising results, questions remain about what factors drove and modulated the Kauri Downturn and how the NZ hydroclimate regime progressed into the early Holocene climate amelioration.

8.6 References

1. Araguás-Araguás, L., Froehlich, K. and Rozanski, K., 2000. “Deuterium and oxygen-18 isotope composition of precipitation and atmospheric moisture”. *Hydrological processes*, 14(8), pp.1341-1355.

2. Aryal, S.K., Bates, B.C., Campbell, E.P., Li, Y., Palmer, M.J. and Viney, N.R., 2009. “Characterizing and modeling temporal and spatial trends in rainfall extremes”. *Journal of Hydrometeorology*, 10(1), pp.241-253.

3. Baisden, W.T., Keller, E.D., Van Hale, R., Frew, R.D. and Wassenaar, L.I., 2016. Precipitation isoscapes for New Zealand: enhanced temporal detail using precipitation-weighted daily climatology. *Isotopes in environmental and health studies*, 52(4-5), pp.343-352.

4. Bard, E., Arnold, M., Hamelin, B., Tisnerat-Laborde, N. and Cabioch, G., 1998. Radiocarbon calibration by means of mass spectrometric 230 Th/234 U and 14 C ages of corals: an updated database including samples from Barbados, Mururoa and Tahiti. *Radiocarbon*, 40(3), pp.1085-1092.

5. Bard, E., Rostek, F. and Ménot-Combes, G., 2004. Radiocarbon calibration beyond 20,000 14C yr BP by means of planktonic foraminifera of the Iberian Margin. *Quaternary research*, 61(2), pp.204-214.

6. Barrell, D.J., Almond, P.C., Vandergoes, M.J., Lowe, D.J., Newnham, R.M. and INTIMATE members, 2013. A composite pollen-based stratotype for inter-regional evaluation of climatic events in New Zealand over the past 30,000 years (NZ-INTIMATE project). *Quaternary Science Reviews*, 74, pp.4-20.

7. Björck, S., Walker, M.J., Cwynar, L.C., Johnsen, S., Knudsen, K.L., Lowe, J.J. and Wohlfarth, B., 1998. An event stratigraphy for the Last Termination in the North Atlantic region based on the Greenland ice-core record: a proposal by the INTIMATE group. *Journal of Quaternary Science*: Published for the Quaternary Research Association, 13(4), pp.283-292.

8. Blunier, T., Schwander, J., Stauffer, B., Stocker, T., Dällenbach, A., Indermühle, A., Tschumi, J., Chappellaz, J., Raynaud, D. and Barnola, J.M., 1997. Timing of the Antarctic Cold Reversal and the atmospheric CO2 increase with respect to the Younger Dryas event. *Geophysical Research Letters*, 24(21), pp.2683-2686.

9. Boswijk, G., 2005. A history of kauri. Australia and New Zealand Forest Histories. Araucarian Forests, Australian Forest History Society, Kingston, Australia, pp.19-26.

10. Boswijk, G., Fowler, A., Lorrey, A., Palmer, J. and Ogden, J., 2006. Extension of the New Zealand kauri (Agathis australis) chronology to 1724 BC. *The Holocene*, 16(2), pp.188-199.

11. Brauer, A., Günter, C., Johnsen, S.J. and Negendank, J.F., 2000. Land-ice teleconnections of cold climatic periods during the last Glacial/Interglacial transition. *Climate Dynamics*, 16, pp.229-239.

12. Brookman, T.H., 2014. Stable isotope dendroclimatology of New Zealand kauri (Agathis australis (D. don) lindl.) and cedar (Libocedrus bidwillii hook. F.). PhD Thesis, *University of Canterbury*, New Zealand.

13. Burr, G.S., Beck, J.W., Taylor, F.W., Récy, J., Edwards, R.L., Cabioch, G., Corrège, T., Donahue, D.J. and O'malley, J.M., 1998. A high-resolution radiocarbon calibration between 11,700 and 12,400 calendar years BP derived from 230 Th ages of corals from Espiritu Santo Island, Vanuatu. *Radiocarbon*, 40(3), pp.1093-1105.

14. Burr, G.S., Galang, C., Taylor, F.W., Gallup, C., Edwards, R.L., Cutler, K. and Quirk, B., 2004. Radiocarbon results from a 13-kyr BP coral from the Huon Peninsula, Papua New Guinea. *Radiocarbon*, 46(3), pp.1211-1224.

15. Carlson, A.E. and Clark, P.U., 2012. Ice sheet sources of sea level rise and freshwater discharge during the last deglaciation. *Reviews of Geophysics*, 50(4).

16. Correge, T., Gagan, M.K., Beck, J.W., Burr, G.S., Cabioch, G. and Le Cornec, F., 2004. Interdecadal variation in the extent of South Pacific tropical waters during the Younger Dryas event. *Nature*, 428(6986), pp.927-929.

17. Crowley, T.J., 1992. North Atlantic deep water cools the Southern Hemisphere. Paleoceanography, 7(4), pp.489-497.

18. Dansgaard, W., 1964. Stable isotopes in precipitation: *Tellus*, v, 16.

19. Denton, G.H., Anderson, R.F., Toggweiler, J.R., Edwards, R.L., Schaefer, J.M. and Putnam, A.E., 2010. The last glacial termination. *Science*, 328(5986), pp.1652-1656.

20. De Deckker, P., Moros, M., Perner, K. and Jansen, E., 2012. Influence of the tropics and southern westerlies on glacial interhemispheric asymmetry. *Nature Geoscience*, 5(4), pp.266-269.

21. De Deckker, P., Abed, R.M., De Beer, D., Hinrichs, K.U., O'Loingsigh, T., Schefuß, E., Stuut, J.B.W., Tapper, N.J. and Van Der Kaars, S., 2008. Geochemical and microbiological fingerprinting of airborne dust that fell in Canberra, Australia, in October 2002. *Geochemistry, Geophysics, Geosystems*, 9(12).

22. Edwards, T.W., 1993. Interpreting past climate from stable isotopes in continental organic matter. *GEOPHYSICAL MONOGRAPH-AMERICAN GEOPHYSICAL* UNION, 78, pp.333-333.

23. Ecroyd, C.E., 1982. Biological flora of New Zealand 8. Agathis australis (D. Don) Lindl.(Araucariaceae) Kauri. *New Zealand Journal of Botany*, 20(1), pp.17-36.

24. Fairbanks, R.G., Mortlock, R.A., Chiu, T.C., Cao, L., Kaplan, A., Guilderson, T.P., Fairbanks, T.W., Bloom, A.L., Grootes, P.M. and Nadeau, M.J., 2005. Radiocarbon calibration curve spanning 0 to 50,000 years BP based on paired 230Th/234U/238U and 14C dates on pristine corals. *Quaternary Science Reviews*, 24(16-17), pp.1781-1796.

25. Fowler, A., Boswijk, G. and Ogden, J., 2004. Tree-ring studies on Agathis australis (kauri): a synthesis of development work on Late Holocene chronologies. *Tree-Ring Research*, 60(1), pp.15-29.

26. Fowler, A. and Boswijk, G., 2007. Five centuries of ENSO history recorded in Agathis australis (kauri) tree rings. Peter Kershaw AND Jerome Chappellaz. *PAGES News: Past Global Changes.* Vol. 15, No. 2

27. Fowler, A., Palmer, J., Salinger, J. and Ogden, J., 2000. Dendroclimatic interpretation of tree-rings in Agathis australis (kauri): 2. Evidence of a significant relationship with ENSO. *Journal of the Royal Society of New Zealand*, 30(3), pp.277-292.

28. Fowler, A.M., Boswijk, G., Lorrey, A.M., Gergis, J., Pirie, M., McCloskey, S.P., Palmer, J.G. and Wunder, J., 2012. Multi-centennial tree-ring record of ENSO-related activity in New Zealand. *Nature Climate Change*, 2(3), pp.172-176.

29. Gat, J.R., 2000. Atmospheric water balance—the isotopic perspective. *Hydrological processes*, 14(8), pp.1357-1369.

30. Gray, L.J., Beer, J., Geller, M., Haigh, J.D., Lockwood, M., Matthes, K., Cubasch, U., Fleitmann, D., Harrison, G., Hood, L. and Luterbacher, J., 2010. Solar influences on climate. *Reviews of Geophysics*, 48(4).

31. Green, J.D. and Lowe, D.J., 1985. Stratigraphy and development of c. 17 000 year old Lake Maratoto, North Island, New Zealand, with some inferences about postglacial climatic change. *New Zealand journal of geology and geophysics*, 28(4), pp.675-699.

32. Grimm, A.M. and Tedeschi, R.G., 2009. ENSO and extreme rainfall events in South America. *Journal of Climate*, 22(7), pp.1589-1609.

33. Hajdas, I., Lowe, D.J., Newnham, R.M. and Bonani, G., 2006. Timing of the late-glacial climate reversal in the Southern Hemisphere using high-resolution radiocarbon chronology for Kaipo bog, New Zealand. *Quaternary Research*, 65(2), pp.340-345.

34. Hinojosa, J.L., Moy, C.M., Vandergoes, M., Feakins, S.J. and Sessions, A.L., 2019. Hydrologic change in New Zealand during the last deglaciation linked to reorganization of the Southern Hemisphere westerly winds. *Paleoceanography and Paleoclimatolog*y, 34(12), pp.2158-2170.

35. Hua, Q., Barbetti, M., Zoppi, U., Fink, D., Watanasak, M. and Jacobsen, G.E., 2004. Radiocarbon in tropical tree rings during the Little Ice Age. *Nuclear Instruments and Methods in Physics Research Section B: Beam Interactions with Materials and Atoms*, 223, pp.489-494.

36. Hogg, A., Southon, J., Turney, C., Palmer, J., Ramsey, C.B., Fenwick, P., Boswijk, G., Büntgen, U., Friedrich, M., Helle, G. and Hughen, K., 2016. Decadally resolved lateglacial radiocarbon evidence from New Zealand kauri. *Radiocarbon*, 58(4).

37. Hua, Q., Barbetti, M., Fink, D., Kaiser, K.F., Friedrich, M., Kromer, B., Levchenko, V.A., Zoppi, U., Smith, A.M. and Bertuch, F., 2009. Atmospheric 14C variations derived from tree rings during the early Younger Dryas. *Quaternary Science Review*s, 28(25-26), pp.2982-2990.

38. Hughen, K.A., Baillie, M.G., Bard, E., Beck, J.W., Bertrand, C.J., Blackwell, P.G., Buck, C.E., Burr, G.S., Cutler, K.B., Damon, P.E. and Edwards, R.L., 2004. Marine04 marine radiocarbon age calibration, 0–26 cal kyr BP. *Radiocarbon*, 46(3), pp.1059-1086.

39. Kahmen, Ansgar, et al. 2011 Cellulose δ18O is an index of leaf-to-air vapor pressure difference (VPD) in tropical plants. *Proceedings of the National Academy of Sciences* 108.5: 1981-1986.

40. Kaplan, M.R., Schaefer, J.M., Denton, G.H., Barrell, D.J., Chinn, T.J., Putnam, A.E., Andersen, B.G., Finkel, R.C., Schwartz, R. and Doughty, A.M., 2010. Glacier retreat in New Zealand during the Younger Dryas stadial. *Nature*, 467(7312), pp.194-197.

41. Kawamura, K., Parrenin, F., Lisiecki, L., Uemura, R., Vimeux, F., Severinghaus, J.P., Hutterli, M.A., Nakazawa, T., Aoki, S., Jouzel, J. and Raymo, M.E., 2007. Northern Hemisphere forcing of climatic cycles in Antarctica over the past 360,000 years. *Nature*, 448(7156), pp.912-916.

42. Lauterbach, S., Brauer, A., Andersen, N., Danielopol, D.L., Dulski, P., Hüls, M., Milecka, K., Namiotko, T., Obremska, M., Von Grafenstein, U. and Declakes Participants, 2011. Environmental responses to Lateglacial climatic fluctuations recorded in the sediments of pre-Alpine Lake Mondsee (northeastern Alps). *Journal of Quaternary Science*, 26(3), pp.253-267.

43. Liñán, I.D., Gutiérrez, E., Helle, G., Heinrich, I., Andreu-Hayles, L., Planells, O., Leuenberger, M., Bürger, C. and Schleser, G., 2011. Pooled versus separate measurements of tree-ring stable isotopes. *Science of the Total Environment*, 409(11), pp.2244-2251.

44. Lorrey, A.M. and Ogden, J., 2005. Tree-ring analysis of subfossil kauri (Agathis australis) from Omaha Flats, Tawharunui Peninsula, New Zealand. *New Zealand Tree-ring Site Report*, 22.

45. Lorrey, A.M., Brookman, T.H., Evans, M.N., Fauchereau, N.C., Macinnis-Ng, C., Barbour, M.M., Criscitiello, A., Eischeid, G., Fowler, A.M., Horton, T.W. and Schrag, D.P., 2016. Stable oxygen isotope signatures of early season wood in New Zealand kauri (Agathis australis) tree rings: Prospects for palaeoclimate reconstruction. *Dendrochronologia*, 40, pp.50-63.

46. Lowe, D.J., Shane, P.A., Alloway, B.V. and Newnham, R.M., 2008. Fingerprints and age models for widespread New Zealand tephra marker beds erupted since 30,000 years ago: a framework for NZ-INTIMATE. *Quaternary Science Reviews*, 27(1-2), pp.95-126.

47. Lowe, D.J., Blaauw, M., Hogg, A.G. and Newnham, R.M., 2013. Ages of 24 widespread tephras erupted since 30,000 years ago in New Zealand, with re-evaluation of the timing and palaeoclimatic implications of the Lateglacial cool episode recorded at Kaipo bog. *Quaternary Science Reviews*, 74, pp.170-194.

48. Lüttge, U. and Kluge, M., 2012. Botanik: die einführende Biologie der Pflanzen. *John Wiley & Sons*.

49. Marchitto, T.M., Lehman, S.J., Ortiz, J.D., Flückiger, J. and van Geen, A., 2007. Marine radiocarbon evidence for the mechanism of deglacial atmospheric CO2 rise. *Science*, 316(5830), pp.1456-1459.

50. Marcott, S.A., Bauska, T.K., Buizert, C., Steig, E.J., Rosen, J.L., Cuffey, K.M., Fudge, T.J., Severinghaus, J.P., Ahn, J., Kalk, M.L. and McConnell, J.R., 2014. Centennial-scale changes in the global carbon cycle during the last deglaciation. *Nature*, 514(7524), pp.616-619.

51. Merkt, J. and Müller, H., 1999. Varve chronology and palynology of the Lateglacial in Northwest Germany from lacustrine sediments of Hämelsee in Lower Saxony. *Quaternary International*, 61(1), pp.41-59.

52. Newnham, R.M. and Lowe, D.J., 2000. Fine-resolution pollen record of late-glacial climate reversal from New Zealand. *Geology*, 28(8), pp.759-762.

53. Ogden, J., Wilson, A., Hendy, C., Newnham, R.M. and Hogg, A.G., 1992. The late Quaternary history of kauri (Agathis australis) in New Zealand and its climatic significance. *Journal of biogeography*, pp.611-622.

54. Ogden, J. and Ahmed, M., 1989. Climate response function analyses of kauri (Agathis australis) tree-ring chronologies in northern New Zealand*. Journal of the Royal Society of New Zealand*, 19(2), pp.205-221.

55. Palmer, J.G., Turney, C.S., Cook, E.R., Fenwick, P., Thomas, Z., Helle, G., Jones, R., Clement, A., Hogg, A., Southon, J. and Ramsey, C.B., 2016. Changes in El Niño–Southern Oscillation (ENSO) conditions during the Greenland Stadial 1 (GS-1) chronozone revealed by New Zealand tree-rings. *Quaternary Science Reviews*, 153, pp.139-155.

56. Palmer, J. and Ogden, J., 1983. A dendrometer band study of the seasonal pattern of radial increment in kauri (Agathis australis). *New Zealand journal of botany*, 21(2), pp.121-125.

57. Paul, D., Skrzypek, G. and Fórizs, I., 2007. Normalization of measured stable isotopic compositions to isotope reference scales–a review. Rapid Communications in Mass Spectrometry: *An International Journal Devoted to the Rapid Dissemination of Up-to-the-Minute Research in Mass Spectrometry*, 21(18), pp.3006-3014.

58. Pauly, M., Helle, G., Miramont, C., Büntgen, U., Treydte, K., Reinig, F., Guibal, F., Sivan, O., Heinrich, I., Riedel, F. and Kromer, B., 2018. Subfossil trees suggest enhanced Mediterranean hydroclimate variability at the onset of the Younger Dryas. *Scientific reports,* 8(1), pp.1-8.

59. Pauly, M., Helle, G., Büntgen, U., Wacker, L., Treydte, K., Reinig, F., Turney, C., Nievergelt, D., Kromer, B., Friedrich, F., Sookdeo, A., Heinrich, I., Riedel, F., Balting, D., Brauer, A., 2020. Tree-ring stable isotopes from Swiss subfossil pines reveal Late Glacial climate variability over the North Atlantic/European sector. *Quaternary Science Reviews* (247) 106550.

60. Pedro, J.B., Van Ommen, T.D., Rasmussen, S.O., Morgan, V.I., Chappellaz, J., Moy, A.D., Masson-Delmotte, V. and Delmotte, M., 2011. The last deglaciation: timing the bipolar seesaw. *Climate of the Past, European Geosciences Union*

61. Rach, O., Brauer, A., Wilkes, H. and Sachse, D., 2014. Delayed hydrological response to Greenland cooling at the onset of the Younger Dryas in western Europe. *Nature Geoscience*, 7(2), pp.109-112.

62. Rasmussen, S.O., Bigler, M., Blockley, S.P., Blunier, T., Buchardt, S.L., Clausen, H.B., Cvijanovic, I., Dahl-Jensen, D., Johnsen, S.J., Fischer, H. and Gkinis, V., 2014. A stratigraphic framework for abrupt climatic changes during the Last Glacial period based on three synchronized Greenland ice-core records: refining and extending the INTIMATE event stratigraphy. *Quaternary Science Reviews*, 106, pp.14-28.

63. Renssen, H., Mairesse, A., Goosse, H., Mathiot, P., Heiri, O., Roche, D.M., Nisancioglu, K.H. and Valdes, P.J., 2015. Multiple causes of the Younger Dryas cold period. *Nature Geoscience*, 8(12), pp.946-949.

64. Ryan, M.T., 2017. Late Quaternary vegetation and climate history reconstructed from palynology of marine cores off southwestern New Zealand. *PhD Thesis, Victoria University of Wellington*.

65. Saurer, M., Kress, A., Leuenberger, M., Rinne, K. T., Treydte, K. S., & Siegwolf, R. T., 2012. Influence of atmospheric circulation patterns on the oxygen isotope ratio of tree rings in the Alpine region. *Journal of Geophysical Research: Atmospheres*, 117(D5).

66. Schollaen, K., Baschek, H., Heinrich, I., Slotta, F., Pauly, M. and Helle, G., 2017. A guideline for sample preparation in modern tree-ring stable isotope research. *Dendrochronologia*, 44, pp.133-145.

67. Schollaen, K., Heinrich, I., Neuwirth, B., Krusic, P.J., D'Arrigo, R.D., Karyanto, O. and Helle, G., 2013. Multiple tree-ring chronologies (ring width, δ13C and δ18O) reveal dry and rainy season signals of rainfall in Indonesia. *Quaternary Science Reviews*, 73, pp.170-181.

68. Schöngart, J., Piedade, M.T.F., Ludwigshausen, S., Horna, V. and Worbes, M., 2002. Phenology and stem-growth periodicity of tree species in Amazonian floodplain forests. *Journal of Tropical Ecology*, pp.581-597.

69. Steffensen, J.P., Andersen, K.K., Bigler, M., Clausen, H.B., Dahl-Jensen, D., Fischer, H., Goto-Azuma, K., Hansson, M., Johnsen, S.J., Jouzel, J. and Masson-Delmotte, V., 2008. High-resolution Greenland ice core data show abrupt climate change happens in few years. *Science*, 321(5889), pp.680-684.

70. Stocker, T.F., 1998. The seesaw effect. *Science*, 282(5386), pp.61-62.

71. Treydte, K.S., Schleser, G.H., Helle, G., Frank, D.C., Winiger, M., Haug, G.H. and Esper, J., 2006. The twentieth century was the wettest period in northern Pakistan over the past millennium. *Nature*, 440(7088), pp.1179-1182.

72. Treydte, K., Frank, D., Esper, J., Andreu, L., Bednarz, Z., Berninger, F., Boettger, T., D'alessandro, C.M., Etien, N., Filot, M. and Grabner, M., 2007. Signal strength and climate calibration of a European tree-ring isotope network. *Geophysical Research Letters*, 34(24).

73. Turney, C.S., Fifield, L.K., Hogg, A.G., Palmer, J.G., Hughen, K., Baillie, M.G., Galbraith, R., Ogden, J., Lorrey, A., Tims, S.G. and Jones, R.T., 2010. The potential of New Zealand kauri (Agathis australis) for testing the synchronicity of abrupt climate change during the Last Glacial Interval (60,000–11,700 years ago). *Quaternary Science Reviews*, 29(27-28), pp.3677-3682.

74. Ummenhofer, C.C. and England, M.H., 2007. Interannual extremes in New Zealand precipitation linked to modes of Southern Hemisphere climate variability. *Journal of Climate*, 20(21), pp.5418-5440.

75. von Grafenstein, U., Erlenkeuser, H., Brauer, A., Jouzel, J. and Johnsen, S.J., 1999. A mid-European decadal isotope-climate record from 15,500 to 5000 years BP. *Science*, 284(5420), pp.1654-1657.

76. WAIS Divide Project Members, 2015. Precise interpolar phasing of abrupt climate change during the last ice age. *Nature*, 520(7549), p.661.

77. van Geel, B., Buurman, J., Brinkkemper, O., Schelvis, J., Aptroot, A., van Reenen, G. and Hakbijl, T., 2003. Environmental reconstruction of a Roman Period settlement site in Uitgeest (The Netherlands), with special reference to coprophilous fungi. *Journal of Archaeological Science*, 30(7), pp.873-883.

78. Wieloch, T., Helle, G., Heinrich, I., Voigt, M. and Schyma, P., 2011. A novel device for batch-wise isolation of α-cellulose from small-amount wholewood samples. *Dendrochronologia*, 29(2), pp.115-117.

79. Willems, P., 2013. Adjustment of extreme rainfall statistics accounting for multidecadal climate oscillations. *Journal of Hydrology*, 490, pp.126-133.

80. Xu, C., Ge, J., Nakatsuka, T., Yi, L., Zheng, H. and Sano, M., 2016. Potential utility of tree ring δ18O series for reconstructing precipitation records from the lower reaches of the Yangtze River, southeast China. *Journal of Geophysical Research: Atmospheres*, 121(8), pp.3954-3968.

S8.7. Stable Isotopes in Kauri Tree Rings

The basic source of oxygen atoms in the tree-ring cellulose is atmospheric precipitation. Variations in $\delta^{18}O$ of precipitation ($\delta^{18}O_{prec}$) are determined by fractionation processes which occur during temperature- and humidity-dependent phase changes associated with evaporation and condensation (e.g. Dansgaard 1964; Gat 2000). $\delta^{18}O_{prec}$ is also known to reflect rainout history and atmospheric circulation patterns along given air mass trajectories (e.g. Araguas-Araguas et al., 2000).

$\delta^{18}O$ within tree-ring cellulose ($\delta^{18}O_{cell}$) is related to the $\delta^{18}O$ of the precipitation source via soil water representing an average $\delta^{18}O$ over several precipitation events modified by partial evaporation from the soil (depending on soil texture and porosity), as well as by a possible time lag, depending on rooting depth (Saurer et al. 2012). $\delta^{13}C_{cell}$ is taken up at the leaf level in the form of CO_2, with the proportion of heavy to light carbon (^{13}C, ^{12}C) impacted by relative humidity driven stomatal conductance (Farquhar et al., 1982). Similar to $\delta^{13}C_{cell}$, variability of $\delta^{18}O_{cell}$ is affected by evaporative ^{18}O-enrichment of leaf water governed by leaf-to-air vapour pressure deficit (e.g. Kahmen et al., 2011).

Intra-annual tree-ring isotope data ($\delta^{18}O$ and $\delta^{13}C$) by Brookman (2014) demonstrated that isotopic maxima occurred in kauri wood formed during SH spring (September – November) and minima prevail in late season wood formed during SH summer/autumn; the latter potentially capturing extra-tropical cyclones as depleted $\delta^{18}O$ (negative correlation to precipitation amount and positive correlation to relative humidity). This seasonal pattern is rather similar to intra-seasonal $\delta^{18}O$ tree-ring stable isotope variability from sites in Indonesia

(Schollaen et al. 2013) and southeast China (Xu et al. 2015), characterised by monsoonal seasonal rainfall. Lorrey et al. (2016) demonstrated opposing relationships to climate when analyzing only the early season wood (ESW) portion of kauri tree rings, in particular, negative correlations to temperature. These contrasting results prove that the portion of the annual ring measured in kauri trees can greatly impact the sensitivity of stable isotopes therein to different climate variables, as ESW tends to provide enriched $\delta^{18}O$ and $\delta^{13}C$ compared to whole ring analysis. For further details on oxygen stable isotope transfer in the arboreal system of kauri cf. Lorrey et al. (2016) and citations therein.

S8.8. Site conditions

New Zealand climate is influenced by a complex mix of surrounding atmospheric systems (Figure 8.2c), including incoming moist maritime air masses arriving from all directions, modulated by ENSO conditions. The climate of the area in which kauri naturally grow today is generally warm and humid with annual rainfall varying from 1000 to 2500mm and a mean annual temperature from 13 to 16°C (Ecroyd 1982). Snowfalls are uncommon and frosts are rather rare and not severe in the kauri habitat; ranging from sea level to no more than 450m above sea level, hence kauri is predominately a lowland species. The natural distribution of modern kauri is focused in the North Island and many offshore islands between 38°07`S and 34°06`S (Ecroyd 1982).

North Island is subject to the 'roaring forties' prevailing winds arriving from the west as well as tropical La Nina winds flowing from the north. Kauri trees within this region begin their annual growth in SH spring (Palmer & Odgen 1983), with a peak in growth occurring in between December and February (SH summer; Ecroyd 1982) and dormancy lasting from June to August (SH winter; Lüttge & Kluge 2012). Climate-growth relationships have demonstrated positive correlations between kauri growth and hot/dry weather, whereas slow growth is correlated to high humidity, precipitation and cool temperatures (Ogden and Ahmed 1989). Accordingly, during El Nino periods when North Island is experiencing warm and dry conditions, tree-ring growth is enhanced. On the other hand, during cool and humid La Nina periods, conditions are less optimal for tree-ring growth.

Variable	Oxygen	Carbon
Mean	0.02	0.19
Range	-0.76 to 0.88	-0.44 to 0.80
Pre-Downturn (~13 000 - 12 625 cal BP)	-0.76 to 0.07 (-0.23)	-0.44 to 0.80 (0.13)
Downturn (~12 625 - 12 375 cal BP)	-0.07 to 0.55 (0.22)	-0.26 to 0.48 (0.13)
Post-Downturn (~12 375 - 11 850 cal BP)	-0.22 to 0.28 (0.07)	-0.27 to 0.64 (0.28)

Table S8.1. Inter-tree correlations for oxygen ($\delta^{18}O_{cel}$) and carbon ($\delta^{13}C_{cel}$) from KAU-ISO.

Isotope	Modern/Ancient	Range	Mean	Mean inter-annual variability
$\delta^{18}O$	Modern	28.8 to 36.8‰ (8.0‰)	31.9‰	0.70‰
$\delta^{18}O$	Ancient	28.9 to 31.8‰ (2.9‰)	30.5‰	0.74‰
$\delta^{13}C$	Modern	-19.9 to -25.5‰ (5.5‰)	-22.8‰	0.33‰
$\delta^{13}C$	Ancient	-22.3 to -23.4‰ (1.1‰)	-22.8‰	0.40‰

Table S8.2. Mean, range and inter-annual variability of stable oxygen and carbon isotopes in modern (Brookman et al. 2014) and subfossil (this study) tree-rings from New Zealand North Island.

Variable	La Niña-like conditions	YD Downturn
Precipitation	High	High
Temperature	High	Low
Sea Level Pressure	High	Low
Humidity	High	High
Tree Growth	Low	Low

Table S8.3. A comparison of hydroclimate conditions during modern La Niña situations compared to the YD downturn from tree-ring data and PaleoView TraCE21ka climate model outputs.

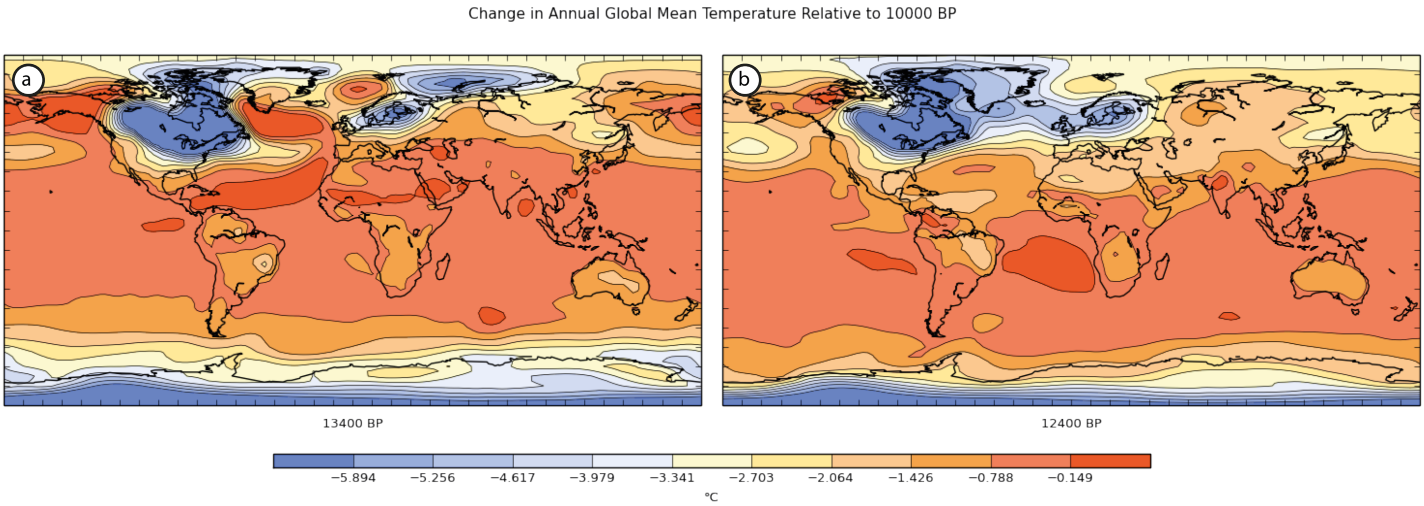

Figure S8.1. Reconstructed average global mean temperature using PaleoView (coupled atmosphere-ocean general circulation TraCE-21ka) during the (a) Bolling-Allerod (~13 400 cal BP), and (b) the Younger Dryas (12 400 cal BP). The difference between the two maps demonstrating the relative widespread cooling of the North Atlantic region across Greenland during the Younger Dryas, in contrast to the warming felt in the Southern Hemisphere.

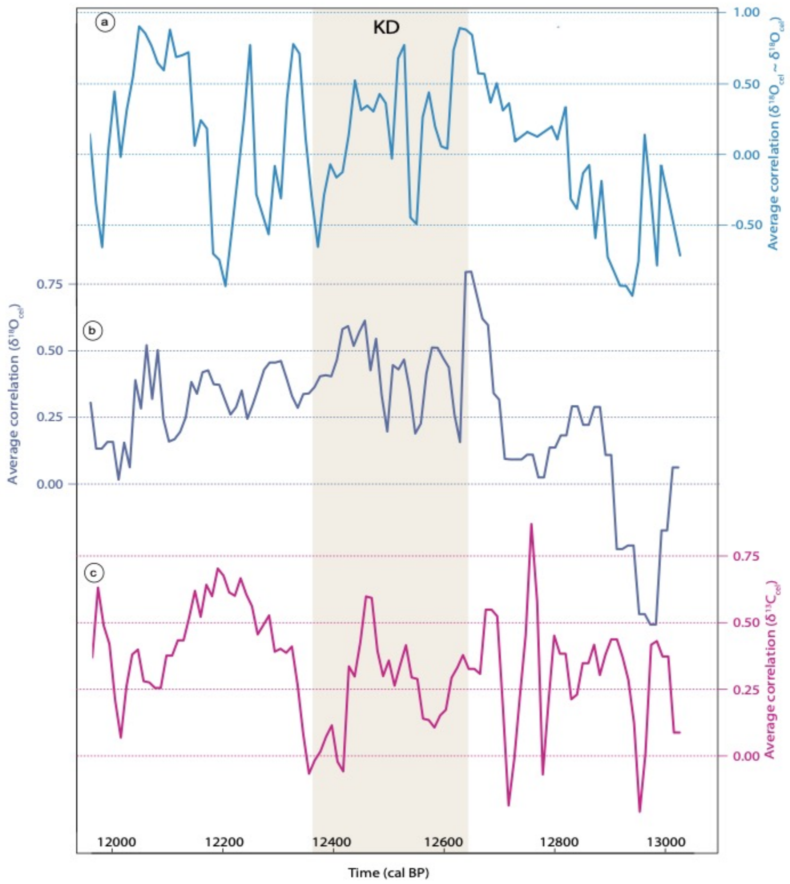

Figure S8.2. Correlation of trees within the KAU-ISO chronology. (a) Correlation of mean $\delta^{13}C_{cel}$ and $\delta^{18}O_{cel}$. Average correlation calculated from running correlation of each tree for (b) $\delta^{18}O_{cel}$, and (c) $\delta^{13}C_{cel}$; the Kauri Downturn (KD) is highlighted.

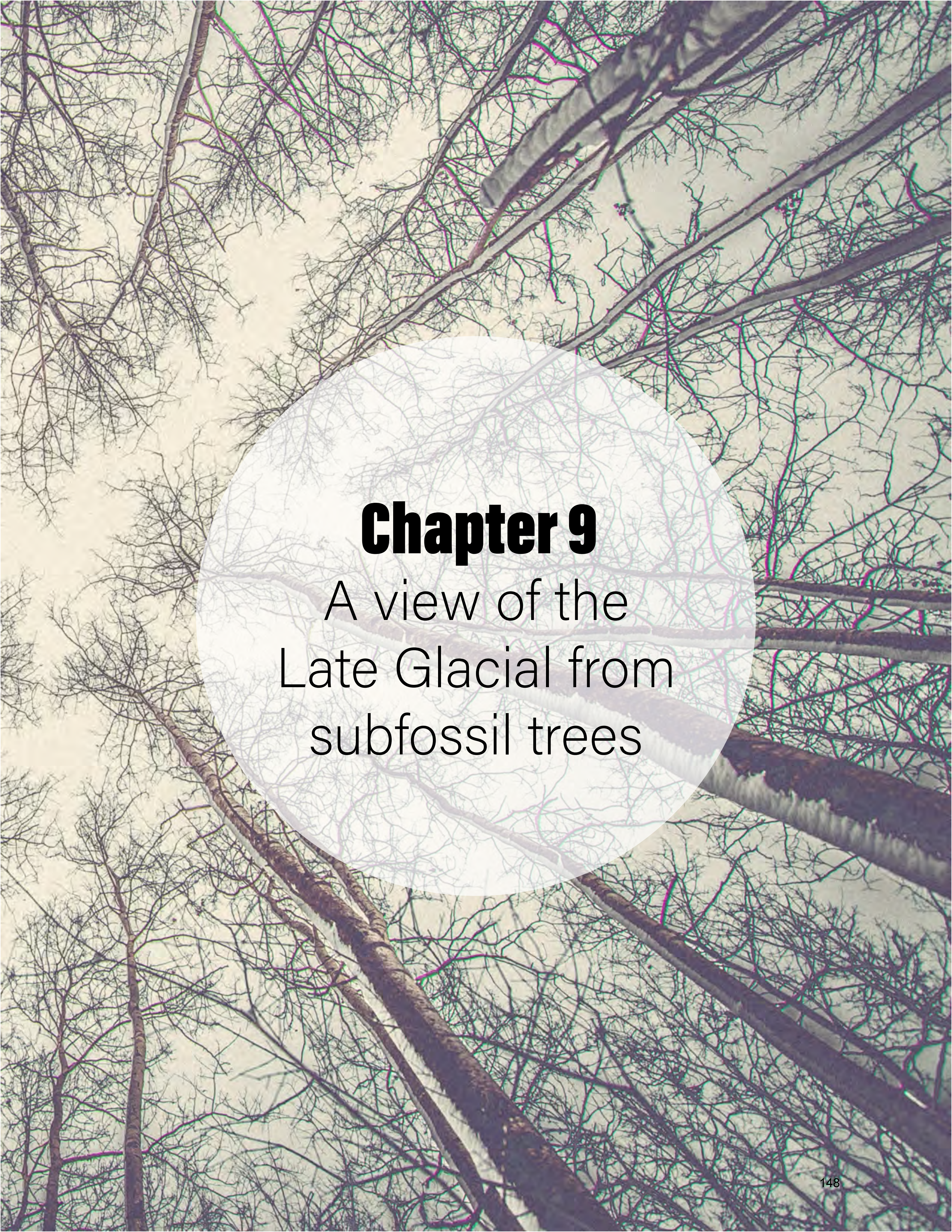

Chapter 9
A view of the
Late Glacial from
subfossil trees

9. A view of the Late Glacial from subfossil trees

The study of dendroclimatology generally depends on three main assumptions:

(1) The principle of uniformitarianism, which assumes that the physical conditions that exist today must have always existed in a similar state in the past;
(2) The relationship between climate conditions and tree-ring parameters (growth rings and stable isotopes) have remained stable through time, and;
(3) Environmental conditions are consistent across local sites, and therefore impact all of the trees consistently within a cohort.

Whilst these principles generally apply to many modern era dendroclimatology studies, this thesis has provided evidence that they partially breakdown in the application with subfossil wood material during the Late Glacial. Through the analysis of high temporal resolution proxy records - which are still relatively rare in the Late Glacial – it is becoming clear that the climate system in the Late Glacial operated differently than today. At the moment, the only annual chronologies available are: (1) Greenland ice core $\delta^{18}O$ (Steffensen et al. 2008), (2) molecular biomarkers from Meerfelder Maar varved sediments (Obreht et al. 2020) and (3) the dual tree-ring stable isotope records ($\delta^{18}O$, $\delta^{13}C$) presented in this thesis from Switzerland, France and New Zealand. These studies have shown that contemporary environmental conditions do not necessarily hold in deep time, as climate in the *Late Glacial demonstrate extremes beyond the envelope of variability experienced within the instrumental record*.

Global climate model (GCM) simulations – which provide multi-decadal temporal resolution - are a useful tool in (a) understanding background climate state conditions in deep time, (b) verifying proxy-climate reconstructions, (c) investigating additional climate parameters and (d) interpreting climate oscillations at various geographic scales (expanding the local proxy signatures to regional to hemispheric model outputs). Based on the conclusions from this thesis (and results from other high-resolution paleoclimate records), it is recommended to use GCMs in addition to proxy records to contextualise the results.

Research in this thesis, as well as modern studies (Kress et al. 2010, Reynolds-Henne et al. 2007, Seftigen et al. 2011), have confirmed that the *relationship between tree-ring stable isotopes and climate conditions are not necessarily stable through time*. In the case of the subfossil trees presented in this work, the instability in climate-proxy relationships is due to the competing impact of local site conditions on tree-ring parameters (e.g. precipitation percolation through soil, permafrost, local weather extremes) and regional/hemispheric air masses (e.g. opposing influence of the North Atlantic, Continental and Mediterranean airmasses in Europe, as well as the circumpolar westerlies, east Australian current and roaring forties in New Zealand). These conditions impact the stable isotope signatures taken up my trees both at the roots ($\delta^{18}O$ from sourcewater) as well as the fractionation of stable isotopes as a result of relative humidity changes (e.g. stomata closure leading to reduced $\delta^{13}C$ uptake and $\delta^{18}O$ enrichment). Careful consideration of the site conditions, tree species and modern calibrations is required to detangle local influences from regional/hemispheric signals beyond the instrumental record.

Local site conditions, particularly of the trees from the Swiss Plateau, seemed to impact the population signal of both the tree-ring widths (Reinig et al. 2018) as well as the stable isotopes (Paper 1). These pine trees grew on an unstable slope, in an environment with discontinuous permafrost – both of which could have potentially impacted the $\delta^{18}O$ signature within the tree-ring widths by inconsistently altering the water taken up at the roots in a small region. While the general geological setting is known, a robust survey of the site (and tree positions) during excavation not undertaken, which could have provided clues into the microsite conditions impacting the population signal and cross-dating of the Swiss trees. However, the statistical cross-dating of the trees to develop the Swiss chronology (Reinig et al. 2018) was aided by high resolution radiocarbon dating (see co-authored publications: Sookdeo et al. 2020, Sookdeo et al. 2019, Reinig et al. 2020); a method which can be used to assist in chronology development when multiple potential tree positions exist.

Differences in tree-ring stable isotope correlation between trees was also likely a result of wood decay (Paper 1), impacting the trees in the Swiss Plateau more strongly than those from the southern French Alps (Paper 2) or New Zealand kauri (Paper 3), particularly around the bark and outer rings. Whilst preliminary, trees with stronger visual decay (discolouration and brittle texture) seemed to have lower intra-tree correlations between isotopes ($\delta^{18}O$ vs. $\delta^{13}C$; due to preferential decay of $\delta^{13}C$) as well as lower inter-tree correlations. Due to this finding, *subfossil tree-ring stable isotope chronologies may require more than the typical 4-5 overlapping trees to produce adequate population signals, compared to modern stable isotope chronologies*. A robust protocol for characterising wood decay – including cellulose preservation, wood texture and colour – should be developed to subset trees before developing a stable isotope chronology.

Despite some noise in the data resulting from local influences (and potentially wood decay), the records in this thesis have proven that *largescale climate anomalies (which are often of more research interest than local variations) can be adequately captured in stable isotopes of subfossil pine and kauri trees*; such as the oscillating polar front (Papers 1-2) and ocean circulation changes around New Zealand (Paper 3). These are generally recorded as significant depletions or enrichments of $\delta^{18}O$, as well as increases in $\delta^{18}O$ inter-annual variability; the caveat being that those widespread conditions are recorded more strongly in tree-ring stable isotopes during extreme (over average) and wet (over humid) conditions, and only when the climate oscillations are expressed during the growing season.

While some NH Late Glacial climate oscillations were recorded in the chronologies presented (i.e. GS-1 in Switzerland and France), other oscillations (e.g. GI-1b) were not articulated as well in the tree-ring stable isotopes compared to lacustrine sediments (e.g. Lauterbach et al. 2011) and Greenland ice core records (e.g. Rasmussen et al. 2014). This could be in part due to these events being predominantly winter occurrences but may also be influenced by the short lifespans of the individual trees, as low frequency climate variability is difficult to maintain in short-lived trees (also seen in Saurer et al. 2012 and Cook et al. 2019). This would impact subfossil Scots pine trees from Europe (lifespans average 100-200 years) more strongly compared to millennial-lived subfossil kauri trees from New Zealand.

References (Chapter 9)

Cook, Edward R., et al. "A Euro-Mediterranean tree-ring reconstruction of the winter NAO index since 910 CE." Climate Dynamics 53.3-4 (2019): 1567-1580.

Kress, Anne, et al. "A 350-year drought reconstruction from Alpine tree ring stable isotopes." Global Biogeochemical Cycles 24.2 (2010).

Lauterbach, Stefan, et al. "Environmental responses to Lateglacial climatic fluctuations recorded in the sediments of pre-Alpine Lake Mondsee (northeastern Alps)." Journal of Quaternary Science 26.3 (2011): 253-267.

Obreht, Igor, et al. "An annually resolved record of Western European vegetation response to Younger Dryas cooling." Quaternary Science Reviews 231 (2020): 106198.

Rasmussen, Sune O., et al. "A stratigraphic framework for abrupt climatic changes during the Last Glacial period based on three synchronized Greenland ice-core records: refining and extending the INTIMATE event stratigraphy." Quaternary Science Reviews 106 (2014): 14-28.

Reinig, Frederick, et al. "New tree-ring evidence for the Late Glacial period from the northern pre-Alps in eastern Switzerland." Quaternary Science Reviews 186 (2018): 215-224.

Reinig, Frederick, et al. "Extending the world’s longest tree-ring chronology throughout the Younger Dryas" (2020, submitted)

Reynolds-Henne, C. E., et al. "Temporal stability of climate-isotope relationships in tree rings of oak and pine (Ticino, Switzerland)." Global Biogeochemical Cycles 21.4 (2007).

Saurer, Matthias, et al. "Influence of atmospheric circulation patterns on the oxygen isotope ratio of tree rings in the Alpine region." Journal of Geophysical Research: Atmospheres 117.D5 (2012).

Seftigen, Kristina, et al. "The influence of climate on 13C/12C and 18O/16O ratios in tree ring cellulose of Pinus sylvestris L. growing in the central Scandinavian Mountains." Chemical Geology 286.3-4 (2011): 84-93.

Sookdeo A., Kromer B., Adolphi F., Beer J., Brehm N., et al. 2020. "Tree-ring radiocarbon reveals reduced solar activity during Younger Dryas cooling. " (2020, Submitted)

Sookdeo, Adam, et al. "Quality dating: a well-defined protocol implemented at ETH for high-precision 14C-Dates tested on late glacial wood." Radiocarbon (2019): 1-9.

Steffensen, Jørgen Peder, et al. "High-resolution Greenland ice core data show abrupt climate change happens in few years." Science 321.5889 (2008): 680-684.

Chapter 10
Conclusions

10. Conclusions

The study of past climates (paleoclimatology) using natural archives (trees, corals, ice cores, lake sediments) offers an opportunity to improve the predictability of future climate change. Examples from the past provide information on climatic variability, abrupt events as well as earth system feedbacks and responses to external forcing, on timescales that exceed the relatively short period of instrumental climate data. By improving the understanding of dynamics controlling climate on long time scales, Global Climate Model (projections can be better constrained, providing more accurate information to inform policy and decision-making at international to local levels.

Late Glacial climate oscillations have been chronicled in climate proxy records across the globe, yet the underlying processes controlling regional differences of both modern and previous climate events remain unclear. This is mainly due to the relatively coarse temporal resolution (multi-decadal to centennial scale) of available paleoclimate records, which cannot necessarily detect short-term oscillations. In this thesis, tree-ring stable isotopes were used, which offer an annually resolved proxy, with the potential to capture rapid hydroclimate changes through the reconstruction of precipitation and relatively humidity. From long-term atmospheric circulation changes such a climate deterioration in the South Pacific (Paper 3) to short-term events including polar outbreak storms in the Mediterranean (paper 2) – this thesis has exemplified the power (as well as challenges – paper 1) of using subfossil tree-ring stable isotopes to track climate variability in the Late Glacial.

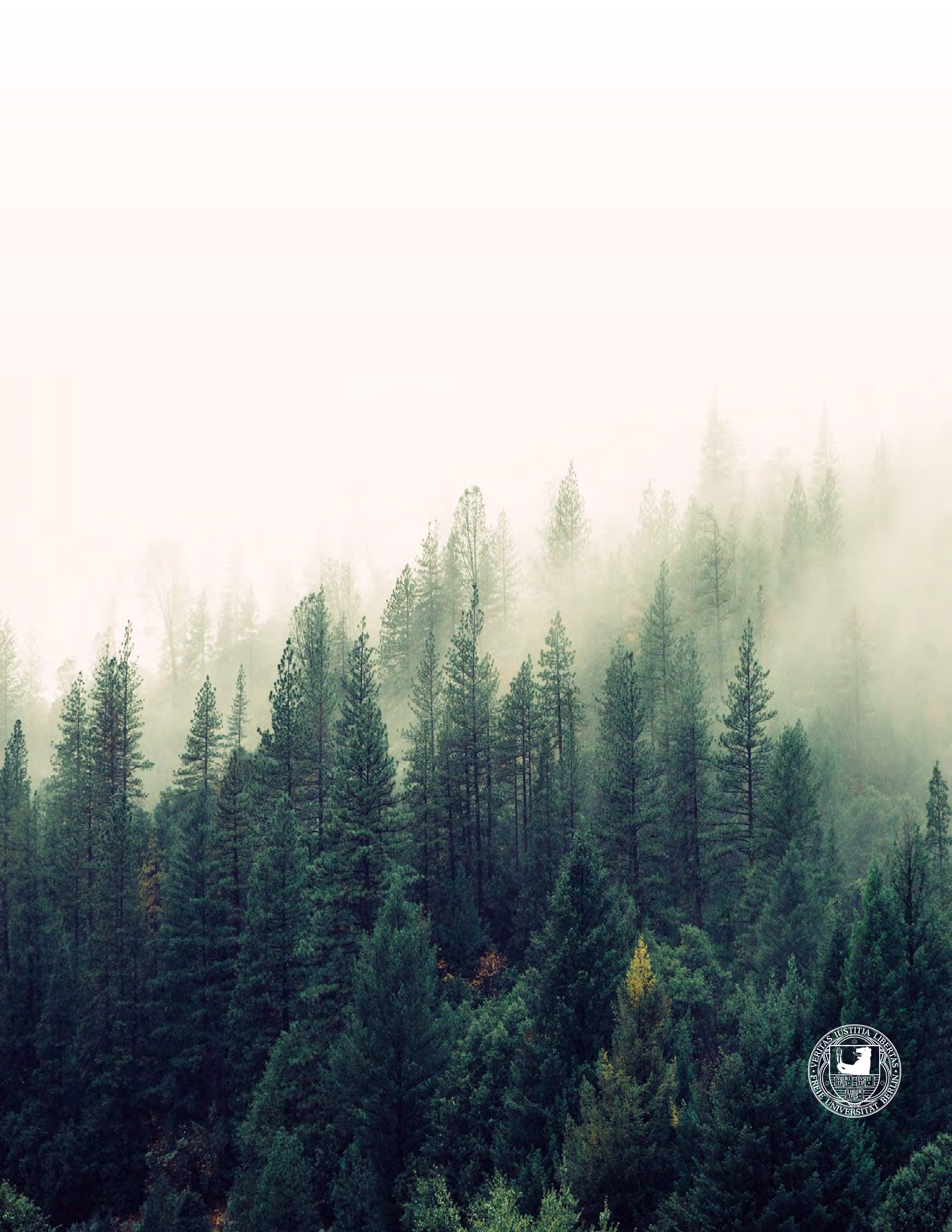
VERITAS IUSTITIA LIBERTAS
FREIE UNIVERSITÄT BERLIN